12-2018

Implementation of Soft Lithography for the Fabrication of Stacked Dielectric Elastomer Actuators for Soft Robotics

Mert Corbaci
mc5042@rit.edu

R·I·T

Implementation of Soft Lithography for the Fabrication of Stacked Dielectric Elastomer Actuators for Soft Robotics

by

Mert Corbaci

A dissertation submitted in partial fulfillment of the
requirements for the degree of
Doctor of Philosophy
in
Microsystems Engineering

Microsystems Engineering
Kate Gleason College of Engineering

Rochester Institute of Technology
Rochester, New York

December 2018

Implementation of Soft Lithography for the Fabrication of Stacked Dielectric Elastomer Actuators for Soft Robotics
by
Mert Corbaci

Committee Approval:
We, the undersigned committee members, certify that we have advised and/or supervised the candidate on the work described in this dissertation. We further certify that we have reviewed the dissertation manuscript and approve it in partial fulfillment of the requirements of the degree of Doctor of Philosophy in Microsystems Engineering.

Dr. Kathleen Lamkin-Kennard Date
Professor, Mechanical Engineering (Dissertation Advisor)

Dr. Karl D. Hirschman Date
Professor, Electrical and Microeletronic Engineering

Dr. Thomas W. Smith Date
Professor, Chemistry and Microsystems Engineering

Dr. Wayne Walter Date
Professor Emeritus, Mechanical Engineering

Certified by:

Dr. Bruce W. Smith Date
Director, Microsystems Engineering Program

Acknowledgements

I would like to express my gratitude to my advisor, Dr. Kathleen Lamkin-Kennard, for her guidance, encouragement and understanding. Many thanks to Prof. William Humphrey, Drs. Karl Hirschman, Thomas Smith, Wayne Walter, Denis Cormier, Thomas Gaborski, Richard Hailstone, and Bruce Smith for all their contributions and for being inspiring teachers; all the members of the Lab Talks group for their valuable discussions; everyone at RIT SMFL, AM Print Center and the Construct at RIT for their technical support, Lisa Zimmerman for always helping me with a smile.

I gratefully acknowledge the financial support of Google Inc, RIT Microsystems Engineering and Mechanical Engineering departments.

Thanks to all the members of the Llama office (Yukee, Mario, Elisabeth, Jimmy, Simon and Jenny) for the delicious food and the best times at RIT; to my closest friends in Boston, Istanbul, West Lafayette and Malmö for their moral support. Special thanks to Olivia Scheibel and Mustafa Koz for all the fun, for their technical assistance and guidance, and for their friendship.

I am grateful to my parents, Ergül and Faik Çorbaci, for their continuous support, never diminishing love and trust; to my grand-parents, Zeliha and Hasan Yildiz, for raising me and teaching me how to learn. Finally to my partner, Deniz Çetin: thank you for encouraging me to push my limits and for always being there for me regardless of the circumstances.

Abstract

Advancements in software engineering have enabled the robotics industry to transition from the use of giant industrial robots to more friendly humanoid robots. Soft robotics is one of the key elements needed to advance the transition process by providing a safer way for robots to interact with the environment. Electroactive polymers (EAPs) are one of the best candidate materials for the next generation of soft robotic actuators and artificial muscles. Lightweight dielectric elastomer actuators (DEAs) provide optimal properties such as high elasticity, rapid response rates, mechanical robustness and compliance. However, for DEAs to become widely used as artificial muscles or soft actuators, there are current limitations, such as high actuation voltage requirements, control of actuation direction, and scaling, that need to be addressed.

This study presents a novel approach inspired by the natural skeletal muscles to overcome the drawbacks of conventional DEAs. Instead of fabricating a large DEA device, smaller sub-units can be fabricated and bundled together to form larger actuators, similar to the way myofibrils form myocytes in skeletal muscles. Soft lithography and other microfabrication techniques were utilized to allow fabrication of silicone based multilayer stacked DEA structures, composed of hundreds of micro-sized DEA units with mechanically compliant electrodes. Experiments show that free-standing multilayer DEA structures can be fabricated using existing microfabrication

tools. Three fabrication approaches, using spin coating, film casting and injection molding were evaluated to improve the repeatability of the fabrication process. Multi-layer DEA fibers can be actuated in sub-kV range while maintaining actuation ratio above 5%.

Contents

List of Figures

List of Tables

Chapter 1

Introduction

1.1 Robotics

A robot refers to a mechanical or virtual agent that is artificially designed and that can accomplish a predesignated set of tasks automatically or under the control of a computer. A robot can be an autonomous robot in an industrial plant, carrying out manufacturing tasks like lifting a half a ton steel block, painting a car, drilling a hole on an aluminum sheet or cutting through a piece of glass with sub-mm precision. Alternatively, it can be a humanoid service robot designed to assist and to help people do daily tasks like cleaning, providing security, communicating with others or moving from one place to another. No matter what a robot is designed for, it always requires three main components; a frame for a physical body (i.e. skeleton), actuators for movement (i.e. muscles), and a controlling center (i.e. brain).

As the list of potential tasks that robots can perform gets more complex, robots require more components for accuracy and precision. Robots can be equipped with hundreds of sensors, providing feedback to the controlling center from the environ-

ment and from the actuators of the robot. Each robot, however, is designed for accomplishing predesignated tasks in a specific environment and for interacting with specific types of objects, as it is usually cumbersome and sometimes even impossible to determine and process in real-time how a robot is interacting with objects and its environment. Nevertheless, robots are becoming more integrated in our daily lives and they need to be compliant with both the living subjects around them and the objects with which they are required to interact.

The concept of robotics can be traced back to Greek mythology, specifically Talos, a giant bronze automaton that was sent to protect Europe [1]. In the 200s B.C., Greek mathematicians and inventors like Archimedes and Ctesibus designed the first mechanical systems with movable figures that constituted the foundation of modern robotics [2]. Like in every era, they had tried to fulfill the needs of their people by building structures to carry water around (Archimedes screw), to defend cities (Archimedes claw), or to measure time (water clocks). The mechanical systems did not necessarily resemble any kind of modern day robot, but were made of gears, pulleys and screws, which are still used to move structures. In the 15^{th} century, Leonardo da Vinci introduced a 'mechanical knight', the first ancestor of what we call a humanoid robot today [3]. The 'knight' was controlled by pulling strings that were mechanically attached to wooden moving parts, similar to the parts Archimedes and others used in Ancient Greece.

In 1961, the first industrial robot, Unimate, shown in Figure 1.1, was integrated into the manufacturing facility of General Motors [4]. It was a 4000 lb machine with 6 programmable axes of motion and could handle parts weighing 500 lbs [5]. Since then, industrial robots have been implemented into the assembly lines of many different manufacturers and became a billion industry in 2014, including software and

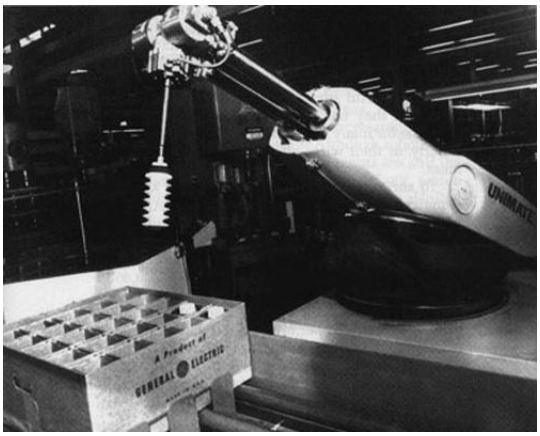

Figure 1.1: The first industrial robot, Unimate, weighed around 1.8 tons and had 6 fully programmable axes of motion.

systems engineering costs [6].

In just a few centuries, robots have transformed from complicated hand-made puppets to ultra-precision high-speed machines that are used world-wide. The main difference between the two is the integration of a "brain" that controls the devices. Instead of a person holding strings, modern robots are controlled by computers that receive inputs from numerous sensors, evaluate them through complex control strategies, then generate output signals for a specified time to actuators, such as motors, to generate motions.

With significant advancements in microelectronics, control theory and embedded systems, robots can maintain sub-millimeter precision while delivering force outputs hundreds of times larger than humans can. The same advancements that led to the proliferation of industrial robots has also allowed them to reach beyond the factory floors and become more and more immersed in our daily lives. However, the usefulness of robots outside of factory environments is often limited because they are made of stiff, highly geared components that may be dangerous to humans. Rigid components also limits their ability to interact with fragile objects that require delicate handling.

Figure 1.2: Honda's Asimo is one of the first modern humanoid robots. *Source:* *https://upload.wikimedia.org/wikipedia/commons/3/39/ASIMO_4.28.11.jpg*

Although many companies are developing humanoid robots, such as Honda's Asimo, shown in Figure 1.2, or Boston Dynamics' Atlas, shown in Figure 1.3, these robots are still limited in the amount they interact with humans because of the potential risk they pose. Currently, robots that work around humans are limited to doing low power, low risk activities, such as vacuuming floors or entertaining people. The safety risks could be minimized if robots instead had soft, lightweight, flexible components that could interact with fragile and living things more freely.

1.2 Soft Robotics

Soft robotics is a new and emerging field that aims to develop robots with soft structures to provide a safer and more flexible working environment where robots can interact with humans and other objects, with abated safety concerns, yet still be able

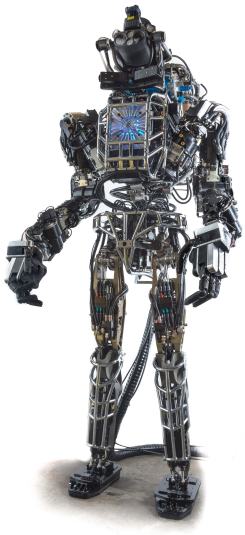

Figure 1.3: Atlas by Boston Dynamics *Source:* *https://upload.wikimedia.org/wikipedia/commons/8/81/Atlas_frontview_2013.jpg*

carry out significant tasks that conventional rigid robots cannot [7]. In a conventional robotic system, actuators and/or grippers provide physical interaction with the surroundings. However, the robots are traditionally manufactured using tough, stiff materials and geared structures. Actuators can be electromechanical in nature or pneumatic or hydraulic based, meaning that they use pressurized fluids in order to do the desired work. Pressurized systems typically work with high pressures and therefore require stiff and tough components that can still pose danger to people and fragile objects in case of a malfunction or an accident.

Soft robots aim to replace these conventional systems with more natural, bio-inspired actuation mechanisms that are built using polymer based soft materials. Most of the soft bio-mimetic actuation systems have the ability to change their shape or volume when an external stimulus is applied. Depending on the type of the actuator, the working mechanism may rely on migration of ions, transfer of a fluid from one point to another, or transfer of electronic charges within the actuator. One example

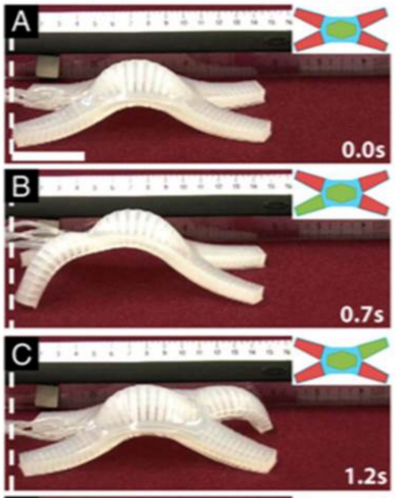

Figure 1.4: A crawling soft robot developed by Prof. Whitesides Research Group at Harvard University. *Source:* `https://gmwgroup.harvard.edu/`

of soft robots is shown in Figure 1.4. The soft crawler robot is made of a highly elastic soft polymer and has empty air sacs inside. When the air sacs are selectively inflated, the robot can crawl in a desired direction.

In order to better understand the difference between conventional actuators and biomimetic soft robotic actuators, intrinsic mechanical properties, like Young's modulus, hardness, and the toughness of materials used in each system should be compared. Young's modulus is a measure of a materials stiffness and is a measure of how much force is required in order to deform a material in the elastic regime. Hardness of a material defines how much force the material can resist before it undergoes plastic deformation. Toughness is a materials ability to absorb energy (the total amount of energy) without catastrophic failure while it is deforming plastically.

Table 1.1 compares the tensile strength and elastic modulus of some of the commonly used metal alloys, glass, silicon, some common polymers and human bone tissue. As seen in Table 1.1, the elastic moduli and tensile strength of the metal alloys are about 10 times higher than those of human bone. On the other hand, some

commonly used polymers like nylon, polyethylene and silicone have elastic moduli and tensile strengths much less than human bone. These values indicate that those polymeric materials, even if they come into contact with humans, would not likely cause any fatal injury.

Table 1.1: Comparison of mechanical properties of commonly used metal alloys and polymers, glass, silicon and human bone.

Material	**Modulus of Elasticity (MPa)**	**Tensile Strength (MPa)**
1040 Steel Alloy cie	2.0×10^5	$520 - 590$
2024-O Aluminum Alloy	7.31×10^4	$186 - 240$
Borosilicate Glass	7.0×10^4	69
Single Crystal Silicon ($< 100 >$)	1.29×10^5	130
Nylon 6,6	3.79×10^3 (max)	94.5 (dry)
LD Polyethylene	1.72×10^2	$8.3 - 31.4$
HD Polyethylene	1.08×10^3	$22.1 - 31.0$
Human Bone	1.17×10^4	61.8
Silicone	$0.2 - 1.5$	

Throughout the history of the humankind, ceramics and metals have been the dominant materials for designing and making tools, as both of them are readily available in nature as raw materials and they don't require complex chemical compounds to fabricate or manufacture. Although some polymers, e.g. natural rubber, are found in nature, most of them are fabricated using different chemical compounds and require complex synthesis techniques that were not readily available until recently. Therefore, technological advancements associated with polymeric materials have started to take place only in the last century.

Despite the fact that polymers have begun to flourish as alternative materials much later than metals and ceramics, they have advanced more significantly in a much shorter time. The mechanical properties, lightweight nature, pliability, elasticity, ease of processing and low cost of fabrication have allowed polymers to replace

other materials in a range of applications including robotics. One significant class of polymers, called active polymers, refers to polymer based materials or structures that respond to external stimuli (i.e. pressure, pH, temperature, electricity) by changing their shape or size [8]. Due to their sensitivity to different stimuli, active polymers could readily be used as sensors without needing to integrate more complex digital sensing mechanisms. Active polymers are also lightweight, flexible and resistant to corrosion and thereby offer significant advantages over traditional actuation mechanisms for applications in soft robotics, aerospace, or biomedicine.

Chapter 2

Background

For the last two decades, active polymers have drawn attention from scientists and engineers from different fields due to their unique properties. Amongst these materials, the ones that respond to electricity with a significant change in their size or shape, are referred to as 'electroactive polymers' or 'EAPs'. In 1880, Röntgen observed for the first time that a pre-stretched natural rubber band with a mass attached to its free end could undergo a shape change when it was charged and discharged [9]. However, it wasn't until 2000 when Pelrine et al. [10] reported that approximately 215% actuation could be achieved with acrylic elastomers, that EAPs came into the spotlight for researchers interested in soft robotics.

2.1 Electroactive Polymers

The working principle of electroactive polymers (EAPs) resembles, in a sense, the behaviour of biological muscles. Therefore, since their first development, EAPs have been studied for their potential application as biomimetic artificial muscles. Depending on their activation or response mechanism, EAPs are usually divided into two

Table 2.1: Types of most common electroactive polymers

Electroactive Polymers (EAPs)	
Ionic EAPs	Electronic EAPs
Polymer Gels	Piezoelectric polymers
Ionic Polymer-Metal Composites	Electrostrictive Polymers
Conjugated Polymers	Dielectric Elastomers
Carbon Nanotubes	Carbon Nanotube Aerogels

categories; ionic EAPs and electronic EAPs, as listed in Table 2.1. The physical response in the former type is caused by the diffusion of ions triggered by an electrical current, whereas in the latter, the response is induced by Coulombic forces or the electric field itself. Ionic EAPs can be further sub-divided into the following categories; ionic polymer gels (IPG), ionic polymer metal composites (IPMC), conducting polymers (CP) and carbon nanotubes (CNT) [11]. Some of most commonly used and studied types of electronic EAPs are dielectric EAPs, electrostrictive graft elastomers, electrostrictive paper, electroviscoelastic elastomers, ferroelectric polymers, and liquid crystal elastomers. This study focuses on dielectric electroactive polymers and their use as actuators.

2.1.1 Dielectric Electroactive Polymers

Dielectric electroactive polymers - DEAPs (also referred to as 'dielectric elastomers' - DEs) are a class of electronic EAPs. The physical assembly of a DEAP resembles a capacitor, with a highly elastic dielectric polymer medium between two electrodes. When an electric field is introduced, the conductive parallel plates attract each other due to Coulombic forces between them. The attraction force causes a pressure on the elastic dielectric (known as the Maxwell stress) and deforms the dielectric polymer. Therefore, actuation (compression) occurs in a direction normal to the parallel plates,

as shown in Figure 2.1. In order to conserve volume, the actuator expands in the lateral direction.

A significant drawback of DEAPs is that they typically require a high voltage input, on the order of 3 to 6 kV [8, 12, 13]. The magnitude of the reversible deformation of a DEA device is approximated by

$$\frac{\Delta z}{z_0} = \epsilon_0 \epsilon_r \frac{U^2}{z_0^2 Y} \tag{2.1}$$

where z_0 is the initial dielectric thickness (which is also the initial separation distance between the conductive layers), Δz is the difference between the final thickness (z) and the initial thickness (z_0) of the dielectric, U is the magnitude of applied voltage, Y is Young's modulus of the dielectric layer, ϵ_0 and ϵ_r are permittivity of free space and relative permittivity of the dielectric layer respectively.

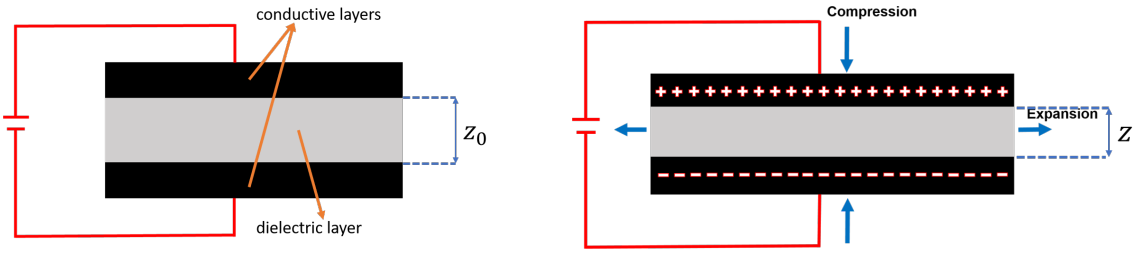

Figure 2.1: Schematic (side view) showing the structure and the actuation mechanism of a simple dielectric elastomer actuator (black layer represents the conductive material, gray is representing the dielectric material). When a voltage threshold is reached, the attraction force between the conductive layers induces a Maxwell stress on the dielectric layer and deforms it in the lateral direction.

The actuation ratio (z/z_0) of a DEAP can be increased by increasing the input voltage, decreasing the elastic modulus of the dielectric or decreasing the distance between the parallel plates. For end applications, such as robotics, it is generally more practical to work with lower operating voltages, thus decreasing the elastic modulus

or the thickness of the dielectric polymer to increase actuation ratios is preferred over increasing the input voltage. Elastic modulus is an intrinsic property, therefore it depends on the material being used in the device. Decreasing the separation distance, on the other hand, can be achieved independent of the material choice. While decreasing the separation distance would increase the actuation ratio, it will diminish the total actuation distance. Thus, alternate approaches would be needed to retain the total actuation distance. One approach would be to fabricate stacked actuator structures comprised of multiple "DEA units" connected in parallel to each other. This way, the total actuation distance would be retained while the applied voltage would be reduced. Therefore, fabricating stacked actuators would be a viable alternative especially at the micro-scale since the total strain and the power output increase with an increasing number of stacked layers [13].

2.2 Literature Review

DEAs offer many advantages over other actuators, such as rapid response rates, high actuation ratios, lightness, and stretchability. An ionic polymer metal composite (IPMC), which is another type of electroactive polymer, takes a few seconds to complete its full range of motion. As it works faster, the actuation ratio (or strain) decreases [14]. Therefore, IPMCs usually work at speeds ranging from 0.1 Hz to 10 Hz. DEAs, on the other hand, can respond to electrical stimulus instantly since they do not rely on ionic transport but electrical conduction. Piezoelectric actuators can provide high actuation forces (100 N to 35 kN) and have rapid response rate (can operate at 50 kHz), but the total strain is usually smaller than 1% [15]. DEAs can deliver much smaller forces but the amount of strain (actuation ratio) can go up to 380% [16].

In recent years, DEA research has focused on overcoming obstacles that limit implementation into real life systems. However, there is still a gap in the field that, if resolved, could change the way soft actuators are used and could proliferate the integration of DEAs in a panoply of applications, which is the fabrication of micro-sized DEAs. A micro-sized DEA could potentially be used in micro-optical systems, robotic devices for aerospace applications, bio-medical devices, micro-robots, micro-pumps/valves, micro-fluidic systems.

To date, DEAP actuators have not transitioned from the experimental stage to a user end product. Most studies in the literature investigate DEAs fabricated using surface coating techniques like spray coating [17], brushing [13] or flame-spray pyrolysis [18], where the conductive coating is applied on a pre-strained dielectric membrane. A pre-strained dielectric membrane returns to its original position when the stress is relieved and the conductive layer on the dielectric crumples due to contraction of the dielectric substrate underneath. This provides conductivity at the high strain ratios seen with DEAs. It has been also reported that pre-stretching the polymer enhances the performance of DEAs [10]. Pelrine et al. reported that pre-straining the dielectric layer of a silicone based DEA increased the actuation ratio from 30 - 40% range to up to 117% [10].

Although introducing pre-strain during fabrication of a DEA enhances its performance, it is not a desirable step to include in the fabrication process. For stacked actuators, the extra time needed to perform pre-strain of each DEA layer would add up to a significant amount of fabrication time for large volume productions. Furthermore, it eliminates the possibility of fabrication of all DEA layers simultaneously, and of fabrication of micro-sized DEAs, since pre-strain has to be introduced to each layer separately while applying the conductive coating. Therefore, eliminating the

pre-strain in the fabrication process and possibly fabricating all layers of a DEA at the same time would be desirable for large volume production of both stacked and single layer actuators, and possibly micro-sized DEAP actuators.

2.2.1 Material Selection for Dielectric Layer

As with all devices, material choice is a key element for fabricating an efficient, stable and durable dielectric elastomer actuator. There are two main components of a DEA that need to be investigated and improved upon in order to meet the requirements, namely the dielectric and conductive layers. The choice of materials for these layers has been the subject of numerous studies in the literature.

One of the essential properties of a DE actuator is its ability to return to its initial state once the stimulus is removed. Therefore, the materials that make up a DEA should be fully elastic in their working ranges. Since the dielectric layer of a DEA is the layer that undergoes most of the physical deformation and stress, its flexibility and elasticity highly impacts the overall performance of the DE actuator.

As Eq. 2.9 indicates, the total actuation of a DE actuator is inversely proportional to the Young's modulus of the dielectric material of the DEA. Therefore, ideally, the Young's modulus of the dielectric material should be as low as possible. However, it should still have high enough strength to be able to provide high force output and withstand heavy loads without going into the plastic deformation regime or reaching catastrophic failure.

In the literature, one of the most commonly studied materials for DEAs is the commercially available 3M^{TM} VHB^{TM} tape [12, 19, 20, 21, 22]. VHB tape is a good candidate for a DEA device in terms of cost, accessibility and ease of fabrication. Large strains (>100%) can be obtained with DEAs made of prestreched VHB tape

for the dielectric layers coated with carbon based electrodes [20, 21]. However, since the thickness of the VHB layer is usually predefined and large [23], the operating voltage is usually in the 3-5 kV range for these actuators. Furthermore, since VHB tape shows viscoelastic behaviour under stress, the actuation cannot be reversed as quickly as some other polymers with negligible viscoelastic behaviour, such as silicones or polyurethanes.

Table 2.2: Physical properties of one-part RTV PDMS (Dow-Corning 732) [24]

Property	Value	Units	Conditions
Density ρ	0.970	$g\,cm^{-3}$	1000 - 12500 cs
Thermal Expansion Coefficient α	9.07×10^{-4}	K^{-1}	$M_v = 1 \times 10^5$ at 25°C
Tensile Strength	2.24	MPa	ASTM D 412
Elongation	550	%	ASTM D 412
Dielectric Strength	21.7	$kV mm^{-1}$	ASTM D 149
Dielectric Constant ϵ	2.8	-	ASTM D 150, at 100Hz
Volume Resistivity	1.5×10^{15}	$\Omega\,cm$	ASTM D 257
Modulus of Elasticity	$0.1 - 3.5$	MPa	ASTM D638

One of the best candidates for the dielectric layer of a DEA is polydimethylsiloxanes (PDMS). PDMS is a commonly studied polymer, especially for biomedical and microfluidic applications due to its biocompatibility and ease of fabrication [25, 26, 27]. PDMS is a siloxane based viscoelastic polymer, but can be solidified using a curing agent and turned into a non-viscoelastic, solid, transparent, flexible and stretchable polymer. Its elasticity, dielectric constant, and some other mechanical characteristics can be modified by changing the amount of the cross-linker agent and the curing temperature [28, 29]. Some of the mechanical properties of commercially available PDMS (Sylgard 184) are given in Table 2.2. The mechanical properties of human tissues are much more similar to PDMS than they are to the metal alloys that are used in traditional robotic devices. Therefore, from a mechanical perspective, it is

much safer for humans to interact with PDMS based DEAs compared to metal-based actuators.

Polyurethanes also have similar properties to PDMS and can also be used for DEA fabrication. Polyurethanes have high dielectric constants, hardness values close to that of PDMS, good mechanical compliance and they can be mixed with conductive particles to form conductive elastic composites [30, 31, 32]. However, especially at high temperatures, PDMS is mechanically and electrically more stable compared to thermoplastic urethanes and the process for fabricating conductive composites is more straightforward compared to urethanes [30, 31, 33].

2.2.2 Material Selection for Conductive Layers

The conductive layer of a DEA structure does not do any physical work while the device is actuating, however it is at least as important as the dielectric layer for the device performance. There are two crucial parameters for the conductive layer: compliance and adherence. Both of these parameters are directly related to the dielectric layer of the DEA, therefore while selecting or designing the materials for a DEA device, the dielectric and conductive layers have to be engineered simultaneously.

Traditionally, conductive layers of electroactive polymers were made of metal thin-films using technologies borrowed from the microelectronics industry, like electron beam evaporation, electroplating, or photolithographic processes [22, 34]. However, having a metal electrode has a few disadvantages. The main drawback is that metals have much higher Young's modulus values than polymers which hinder the full actuation strain range of the polymer based actuators. Also metals, even though they are fabricated as thin-films, have an elasticity range of only about 2-3% whereas for polymers this range can go up to more than 300% [12, 21, 35]. Therefore, metal elec-

trodes break or crack when the actuator is stretched or compressed. Although there are ongoing studies focused on adhering metal electrodes to DEAPs as patterned layers of thin films or corrugated membranes, a more favorable choice is carbon based powders for electrodes [20].

Carbon powders (e.g. carbon black, graphite) are preferred as conductive materials since they maintain conductivity at high strains and they do not significantly affect the stiffness of the device [21]. The powders can be applied onto a polymer sheet usually by brushing or spraying the powder onto the polymer surface. Both the raw material and the fabrication costs of carbon based electrodes are lower than those of metals. However, at high strains, carbon particles can get detached from the polymer due to poor adherence between the two materials.

One approach to overcome this problem is to use carbon based or metal based nano-particles as additives in a polymer matrix to form a conductive polymer composite. There are many alternative conductive fillers to use for making conductive polymer composites. However, a DEAP requires maintaining good conductivity while the composite is stretched even by a few hundred percent. Therefore, while using spherical nano-particles there may be discontinuities within the conductive path along the composite. Overcoming this problem requires high conductive filler content, which affects the mechanical properties of the polymer negatively. This study will investigate various candidate materials and try to optimize the electronic properties with mechanical properties for the conductive layer of a DEAP actuator.

2.2.3 Governing Theory and Voltage Requirements of DEAs

The voltage requirement for actuation of a DEA depends on the distance between the conductive layers, relative permittivity of the dielectric material, and the elastic

modulus of the materials. For a typical DEA, the operating voltage is in the range of 3 to 6 kV. When an voltage V is applied across the conductive parallel plates, each conductive plate obtains a charge Q (either +Q or -Q depending on the polarity). If the surface area of each plate is A, then the surface charge density is given by $\sigma = |Q/A|$. The magnitude of the electric field (E) produced by one of the plates is given in Equation 2.2.

$$E = \frac{\sigma}{2\epsilon_0} = \frac{Q}{2A\epsilon_0} \tag{2.2}$$

Since there are two conductive plates, the total electric field is $E_{total} = 2 \times E$. The potential difference is

$$V = E_{total}d = d\frac{Q}{A\epsilon_o} \tag{2.3}$$

Solving Eq. 2.3 for Q yields:

$$Q = A\epsilon_o\frac{V}{d} \tag{2.4}$$

The Coulombic attraction force (F) exerted on one plate is equal to the charge of that plate times the electric field created by the plates, thus, $F = QE_{total}$. Combining Eq. 2.2 and 2.4 yields

$$F = QE_{total} = A\epsilon_o\frac{V}{d}\frac{Q}{A\epsilon_o} = A\epsilon_o\frac{V}{d}\frac{A\epsilon_o V}{dA\epsilon_o} \tag{2.5}$$

or

$$F = A\epsilon_o \frac{V^2}{d^2} \tag{2.6}$$

As equation 2.6 indicates, the attraction force between the conducting parallel plates is directly related to the square of the applied voltage and inversely related to the distance of separation. Eq. 2.6 assumes that the parallel plates are separated by distance d, however the space between them is empty. In a DEA system, the volume between the plates is filled with a dielectric material and this affects the attraction force between the plates. An additional dielectric constant, ϵ_r is needed, thus Equation 2.6 becomes:

$$F = A\epsilon_o\epsilon_r \frac{V^2}{d^2} \tag{2.7}$$

The attraction force can be converted to the electrostatic pressure (P) applied on the actuator due to the applied voltage by dividing by the surface area of the DEA.

$$P = \epsilon_o\epsilon_r \frac{V^2}{d^2} \tag{2.8}$$

Electrostatic pressure is the stress applied on the dielectric layer of the DEA as a result of the Coulomb forces between the parallel plates caused by the potential difference introduced on the plates. If the Young's modulus of the dielectric material is known, the amount of theoretical actuation ratio of the DEA is

$$\frac{\Delta z}{d} = P/Y = \epsilon_o\epsilon_r \frac{V^2}{Yd^2} \tag{2.9}$$

where Y is Young's modulus of the dielectric material, Δz is the total displacement in the actuation direction.

As equation 2.9 indicates, the actuation ratio of a DEA depends on Young's modulus of the DEA, the dielectric constant of the DEA, the applied voltage, and the distance between the parallel plates. Increasing the efficiency of a DEA means decreasing the applied voltage or increasing the actuation ratio, preferably at the same time. One of the aims of this study is to develop a fabrication technique that will allow the distance of separation of conductive layers to be optimized for high efficiency while maintaining good mechanical properties and retaining the total actuation distance.

2.2.4 Actuation Direction of DEAs

Dielectric elastomers contract in one direction while expanding in the other two directions to conserve volume. Due to this geometric constraint associated with the actuation mechanism, it is not possible to change the actuation direction solely by changing the electrical input into the system. The only way to achieve a different actuation is by designing the DEA in a specific way that will produce the desired actuation direction. This means that for each actuation required in a different direction, a different DEA has to be designed and integrated into the system.

For example, bending motions can be achieved by increasing the conductive layer thickness on one side, thus providing extra stress to cause a bending motion when the device tries to expand in the lateral direction. However, it is not possible to change this behavior while the device is in operation in a device since it requires replacement with a different actuator with a different configuration. If two different motions are required in a system, two DEA devices would have to be implemented. Multiple actuators would increase the total cost, require more space, add extra weight to the system and make it less practical to use or integrate into larger systems. Therefore, having more control over the actuation direction and achieving actuation in more

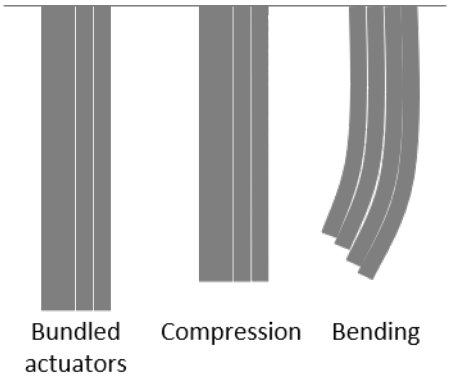

Figure 2.2: Individual DEAs in a bundled DEA structure can be actuated selectively to achieve an actuation in any desired direction.

than one direction only by manipulating the input voltage is an important property that would render DEAs significantly more practical in many applications.

Bundling DEAs together to form larger and more complex actuation systems would enable different actuation mechanisms and actuation in multiple directions within a single actuator system, as shown in Figure 2.2. Actuation direction could be controlled only by modifying the electrical input and stimulating specific actuators without needing to fabricate custom actuators for every application. The multilayer actuator design introduced in this study aims to provide a linear actuator structure, with a fiber-like geometry, that would allow bundling on multiple actuator fibers to create a larger actuator.

2.2.5 Micro-scale Multilayer DEAs

As previously described, several obstacles were encountered when manually fabricating stacked DEAs. Ideally, fabricating all layers of a stacked DEA structure simultaneously would decrease the fabrication time while eliminating the need for an additional adhesive and avoid the inconsistencies associated with the manual fabrication process.

Conventional microfabrication methods allow fabrication of interdigitated electrodes for MEMS devices that resemble the parallel plates on a multilayer stacked DE actuator, where the whole structure is fabricated at the same time. The same fabrication process could be potentially applied to DEA devices to fabricate miniaturized DEAs. However, microfabrication of soft polymers is not trivial since most microfabrication processes are designed for rigid substrates that can have relatively high aspect ratios.

Miniaturizing DEAs could theoretically decrease the operating voltages down to the sub-kV range [36]. However, even at the micro-scale, conventional single layer DEAs face challenges both during fabrication and while in operation. Circular designs, like their macro-sized designs, need a rigid frame to operate as illustrated in Figure 2.3. Furthermore, fabrication of such a structure requires selective etching from the bottom of the substrate to form the required space underneath the actuator [36]. Cantilever designs are easier to fabricate, however, they face another problem. Since the suspended part of the DEA is not rigid, it collapses over the substrate and sticks to the surface making the actuator inoperable [36].

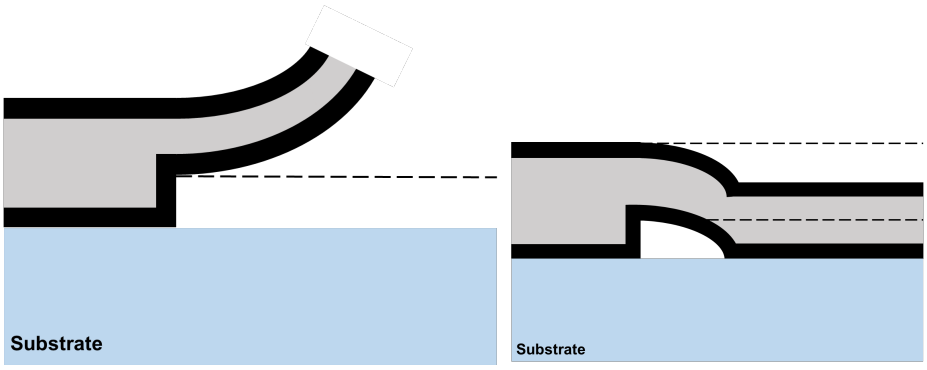

Figure 2.3: Schematics of cantilever type micro-sized DEAP actuators. Soft actuators require a rigid substrate for support. If the cantilever actuator sticks to the substrate due to its own weight, it becomes dysfunctional.

Stacked DEAs could overcome the operational obstacles associated with circular

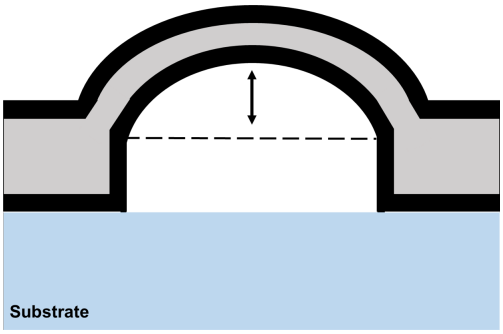

Figure 2.4: Schematic of a dome-shaped micro-sized DEAP actuator.

or cantilever designs since the actuation mechanism does not depend on a rigid substrate and the actuation direction could be translated to be parallel to the length of the actuator (i.e. linear actuation), as opposed to lateral area expansion of the circular actuators or the bending motion of cantilever type actuators. Miniaturized DE stacked actuators were fabricated by Lotz et al [37] in 2011. They showed up to 20% actuation with the stacked design. Spin-coating was used by Lotz et al. [37] to form the dielectric films. Electrodes were deposited by spraying a mixture of graphite powder and isopropanol through a mask onto the dielectric layer. However, this bottom-up approach still required fabrication of each layer one-by-one on top of each other, which poses a problem for high capacity production. Fabricating all layers in a single step would decrease the fabrication time drastically and likely increase uniformity. If one micro-sized stacked actuator consisted of 100 layers, fabricating all layers simultaneously would mean decreasing the fabrication time by a factor of 100.

There have been studies focusing on miniaturization of DEAs using different approaches [36, 38, 39, 40, 41, 42]. Dubois et al. introduced an ion implantation based fabrication method for a membrane type DEA and reported an out-of-plane displacement of 13% at around 1.2 - 1.3 kV [38]. At 13%, the total actuation distance is about 120 μm. This can be a significant amount of deflection for MEMS applications, how-

ever, it is not practical for larger scale applications. Gerratt et al. introduced a fabrication method for a miniaturized cantilever type bidirectional DEA on silicon wafer using deep reactive ion etch for patterning [39]. They have reported significant bending displacement at voltage lower than 1 kV. The total length and width of the fabricated actuator are reported to range from 2 μmu to several millimeters with a depth of 5 μm to 300 μm. The actuator is a cantilever type actuator and can achieve bidirectional actuation, although only in the form of bending motion.

In 2015, Poulin et al. printed a DEA with a 3 μm dielectric membrane and reported 7.5% strain at 245 V [40]. The printed actuators were circular in shape and the actuation occured as lateral expansion (increase in the surface area). They have reported that there is a significant stiffening effect when the dielectric membranes are fabricated thinner. When they compared two actuators with 30 μm and 3 μm dielectric layer thicknesses, they reported a maximum actuation of 14.2% with the 30 μm actuator whereas the 3 μm actuator was limited with 7.5%. However, the thinner actuator also required 10 times lower voltage to operate. In 2017, McCoul et al. improved the same method to allow inkjet 3D printing of UV curable DEAs [42]. The maximum lateral strain (surface area increase) was reported to be 6.1% with 11 μm and 4.7% with 3.3 μm dielectric thickness. The reported actuation voltages are significantly low and promising for practical low voltage applications, however actuation in the form of surface area increase is limited to some specific applications and not very useful for mechanical force generation.

Xiaobin et al. introduced prestretch for micro-fabricated DEAs to increase the actuation ratio and reported about 4% strain at 100 V [43]. They fabricated an actuator with 1.4 μm pre-stretched PDMS membrane coated with stretchable MWCNT/P3DT composite monolayer electrodes.

These studies provide unique contributions for miniaturization of DEAs and reducing the operating voltage of DEAs to sub-kV range. However, all the fabricated DEAs using these methods rely on rigid substrates to work, allow fabrication of single layer or trilayer actuators, provide actuation in micrometer range, output small forces and cannot be scaled up to fabricate larger actuators.

2.2.6 Modeling of Micro-Scale Multilayer DEAs

As explained in Section 2.2.3, the electrostatic pressure causes the mechanical deflection of DEAs and the magnitude of the deflection can be calculated using Equation 2.9. Although this simple model is sufficient to provide a rough estimate of the magnitude of the actuation, it is not an efficient approach for studying a multilayer DEA with a complex geometry.

There have been many studies in the literature focused on the modeling of DEAs with different materials and configurations using various approaches and finite element analysis tools. Wissler et al. simulated the actuation of a pre-strained VHB tape based circular single layer DEA through a finite element model supported by experimental results [44, 45]. Tepel et al. studied the effect of passive surface area in the multilayer configuration and the bulging mechanism due to the constraint introduced by the end caps [46]. Haus et al. proposed a mechanical and electrical model for a PDMS based stack DEA, accounting for the contact resistance of electrical interconnections between DEA layers [47]. Recently, Zhang et al. studied the modeling of DEAs using higher order material characteristics [48]. These studies and many others study the effect of different electrical and mechanical properties, different configurations on actuation of DEAs and improve the numerical models to obtain more accurate simulation data.

2.3 Gaps in the Literature

Dielectric elastomer actuators are promising devices with the potential for many applications in research and industry. There are some major obstacles preventing DEAs from flourishing. One of them is the high voltage requirement. The DEAs fabricated through conventional fabrication approaches usually work in the range of 3 - 6 kV. There have been studies focused on the fabrication of DEAs in micro-scale [36, 38, 39, 40, 41, 42], explained in Section 2.2.3. Although these microfabrication appproaches can reduce the operating voltage down to sub-kV level, the problem with the microfabricated DEAs is that they designed to work in microscale and cannot be scaled up for macroscale application needs. In addition, the conventional DEA structure provides an expansion motion, which is not ideal with a flexible actuator body since it is prone to bending easily. Stacked or multilayer DEAs can help to increase the actuation distance and force, and provide a compressive actuation motion that is more preferable for a soft actuator body. The current microfabrication methods are not designed to allow stacking of many DEA layers.

The conventional materials used for the fabrication of DEAs are also not ideal for microfabrication of DEAs and are not very robust. Carbon based coatings or metal fillers provide good conductivity but sacrifice mechanical integrity due to poor bonding between the conductive coating and the polymer base or the difference in elasticity of the two materials.

Section 2.2.5 examplifies some of the fabrication approaches that have been studied so far to overcome these obstacles. However, there are still gaps in the literature that could help transition DEAs from experimental devices to practical tools. Figure 2.5 depicts the gap that this study aims to address. Combining the existing literature on stacked DEAs, PDMS microstructures and conductive elastomers, it could be possible

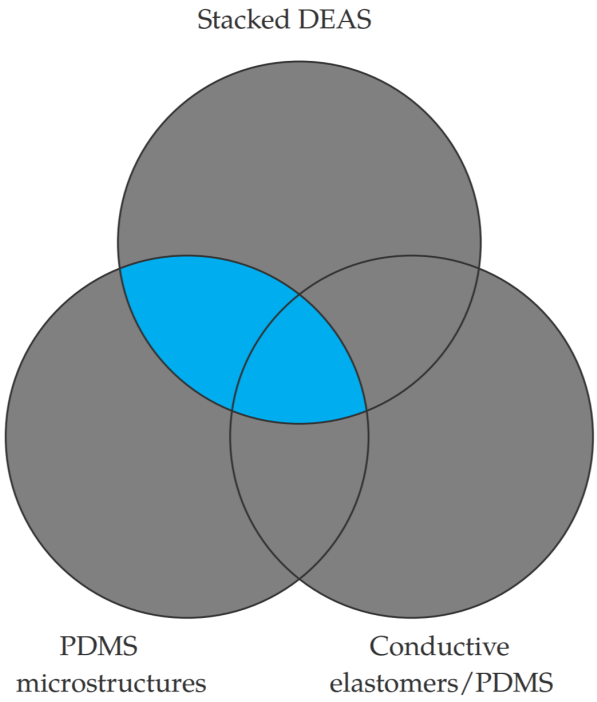

Figure 2.5: The Venn diagram depicts the gaps this study aims to address. Existing literature is shown with gray and the current gaps in the field are shown with blue.

to advance the fabrication of DEAs.

This study investigates the possibility of using conventional microfabrication tools to fabricate multilayer DEAs comprised of micro-sized DEA layers that would work in the sub-kV range with a linear actuation mechanism. This multi-layer DEA:

- can be used as artificial muscles for soft robotics,
- can be scaled up (or down) according to the application needs,
- do not rely on support structures or rigid frames to operate,
- provide a linear actuation mechanism that can be directed to actuate at different angles.

2.3.1 Research Objectives

In order to achieve these goals, the objectives of this study are detailed as follows:

1. Identify and characterize the candidate materials for microfabrication of DEAs:
   Through the prior literature review, CNT/PDMS composite and PDMS were determined as candidate materials for conductive and dielectric materials respectively. The effect of fabrication parameters on the mechanical properties of PDMS and the effect of CNT content in CNT/PDMS composite on electrical and mechanical properties of the composite material were characterized.

2. Fabricate proof of concept DEAs with selected materials:
   Multilayer dielectric elastomer actuators were fabricated using the selected and characterized dielectric and conductive polymers. Fabrication of the devices was done at the macro-scale using conventional fabrication techniques to evaluate the feasibility of using the candidate materials for the fabrication of multilayer DEAs.

3. Develop a micro-scale DEA design that will decrease the actuation voltage range to sub-kV:
   Microfabrication of stacked DEAs, with interdigitated conductive layers, addresses two different gaps. The stacked design enables fabrication of micro-sized actuators that can be scaled up or down and can be used in a variety of applications requiring linear actuation. Microfabrication provides a low voltage input for DEAs by decreasing the separation distance of the conductive parallel plates.

4. Develop and optimize the fabrication method for the micro-scale DEA design:
   Possible fabrication tools and methods were investigated. Three different fab-

rication methods were used to fabricated the micro-sized actuators with the multi-layer design. The repeatibility of the fabrication processes was evaluated.

5. Use numerical simulations to optimize the actuator configuration:

   The fabricated actuators were modeled using multiphysics simulation software. The effect of different design parameters was studied to find the optimum configuration for the multilayer DEAs.

Chapter 3

Materials and Methods

3.1 Characterization of the Materials

The first objective of this study was determined as identifying and characterizing the candidate materials for the microfabrication of DEAs. Based on previous studies in the literature, PDMS was identified as a potential candidate to use a the dielectric material in DEAs due to its pot life, mechanical stability at a wide range of operating temperature, ease of fabrication and biocompatibility, as explained in Section 2.2.1. The mechanical properties of PDMS can change depending on the fabrication parameters and can be fine tuned to meet the requirements. Therefore, the effect of fabrication parameters on the mechanical and electrical properties of PDMS needed to be characterized in order to understand the effects on DEA performance.

3.1.1 Dielectric Material

Section 2.2.3 explains the mechanism behind the actuation of a DE actuator and the parameters that affect the theoretical actuation ratio. The dielectic constant and

Young's modulus are intrinsic properties of any given material. They do not depend on the volume or the shape of the material but can be changed by changing the material composition (by adding fillers/impurities). As mentioned in section 2.2.1, PDMS is a polymer that has a tunable Young's modulus and dielectric constant. By decreasing the amount of curing (or crosslinking) agent, the Young's modulus can be decreased, which results in a more flexible and softer polymer.

Previous studies by Johnston et al. [28] showed that curing temperature can also have a high impact on the properties of PDMS. Table 3.1 shows the Young's modulus of PDMS increases with increasing curing temperature. The ultimate tensile strength however, seems to have an optimum range, as it increases first and then decreases with increasing temperature. According to Table 3.1, 125°C seems to be the best curing temperature to provide a high ultimate tensile strength to PDMS. However, to provide a high actuation ratio, the Young's modulus needs to be small, therefore, lower curing temperatures are more preferable. Depending on application needs, curing temperature can be optimized to balance stiffness with strength.

Table 3.1: Tensile test results of Sylgard 184 PDMS at different curing temperatures by Johnston et al. [28]

Curing Temperature (°C)	Young's Modulus (MPa)	Ultimate Tensile Strength (MPa)
25	1.32	5.13
100	2.05	6.25
125	2.46	7.65
150	2.59	5.24
200	2.97	3.51

In this study, the effects of curing temperature, curing time and the amount of curing agent on elastic modulus of PDMS were investigated. Commercially available Dow Corning Sylgard 184 (Midland, MI) was used to fabricate dog-bone shaped tensile test specimens following the ASTM D638 standard [49]. Tensile test specimens

were prepared to assess the effect of curing agent ratio (Test 1) and the effect of curing time and temperature (Test 2) on the stress-strain behaviour of PDMS.

Sylgard 184 PDMS base (Part A) was mixed with the PDMS curing agent (Part B) at 5:1, 10:1 and 15:1 ratios for Test 1, 10:1 ratio for Test 2 by adding Part B to Part A. The viscous mixture was degassed in a vacuum chamber for 20 minutes. The mixture was poured into the dog-bone shaped aluminum molds with the dimensions specified by the ASTM D638 standard [49]. Any excess PDMS was removed from the molds by sweeping them with a stainless steel film applicator blade. The molded mixture was left at room temperature for 15 minutes to allow the mixture to settle into the molds and form a uniform shape. They were placed in the oven and cured for 35 minutes at 95°C for Test 1, and 10, 20, 35, and 60 minutes at 100°C and 150°C for Test 2 (as shown in Figure 3.2).

The specimens were tested using an Instron 1125 Load Frame with MTS SinTech ReNew system (MTS, Eden Prairie, MN). As shown in Figure 3.1, as the ratio of curing agent to the PDMS base (part A) is increased, the elastic modulus of the PDMS is increased. It is observed that the change in the slope of the stress-strain curve is more drastic when the curing agent amount is lowered in the mixture, compared to when the curing agent amount is higher than the recommended amount. This is because the recommended 10:1 base to curing agent ratio provides enough crosslinker so that the polymer is fully polymerized. When the amount of the curing agent is increased above the recommended amount, it does not affect the crosslinking process significantly and therefore the change in the elastic modulus of crosslinked PDMS is negligible.

Curing time and temperature also impact the mechanical properties of PDMS. Figure 3.2 shows how Sylgard 184 behaves under tension when the curing temperature

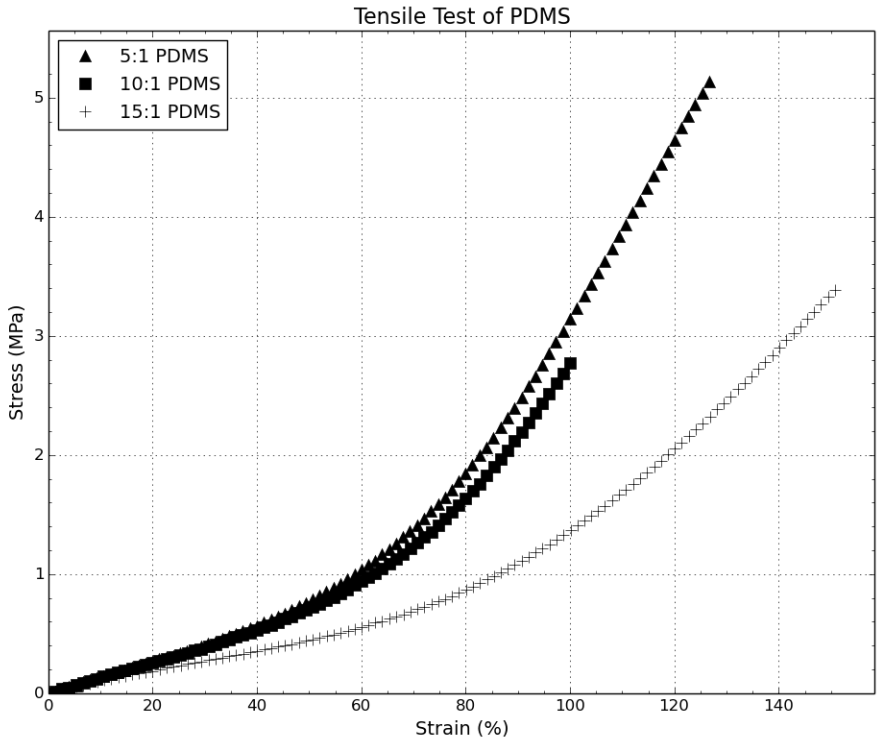

Figure 3.1: Static tensile test results of Sylgard 184 with different curing agent (Part B) content. The ratio indicates the weight ratio of the Sylgard 184 base to the curing agent. As the curing agent content is decreased, the elastic modulus of the PDMS is decreasing.

is held constant at 150°C and the curing time is changed between 10 minutes and 60 minutes. In Figure 3, two different curing temperatures are also compared, namely 100°C and 150°C while the time is held constant at 20 minutes. It is observed that as the curing time decreases, at the same temperature, the elastic modulus of the PDMS specimen goes down. Similarly, as the temperature decreased from 150°C to 100°C, the slope of the curve also decreased. The findings are consistent with those presented by Johnston et al. [28].

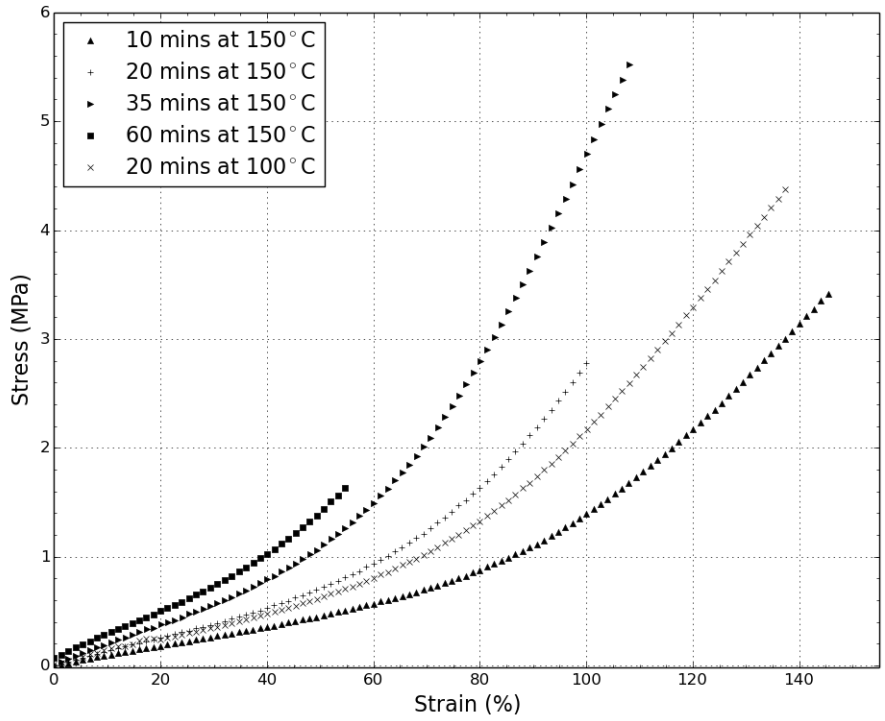

Figure 3.2: Engineering stress vs engineering strain plot of Sylgard 184 with 10:1 base:curing agent ratio cured at 100°C and 150°C for different durations.

3.1.2 Conductive Electrode Material Selection

The conductive layer of a DEA needs to be mechanically compliant with the dielectric polymer, needs to keep its conductivity when strained, and should have good adhesion with the dielectric material. One approach to fulfill these requirements is to use a conductive polymer composite. As preliminary work, carbon black and carbon grease were studied to fabricate a conductive composite. Different compositions of carbon black with PDMS and carbon grease with PDMS were studied to investigate the conductivity, mechanical stability and homogeneity of the composites. It was observed for both composites that high volume fractions of carbon filler were required to achieve good conductivity, i.e. to reach percolation threshold. At high volume concentrations

of conductive filler, polymer composites face issues of crumbling and cracking (Figure 3.3) while curing the polymer since there is not enough polymer content to provide a stable polymer matrix for the composite.

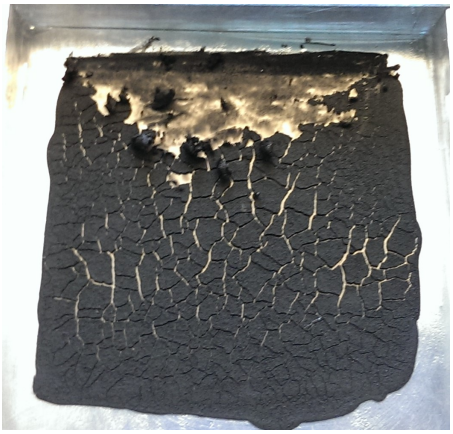

Figure 3.3: Carbon grease polymer composite. After evaporation of the solvent, high carbon grease content caused cracks on the surface.

An alternate material for a compliant stretchable electrode is a composite of carbon nanotubes and polydimethylsiloxane (CNT/PDMS). Carbon nanotubes are a special type of carbon structure that has been observed to have extraordinary electrical and mechanical properties [50]. Since their length/width ratio is significantly larger than spherical nanoparticles, they can sustain the electrical pathway intact in a polymer matrix at much larger strain ranges. Another option to consider as a conductive filler is silver nano-particles. Silver nano-particle - polymer composite systems have been studied in the literature for stretchable electronics [30, 51, 52, 53]. Although silver is a highly conductive material, in order to achieve the same level of conductivity that 1 vol% multi-walled CNT provides in PDMS, about 20 vol% silver nano-particles are needed [51, 52, 54]. High amount of fillers in polymer matrix affects the mechanical properties of the polymer and using silver nanoparticles in large amounts is not cost effective.

CNT/PDMS composites have been investigated in the literature recently, for providing a flexible conductive pathway usually for wearable devices and bio-medical applications [54, 55]. CNT/PDMS composites are reported to reach percolation threshold at lower filler concentrations and achieve higher conductivity compared to other carbon filled polymer composites [55]. In Figure 3.4, percolation threshold concentration for MWCNT/PDMS composite can be estimated as 1 vol%. Conductivity of the composite at 1 vol% MWCNT content is in the range of 1 - 10 S/m.

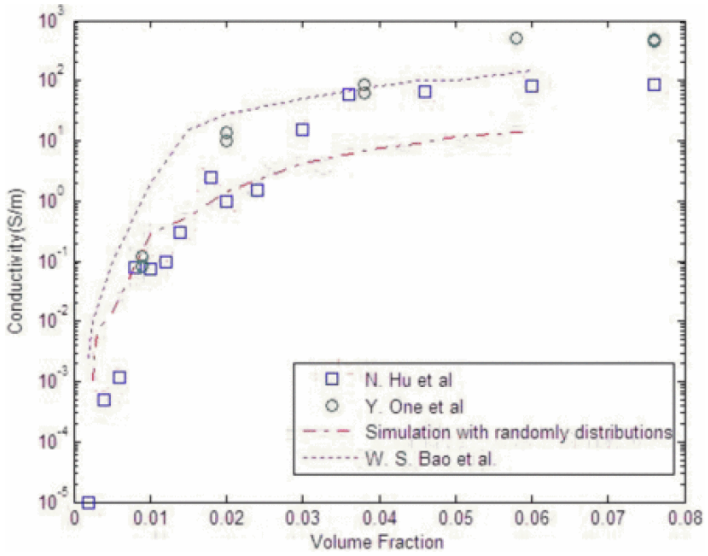

Figure 3.4: Conductivity of MWCNT/PDMS composite depending on volume fraction of randomly distributed MWCNT in the composite. From Ref. [56]

One obstacle when fabricating CNT/PDMS composites is the homogeneity of the CNT distribution in the polymer matrix. Dispersion of carbon nanotubes is rather difficult and different than conventional fillers, like carbon or metal based spherical nano-particles, because of their structure with small diameter (a few nanometers to micrometers), high aspect ratio (> 1000), and low density (about $1.8 g/cm^3$ compared with $4.0 g/cm^3$ density of Al_2O_3) [57]. Due their high surface area and high aspect ratio, CNTs come in heavy entangled bundles which makes their dispersion even more

challenging.

There are several ways to fabricate CNT/polymer composites, including in situ polymerization, solution mixing, chemical modification processes [58]. The conventional method is to use the solution mixing process, which includes dispersion of CNTs in a solvent medium, mixing CNTs with the polymer and evaporating the solvent. However, the solvents used in the process (toluene or chloroform) are hazardous chemicals that can be absorbed into the polymer and may still be present in the polymer in small amounts even after evaporation. Ideally, hazardous solvents should be eliminated from the mixing process.

Optimization of CNT/PDMS Solution Parameters

Dispersion of CNTs in a solvent medium requires a mixing mechanism, such as shear mixing or sonication, to supply an energy to the mixture that is going to overcome the binding energy of the CNT agglomerates. However, the energy delivered by the mixing mechanism to the solution should not exceed the amount required to fracture a nanotube [57, 59]. Therefore, no matter which mixing mechanism is used, energy density (magnitude of energy per volume) must be optimized between the binding energy of the CNT aggregates and fracture resistance of nanotubes.

As explained by Huang et al, ultrasonication and shear mixing provide two entirely different mechanisms for dispersion of CNT aggregates [59]. In ultrasonication, above a certain ultrasonic intensity, cavitation bubbles form. When the cavitation bubbles implode, they create regions with high strain rates within the fluid that can disperse the agglomerated CNT bundles. The distribution of the cavities is not homogeneous and depends on the sonicator geometry and sonication settings. One limitation with ultrasonication is that ultrasound absorption increases with viscosity. Therefore, in

fluids with high viscosities (like uncross-linked PDMS solution), the efficiency of sonication diminishes significantly. Shear mixing can be applicable for both low viscosity and high viscosity media, however, it is more efficient in high viscosity systems. The magnitude of shear stress (σ_s) exerted on the particles in the fluid is defined as the product of the viscosity (η) of the fluid and the fluid strain rate ($\dot{\gamma}$). As the viscosity of the fluid increases, shear stress also increases. In low viscosity fluids (like water, toluene, chloroform), shear stress delivered to CNT clusters goes down to lower than 50 Pa [59], which is not enough to disperse the entangled CNTs. In order to disentangle the MWCNT agglomerates and to disperse them in viscous PDMS, a combination of sonication and shear mixing was used. The following procedure was followed for the fabrication of conductive MWCNT/PDMS composite.

MWCNTs were first dispersed in toluene. MWCNTs were measured and added to a glass beaker and were mixed with toluene, enough to cover the MWCNTs. Approximately 20 ml toluene was added for 1 g of MWCNTs. When transfering the dry MWCNTs, it was observed that MWCNTs were affected by the static electricity, tended to fly off and stick to the surrounding surfaces, thus cause contamination of the laboratory equipment. Using a metal spoon for transfer and adding toluene to the glass beaker prior to adding the MWCNTs helped to prevent this problem.

MWCNT/toluene mixture was mixed for an hour using a magnetic stirrer, starting at 700 rpm and ramping up to 1100 rpm. The mixture was sonicated for 20 minutes in a bath sonicator and transferred back to the magnetic stirrer. After mixing for 2 hours at 700 rpm, Sylgard 184 PDMS base was added to the mixture. MWCNT/PDMS/toluene mixture was left on magnetic stirrer at 1100 rpm overnight. The mixture was sonicated for 20 minutes in the bath type sonicator and placed back on the stirrer. The mixing process continued until the toluene evaporated. As the

toluene evaporated, the mixture became more viscous and the stirring speed had to be lowered to 700 rpm.

Conductivity of MWCNT/PDMS composite

In order to measure the conductivity, MWCNT/PDMS mixture was poured into rectangular aluminum molds and degassed in the vacuum chamber for 30 minutes. The mixture was cured in the oven at 80 °C. The solidified MWCNT/PDMS composite was cut into a cuboid. Copper tape electrodes were connected on opposite sides of the cuboid shaped composite material. The resistance value was measured, resistivity and conductivity values were calculated using the dimensions of the composite. The conductivities of the composites were measured to be in the range of 1 - 6 S/m, with an average of 3.35 S/m, which is close to the theoretical conductivity values at these concentrations for randomly oriented CNTs in polymer matrix, as reported by Liu et al in Figure 3.4 [56].

One of the steps for the fabrication of conductive MWCNT/PDMS composites was to evaporate the solvent before adding the crosslinker and curing the polymer. Shortening the evaporation step would significantly reduce the total fabrication time of the conductive polymer. Therefore, for testing the effect of increased mixing temperature on the fabrication process, the MWCNT/toluene/PDMS base mixture was heated to 110°C. The rest of the procedure for fabricating the conductive polymer was not modified. The conductivity specimens were fabricated using the aforementioned aluminum mold. The resistance measurements indicated that the resulting MWCNT/PDMS composite specimens were significantly less conductive compared to the specimens prepared with the original procedure. Table 3.2 shows the effect of mixing temperature, as well as the solvent medium and the CNT content on the

Table 3.2: The effect of solvent and mixing temperature on conductivity of MWCNT/PDMS composite

Solvent	Mixing Temperature (°C)	Average Conductivity (S/m)
Toluene (8% MWCNT)	25	3.35
Toluene (10% MWCNT)	25	6.0
Toluene	110	3.39×10^{-6}
Chloroform	25	
Chloroform	110	not conductive
No solvent	25	not conductive

conductivity of the resulting composite specimens.

In order to obtain better conductivity and reduce the fabrication time, alternative approaches were tested. As shown in Figure 3.5, heating up the mixture, using a planetary mixer without any solvent, using a probe type sonicator did not seem to provide a composite with high enough conductivity to be considered as a candidate material.

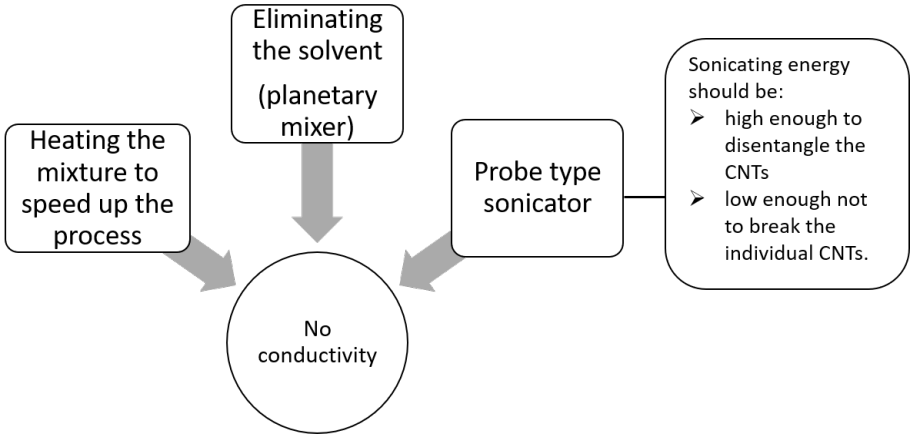

Figure 3.5: Diagram illustrating different attempts to improve conductivity and decreasing the processing time for the conductive composite material.

3.2 Multilayer DEAs

After the dielectric and the conductive materials were characterized and could be fabricated with desired mechanical and electrical properties, the next step was to design a micro-sized DEA to reduce the operating voltage range down to sub-kV level. As explained previously, one way to increase the actuation ratio and decrease the voltage requirement of DEAs is to decrease the distance of separation between the conductive parallel plate layers. However, a decrease in the thickness of the device will decrease the total actuation distance. For example, if one assumes 100 μm for the distance of separation, i.e. thickness of the dielectric layer, and 10% actuation ratio, this will translate to 10 μm of total actuation. If the thickness is decreased by half and is set at 50 μm, from Eq. 2.9, the voltage required to obtain the same actuation ratio would decrease by a multiple of 4 times. However, in this case, the total actuation distance would be 5 μm, i.e. half the original distance. However, if multiple layers of identical DEAs are stacked on top of each other, the actuation distance could be retained while still operating at low voltage, as depicted in Figure 3.6.

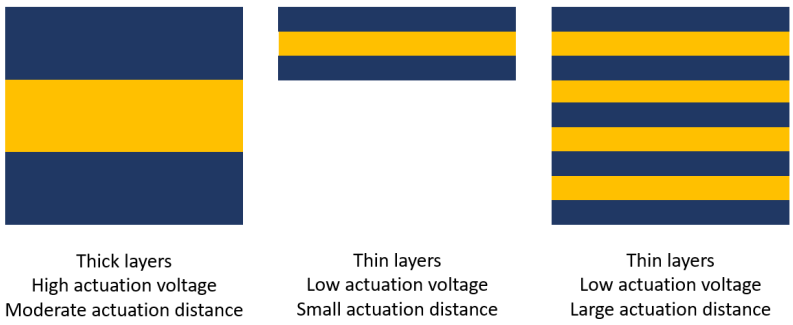

Figure 3.6: Three different DEA models. From left to right: single DEA with thick conductive and dielectric layers, single DEA with thin layers, multilayer DEA with thin layers.

3.2.1 Macro-scale Multilayer DEAs

The second objective of the study was identified as the fabrication of proof of concept DEAs in order to assess the compatibility of the selected materials with the multi-layer DEA structure. In the literature, it has been shown that stacked dielectric elastomer actuators could be fabricated at the macroscale, i.e. with $\approx 2cm$ diameter and 2 to 7 cm total length [13]. Kovacs et al. reported [13] that up to 30% contraction strain could be achieved at 4.2 kV. The main geometrical constraint in the fabricated DEAs was reported to be the active surface area, which is the ratio of the surface area of the conductive parallel plates and the total surface area of the whole structure including the electrical connections that are not contributing to the generated actuation force. As the active surface area decreases, the total actuation ratio diminishes as the passive surface is applying a stress in the opposite direction to the actuation. However, the passive area surrounding the electrodes is necessary to isolate the layers from each other and to prevent dielectric breakdown [13].

As a proof of concept, stacked DEAs at the macroscale were fabricated using the conductive PDMS composite described in Section 3.1.2. All actuators were fabricated on a mechanical grade silicon wafer using the tape casting method with a manual micrometer adjustable film applicator blade. First, the external PDMS layer was cast at 1 mil ($\approx 25.4\mu m$) thickness and cured at 95°C. After curing, a cPDMS layer was cast using an aluminum foil mask to isolate an area on one side required for electrical connection of the counter electrode (next conductive layer) and was cured at the same temperature. The first two steps were repeated, alternating the masking side at each conductive layer, until the desired number of layers were reached. The schematic in Figure 3.7 shows a cross-sectional cut of the stacked DEA structure with the alternating conductive layers on each side.

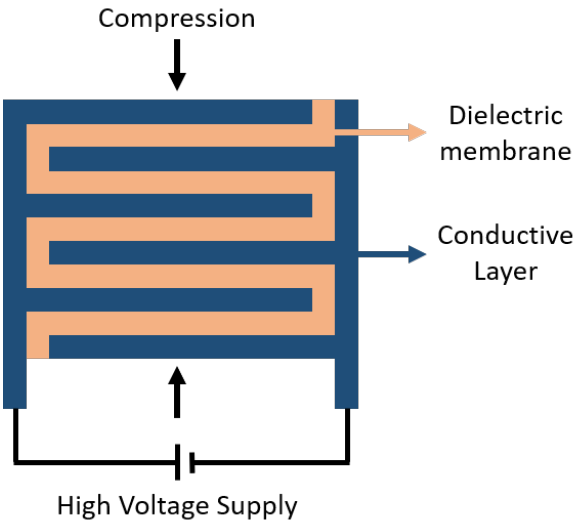

Figure 3.7: Cross sectional view of the stacked DEA structure. Interdigitated conductive layers are isolated from each other by the serpentine shaped dielectric material between. On each side, alternating conductive layers are interconnected and attached to a power source. The actuator is compressed in the perpendicular direction (indicated by the arrows) when a voltage is applied and expands in the lateral direction.

The same procedure was followed to fabricate stacked actuators with dielectric layer thicknesses of 1 mil, 2mils, and 3 mils. Figure 3.8 shows one of the macroscale stacked actuators after fabrication, before attaching the electrical connections for testing. Fig. 3.9 represents an SEM image of a cross-sectional area of another sample of the same stacked multilayer structure and a more detailed image of the conductive CNT/PDMS composite layer.

In order to better highlight the carbon nanotube content and distribution in PDMS, the cross-sectional microscope image was modified in ImageJ. In Figure 3.10, darker portions of the image represent the PDMS layers and the lighter particles show the carbon nanotube distribution in the CNT/PDMS composite.

Actuation tests were performed in order to compare the actuation ratio with varying layer thickness. As shown in Fig. 3.11, with decreasing layer thickness, the

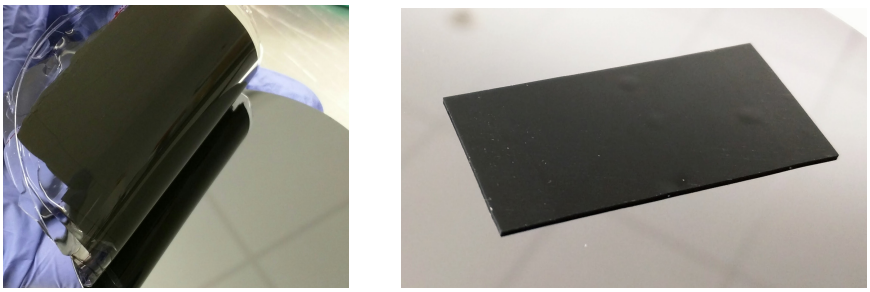

Figure 3.8: Stacked DEAP actuators fabricated on silicon wafer. Left: Peeling off from the wafer after fabrication. Right: Final shape of the actuator before electrical connections.

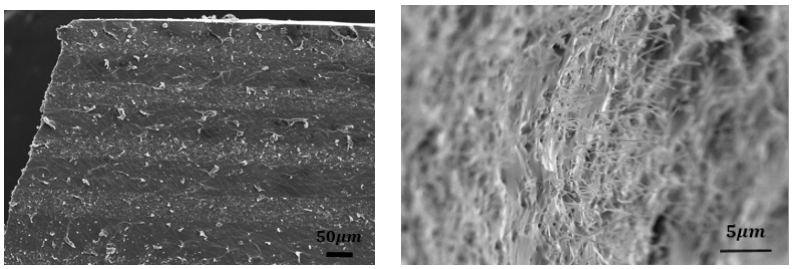

Figure 3.9: Left: SEM image of a cross-sectional area of a stacked DEA sample. Right: Detailed SEM image of a MWCNT/PDMS composite layer in the stacked DEA sample.

total actuation ratio increased. The difference between actuators 1 and 3 shows the effect of active surface area over actuation ratio. Active surface area is the ratio of overlapping conducting layers over the total surface area. A smaller active surface area means the actuator has more passive surface area, which is a combination of the dielectric part and the electrode connections, that is not contributing to actuation, but restricting it.

As represented in Figure 3.11, as the thickness of the layers decreases, the actuation ratio of the actuator increases. The actuation ratio also increases with a larger active surface area. This indicates that the passive surface area should be minimized in order achieve higher performance from the actuator. Decreasing the passive surface area is a more serious challenge for micro-scale stacked actuators since electrical

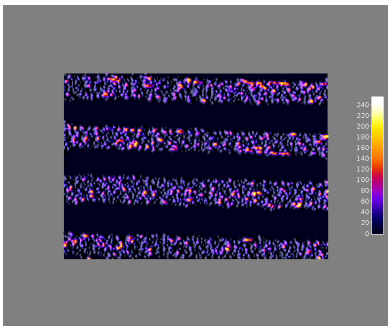

Figure 3.10: Cross-sectional SEM image of stacked DEAP actuator modified in ImageJ software to clearly distinguish the dielectric and the conductive layers and to accentuate the distribution of CNT in CNT/PDMS composite.

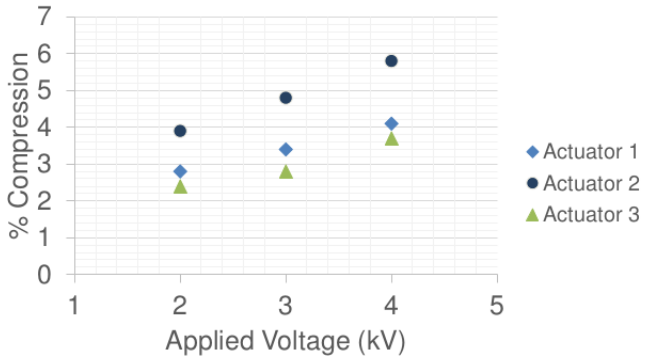

Figure 3.11: Actuation ratio (shown as % compression) versus applied voltage for three different stacked actuators. The number of layers and total surface area was kept constant for all samples. Actuator 1 and 3 has a layer thickness of $\sim 50\mu m$, actuator 2 has a layer thickness of $\sim 26\mu m$. Actuator 3 has 10% smaller active surface area than actuator 1.

connections have to be as small as possible in size, but need to stay intact and provide good electrical conduction.

Even though some of the fabricated samples had a uniform layer thickness and homogeneous CNT distribution, as represented in Figures 3.8 through 3.10, others did not result in good structures due to the manual fabrication process. Figure 3.12 shows how the thickness of layers varied within a single stacked actuator. Figure 3.12 shows that thickness uniformity is more difficult to sustain as the number of layers

increases in a given actuator. In the figure, the lighter areas show the conductive CNT/PDMS composite regions and the darker areas are PDMS dielectric layers. The thickness variation in a single layer in Figure 3.12 increases up to 30% in dielectric layers. Throughout the whole structure, the average thickness difference between two different layers increases to greater than 200%. While the thickness difference between the alternating layers can be tolerated, the variance in individual layers causes a nonuniform electric field that ends up disturbing the actuation mechanism. Rosset et al. reported that a 1 micron thickness inhomogeneity of a 5 μm membrane could cause a 25% difference in the electric field [60]. Like contaminants and voids, the thickness inhomogeneity weakens the membrane and lowers the dielectric breakdown strength of the dielectric layer.

The main reason for nonuniformities in the layer thickness is due to the fabrication method. PDMS has a thermal expansion coefficient of $3.10 \times 10^{-4}\ C^{-1}$. As each layer is fabricated on top of the previous ones, close to 3% expansion and contraction of existing layers occurs with each curing cycle. Since a manual tape casting method is used for fabrication, it is difficult to maintain identical conditions at the end of each fabrication cycle, including tape casting and curing. Furthermore, the whole structure is standing on a rigid substrate with a different thermal expansion coefficient and heat exchange coefficient. As the PDMS layers expand and contract, the rigid substrate does not behave similarly, resulting in bending of the structure as more layers are fabricated and the system goes through heating and cooling cycles. Additionally, the toluene used to disperse the carbon nanotubes in the PDMS is still present in the mixture in small amounts when the conductive polymer solution is cast onto the PDMS layers. When it is placed in the oven for curing, the remaining solvent evaporates and disrupts the surface of the conductive polymer solution when it is

polymerizing. Therefore, it is difficult to maintain consistency throughout the whole fabrication process. If all of the layers could be fabricated in one step, without going through the heating and cooling cycles repeatedly, the thickness of the layers could be more uniform and the polymer would not go through the thermal stress cycles during the process.

Another drawback associated with the manual fabrication of stacked DEAs is the need for adhesives for providing structural integrity. Since conventional fabrication methods require each layer of DEAs to be fabricated individually, each layer must be combined into a stacked device after fabricating single DEA structures using an adhesive additive to ensure the structural integrity of the device. The process is time-consuming to fabricate a DEA and requires additional binding steps, which again contributes to the total fabrication time and could potentially affect the mechanical properties of the actuator adversely.

The results indicated the selected materials could be used for the fabrication of stacked (or multilayer) actuators but the manual fabrication process limited the repeability and would be challenging in smaller scales, with thinner dielectric layers. A more automated process that can also be easily adopted for smaller scale fabrication is needed. In order to eliminate the nonuniformity of the stacked layers due to the manual steps and the thermal shrinkage of PDMS, a microfabrication method that allows the fabrication of all individual layers at once would be preferable. Microfabrication of the DEAs would also eliminate the need for additional adhesives since the alternating PDMS layers would be a single solid body.

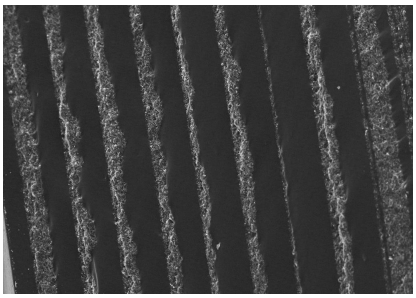

Figure 3.12: SEM image of cross-sectional area of another stacked actuator sample. As the number of layers increases, it is more difficult to obtain uniform layers.

3.2.2 Fabrication Approaches for Biomimetic Multilayer DEAs

After the proof of concept fabrication of the "macro-scale" multi-layer DEAs, the next steps in the objectives were to develop a micro-scale DEA design along with a suitable fabrication method that would allow the "microfabrication" of DEAs with a flexible and scalable approach.

The novel fabrication strategy developed in this work, to fabricate multilayer DEAs, relies on implementing the fabrication process from the side-up, by tilting the structure 90^o, rather than starting from the bottom. All dielectric layers of the stack are thus fabricated at the same time, then the conductive layers are added and cured simultaneously. The method eliminates the time constraints associated with fabricating each layer individually depending on the number of layers. Furthermore, increasing the number of layers in the stack provides a larger actuation distance. Actuation of the DEA is along the length of the DEA, parallel to the attraction force between the conductive layers.

The biomimetically inspired stacked actuator consisted of interdigitated conductive layers, isolated with the dielectric PDMS, as shown in Figure 3.15. A photomask with 20 μm thick interdigitated lines and electrode connections for the voltage input was designed.The schematic in Figure 3.17 shows the cross-sectional view of a por-

tion of the proposed structure from the side (a), from the top (b) and from a low angle perspective (c). Figure 3.17 (c) shows the alternating conductive layers aligned next to one another from left to right. When a voltage difference is introduced to the device, the parallel conductive layers induce electrostatic pressure on each other and the structure shrinks in the horizontal axis. To conserve volume, the structure also expands along the vertical axis. When compared with the traditional sheet-type DEAs, the structure in Figure 3.17 provides a linear actuation mechanism in the form of compression.

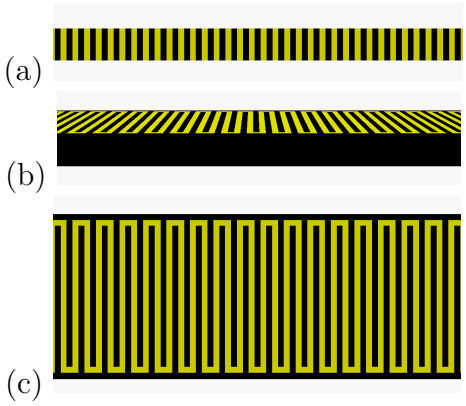

Figure 3.13: Schematics showing the cross-sectional side view (a), a low angle perspective (b) and top view (c) of a stacked DEA structure with alternating layers of conductive (black) and dielectric (yellow) PDMS. Note that the image is not to scale.

Fabrication of the Photoresist Molds

The existing DEA structures rely on the very basic DEA design that is composed of two conductive layers with a dielectric layer between them. Stacking multiple DEAs requires one to fabricate individual DEA structures, then to align and stack them and use an adhesive to connect them together.

A new DEA design was needed for the fabrication of multilayer DEAs in micro-scale. Each alternating layer needed to be isolated from each other but every second

layer needed to be electrically connected. Since the actuators are fabricated in micro-scale, making the electrical connection of hundreds of layers selectively would not be practical. Therefore, an interdigitated electrode structure was designed to be printed on a photomask. With the interdigitated electrode structure, both the conductive parallel layers and their interconnections can be fabricated during the microfabrication process.

For all three fabrication methods, the first step was to fabricate photoresist molds using the photomasks with the designed structures. For the fabrication of the photoresist molds, RCA cleaned 3" mechanical grade silicon wafers were coated with MicroChem SU-8 3050 photoresist at 1000 rpm for 30 seconds with a 500 rpm ramp of 5 seconds. Soft-bake step was done at 95°C for 45 minutes, until the resist film stopped wrinkling when removed from the hotplate. Using the photomasks, the negative photoresist was exposed with UV for a total dose of 250 mJ/cm^2 using Karl Suss MA 150 aligner, using an i-line filter. Post-exposure bake was started at 65°C for 1 minute and finished at 95°C where the wafer was held for 5 minutes. The photoresist was developed with MicroChem SU-8 developer to wash away the uncured SU-8, rinsed with IPA (isopropyl alcohol) and dried. Patterned SU-8 films were hard-baked at 150°C to improve the structural integrity of the relatively high-aspect-ratio features. The thickness of the SU-8 film and the height of the features were measured, using a KLA Tencor P2 profilometer, as 180 μm.

Originals and inverted (negative) versions of the same mask design were printed to use as the photomask for the different methods. For all the photoresist (negative and original) molds, the same fabrication prodecure was followed. PDMS was prepared at a 15:1 base to curing agent ratio and c-PDMS was prepared at a 10:1 ratio, unless otherwise stated.

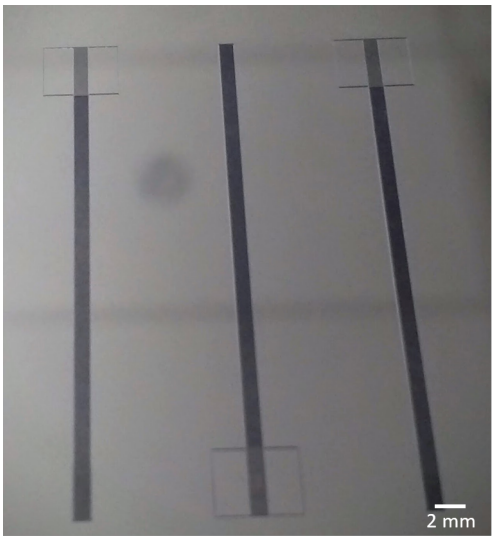

Figure 3.14: Designed pattern transferred to the SU-8 photoresist on silicon wafer. Three separate molds for three devices are shown in the figure.

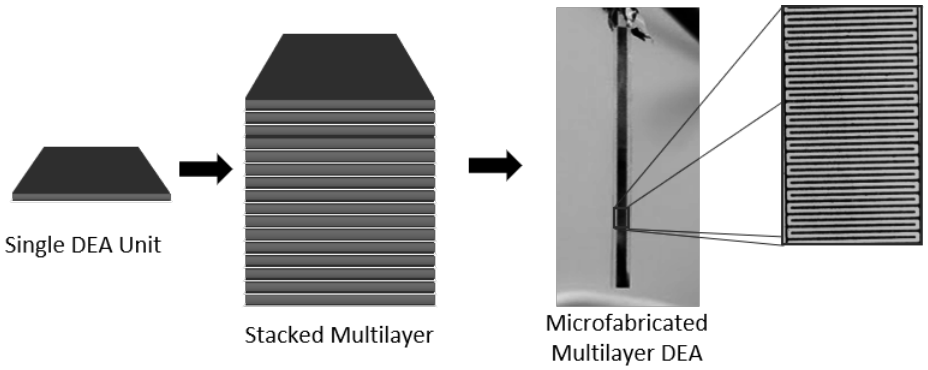

Figure 3.15: a) Schematic representation of a single DEA structure with the dielectric membrane sandwiched between two parallel conductive layers, b) schematic of a stacked DEA structure with many layers of alternating dielectric and conductive elastomers, c) actual stacked DEA fabricated using a microfabrication approach, (d) microscope image of the interdigitated conductive elastomer layers in the photoresist mold.

Having both the dielectric and conductive layers made from the same material (PDMS) provides mechanical compliance for the actuator, however, it poses a challenge for microfabrication as it is not possible to chemically alter one of the layers

without modifying the other. Three different fabrication approaches were investigated, using similar fabrication tools, to study the feasibility of fabrication of multilayer DEAs.

Microfabrication Method I

For Method I, the photoresist molds were fabricated using the original photomask shown in Figure 3.16. The figure shows a screenshot of the photomask design converted to PDF format. The white regions are transparent on the printed photomask and allow the transmission of the UV light (i-line) from the aligner that initiates the crosslinking of the photoresis. The black regions are printed in black ink on the photoresist and block the UV light, preventing the photoresist from crosslinking. When the photoresist is developed, the black regions dissolve and the white features stay crosslinked on the silicon wafers, forming the pattern to be transferred to PDMS.

Figure 3.18 depicts each step of this fabrication approach. As shown in the figure, gray, blue, yellow and black pieces represent the silicon wafer, photoresist, PDMS, c-PDMS, respectively.

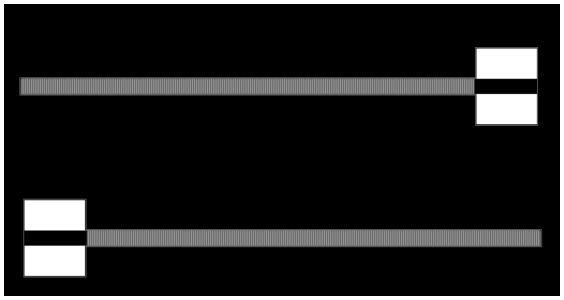

Figure 3.16: Top view of the photomask design used for patterning the photoresist for fabrication method I. The white features are transparent when printed on the photomask and allow the transmission of light onto the photoresist, allowing the illuminated areas of SU-8 to crosslink.

The photoresist molds were coated with PDMS and cured at 80°C for 30 minutes.

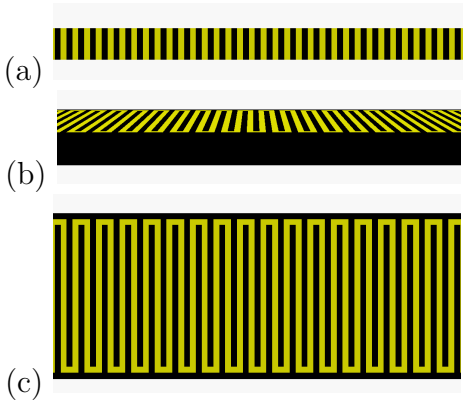

Figure 3.17: Schematics showing the cross-sectional side view (a), a low angle perspective (b) and top view (c) of a stacked DEA structure with alternating layers of conductive (black) and dielectric (yellow) PDMS. Note that the image is not to scale.

The cured PDMS was peeled from the photoresist, which formed the interdigitated dielectric layers and the bottom PDMS layer. The structure was placed on a blank wafer and coated with c-PDMS to fill the gaps in the PDMS to form the conductive interdigitated layers and interconnections for each layer. The excess c-PDMS was removed using a combination of a metal blade and a custom film applicator blade with a PDMS coated edge to isolate individual conductive layers of the stacked DEA. The completed structure was cured and individual devices were cut to obtain free standing stacked fiber-like DEAs.

The schematic in Fig. 3.17 (a) shows the cross-sectional side view of the final structure as depicted in step 8 in Fig. 3.18, without the encapsulation layers at the top and the bottom. Fig. 3.17 (b) depicts the device at a distance as seen from a low angle perpective. Fig. 3.17 (c) shows the same structure from the top, with the interdigitated conductive layers and the dielectric layers between them.

It was observed that when a softer dielectric material with a lower elastic modulus was used for this method, it was more difficult to coat the c-PDMS onto and clean the excess solution from the PDMS dielectric layer. Due to the mechanical pressure

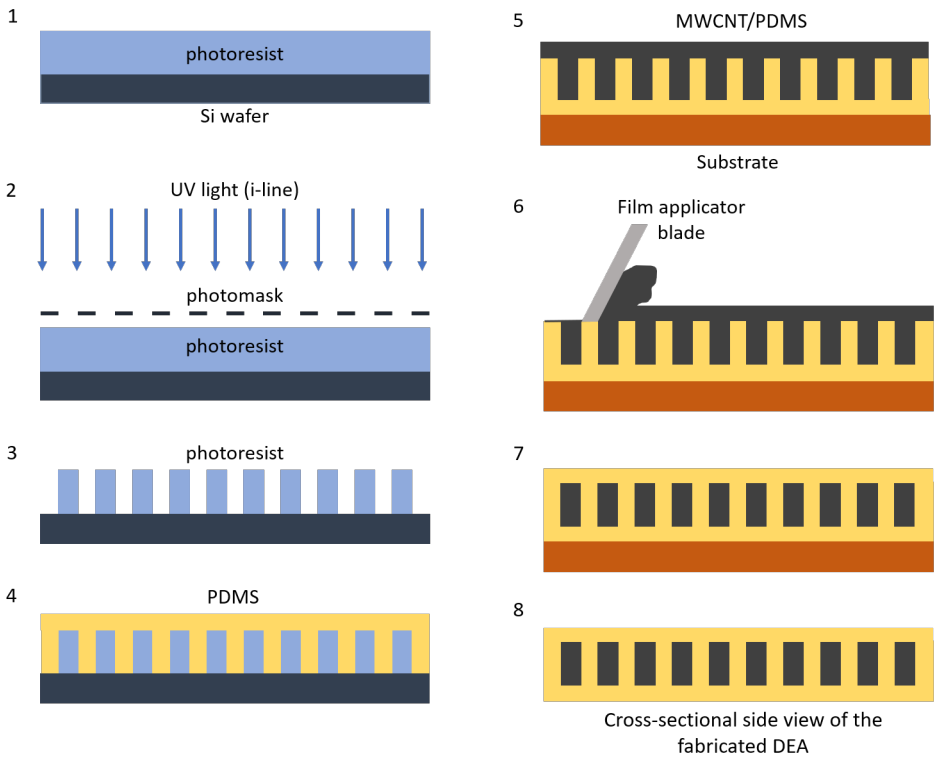

Figure 3.18: Schematics for the process flow for microfabrication Method I. All images show cross sectional side views of a small section of each material/tool used during the fabrication process.

from the cleaning step, high pillars (dielectric layers) tended to deform and collapse.

Microfabrication Method II - Negative Mask

For the second method, a similar process flow was followed. In order to avoid the removal step causing the PDMS pillars to deform, the fabrication order of the dielectric and conductive layers was reversed. The negative versions of the photoresist molds were used for this approach, instead of the original pattern.

After the photoresist molds were prepared, the molds were coated with the c-PDMS mixture, as opposed to PDMS, as shown in Fig. 3.20. The excess c-PDMS was removed using the same tools as in Method I.

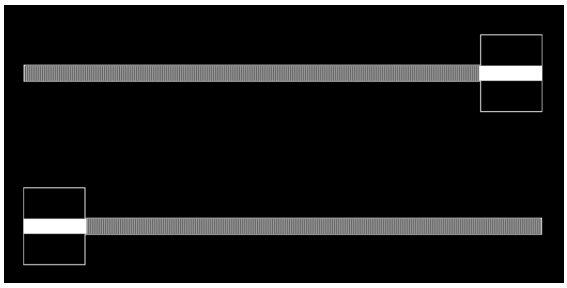

Figure 3.19: Top view of the photomask design used for the fabrication method II, inverse of the mask used for method I. The electrodes are black in this design so that the photoresist will be dissolved where the conductive PDMS patterns will be. The device is surrounded by a white (transparent) line to isolate the patterns from the bulk of the photomask.

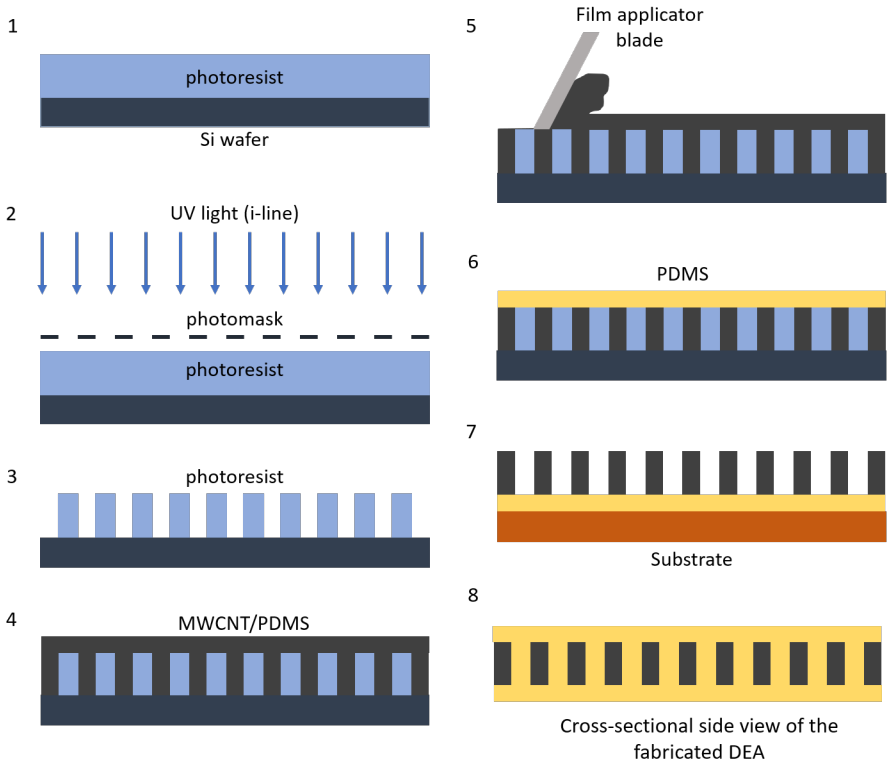

Figure 3.20: Schematics for the process flow for Method II. Conductive layers are fabricated before the dielectric layers.

After curing the c-PDMS, it was coated with a 50 micron PDMS layer and cured again at 80°C. Once the PDMS was solidified, the structure was peeled from the

wafer (from the resist mold) and encapsulated with PDMS on the other side using the same curing procedure. Figure 3.17 shows a representative cross-sectional image of a stacked DEA after this step. Finally, devices were cut from the rest of the polymer and free-standing DEA fibers were obtained.

One of the difficulties associated with this method was the detachment of the conductive MWCNT/PDMS from the SU-8 mold. When peeling the structures from the photoresist mold, after step 6, some of the conductive layers were broken. If one of the active layers is broken, it does not affect the whole actuator. However, if one of the electrode connections is broken, the rest of the actuator would not work. Application of a surfactant on the SU-8 surface could help to overcome this problem. However, as the features get smaller, wetting of the photoresist surface by the PDMS mixture becomes more important than it is in larger scale.

Microfabrication Method III - Injection

An alternative approach to coating the c-PDMS was to inject it into the dielectric structure using a syringe with fine tip needle that could deliver the c-PDMS into the fabricated dielectric structure. Figure 3.21 illustrates the fabrication approach via injection molding schematically. For this approach, the same masks used in Method I were used to fabricate the photoresist mold for forming the initial dielectric structure. The dielectric PDMS formed the serpentine structure and the interdigitated structure for the conductive layers was hollow.

The PDMS was spin coated onto the resist mold and cured, then detached from the mold and placed on a flat surface (i.e. bare silicon wafer or glass substrate). Another PDMS layer was spin coated on a blank wafer (with no mold) to form a thin and flat PDMS sheet. Once it was cured, the thin PDMS sheet was peeled from the

silicon wafer. Both PDMS pieces (flat sheet and the patterned PDMS) were treated with low temperature corona discharge plasma (corona treatment) to functionalize the surfaces. The thin PDMS sheet was carefully placed on top of the patterned PDMS to cover the entire area and seal off all the hollow structures on the PDMS. The two attached pieces were placed in the oven to improve the bonding and baked at 95°C for 30 minutes.

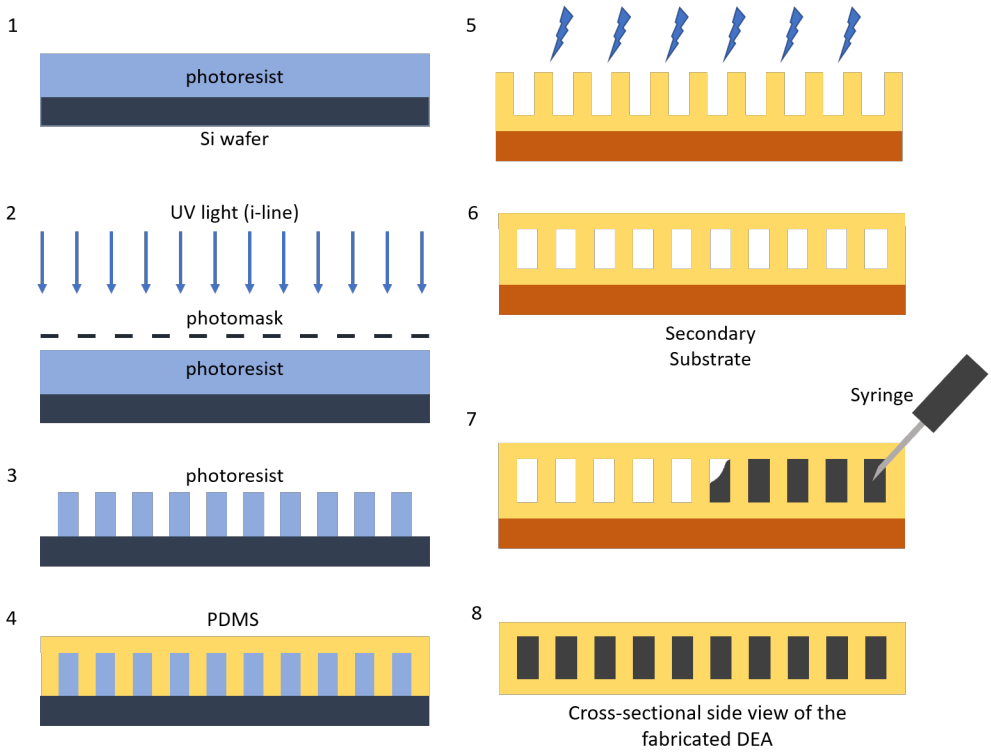

Figure 3.21: Schematic depicting the process flow for the injection molding approach (Method III). Drawings in the figure are not to scale and represent the cross-sectional side views at the center of each structure.

Sealed devices were cut from the bottom end in order to let the trapped air out during the injection process. c-PDMS mixture was injected into the sealed devices to form the conductive DEA layers. However, it was observed that, depending on the viscosity of the c-PDMS mixture, internal pressure during the injection process caused

breaking of the bonds between the PDMS layers and caused leaking. Therefore, sealed PDMS structures were placed in a vacuum chamber and the c-PDMS syringe was inserted into the hollow structure. Vacuum was used to remove the air inside the sealed devices and pull the c-PDMS mixture into the hollow regions.

(a) 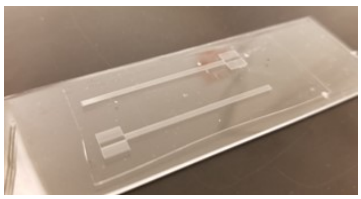 (b) 

Figure 3.22: a) Two PDMS pieces sealed together to form the dielectric part of the stacked DEA structure before injecting the c-PDMS in Method III. b) Injection of c-PDMS. The needle on the right hand side of the figure (b) is placed at the bottom end of the sealed device to let the air out easily from inside the hollow channels into the vacuum chamber.

Figure 3.22 (a) shows the two pieces of PDMS sealed together after the corona treatment step. Two devices in the image were cut from the rest of the PDMS. The needle, attached to the syringe containing the c-PDMS mixture, is inserted into the hollow area that forms the electrode connection for the power input. Another needle is inserted from the opposite end, as shown in Figure 3.22 (b), to introduce vacuum into the chamber.

With this method, the manual step of removing the excess conductive slurry was removed from the fabrication flow. Although this fabrication method did not increase the yield overall, it was observed that with short injection distance, the fabrication yield was significantly higher, as explained later.

3.2.3 Improvements in the Fabrication Methods

Laser Etching

As explained earlier, one of the major problems with the fabrication process (using Method I or II) is to eliminate the excess conductive PDMS slurry and to isolate the alternating conductive layers from each other. A possible approach to eliminate this problem could be to etch the conductive PDMS from the top of the fabricated devices after the fabrication process has been completed. Since the whole structure is made of the same material, chemical etching would be isotropic and is not desired. One possible method could be using laser etching to burn the conductive PDMS with high power laser.

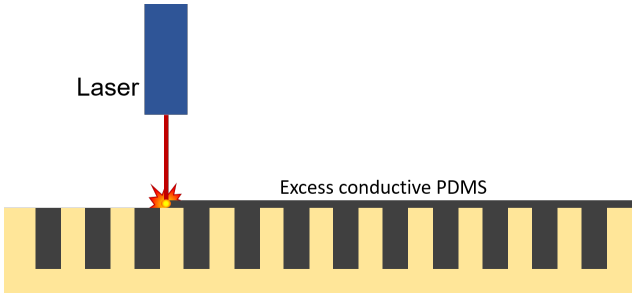

Figure 3.23: Schematic showing a laser cutter burning away the excess conductive PDMS on top of the structure.

Figure 4.1 demonstrates the basic working mechanism of the method that could be used to remove the conductive PDMS from the surface. A set of experiments was carried out to assess the possibility of using a conventional laser cutting tool for etching cPDMS.

As shown in Figure 3.24, both PDMS and cPDMS can be burned and etched away using a laser cutting tool. Figure 3.24 (b) shows the thickness of the cPDMS/PDMS specimen (from the side) that was etched completely using laser. The etching depth is plotted in Figure 3.25 as a function of the laser power. It is observed that at high

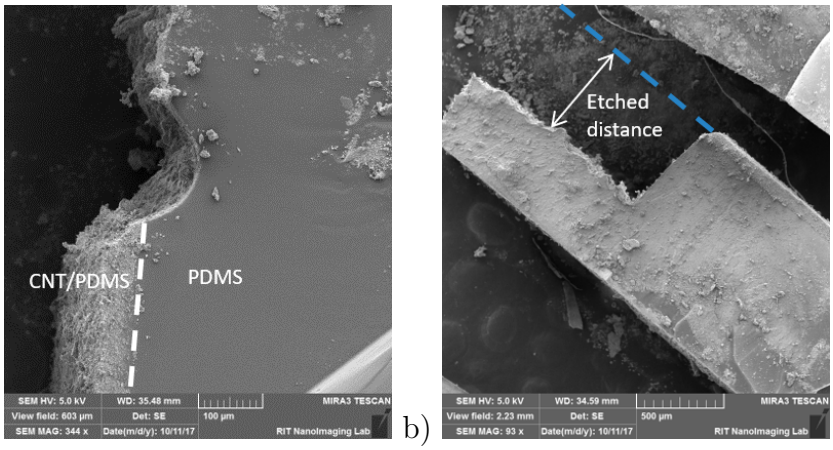

Figure 3.24: (a) SEM image of a cPDMS coated PDMS specimen. The labeled (bottom) part is the unetched specimen, the top part is etched with laser. (b) SEM image of a cPDMS coated PDMS specimen, etched about halfway through its thickness.

power, the etching depth is inconsistent. Below 18%, the etching depth is between 15 and 23 μm and it does not change significantly. The standard deviation for the etching distance below 18% is less than 5%, whereas it is 40% at 30% laser power.

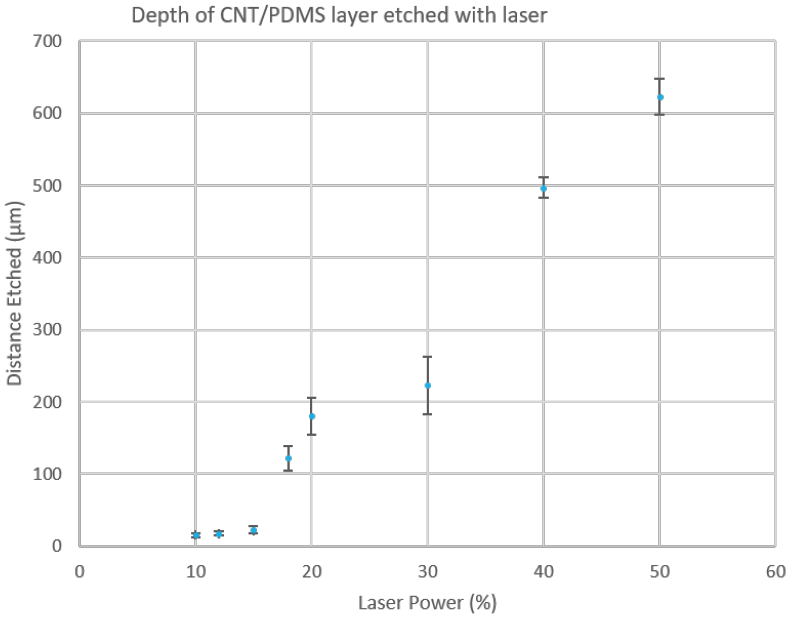

Figure 3.25: Etching depth with changing laser power (given as percentage).

a) 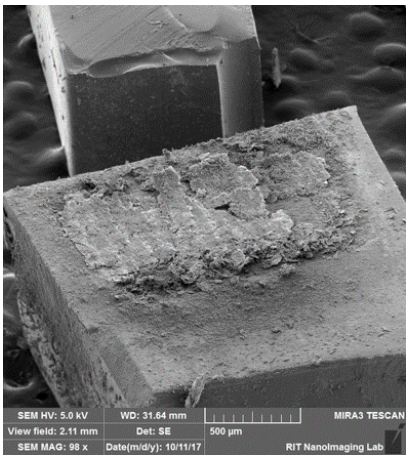

b) 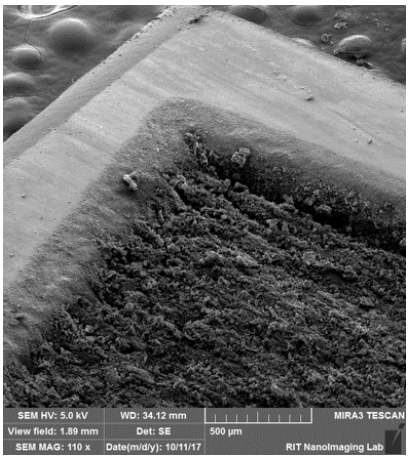

Figure 3.26: (a) Surface of a laser etched cPDMS specimen, with burned cPDMS residue (b) Close-up of an SEM image of a cPDMS coated PDMS specimen.

Since the cPDMS layer covering the devices is thinner than 10 μm, laser etching could be used to eliminate the excess cPDMS from the surface. Even though the variation in etching depth is relatively low and can be used for large scale devices, it could cause significant inconsistencies for smaller scale devices. Another drawback of laser etching is the residual cPMDS left after the etching process. Figure 3.26 shows that the etched surfaces are coated with residual cPDMS layers. Figure 3.26 (b) also shows the variation in etching depth on the surface.

Water Soluble Sacrificial Layer

In order to ease the detachment of the PDMS layers from the photoresist molds, a water soluble sacrificial layer was introduced. Linder et al. [61] studied water soluble sacrificial layers to be in surface micromachining of stand-alone SU-8 structures. One of these sacrificial materials was poly(acrylic acid) (PAA). Using PAA, Linder et al. obtained a water soluble sacrificial layer that was insoluble in common solvents (such as toluene, chloroform, acetone) and SU-8 developer. The thickness of the water diluted PAA layers obtained via spin coating, reported by Linder et al., could go

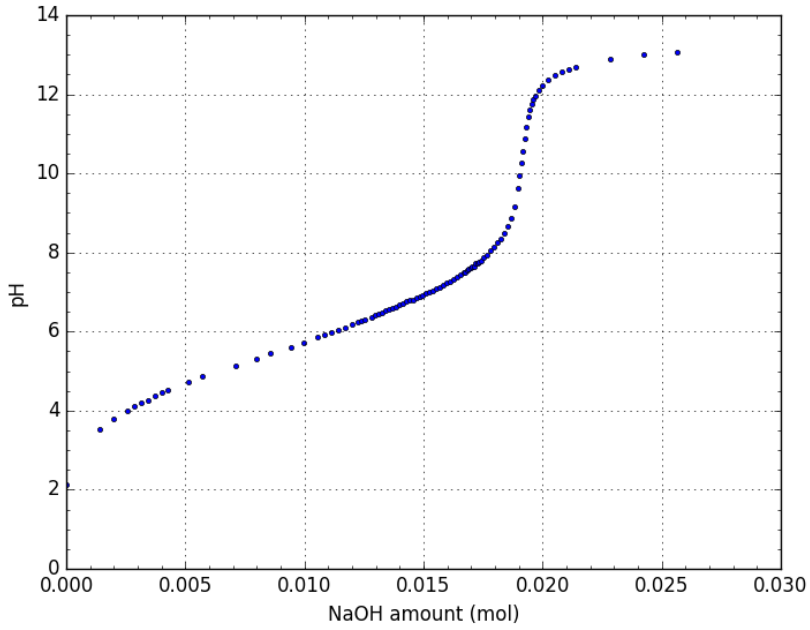

Figure 3.27: The pH of the mixture vs the amount of NaOH added to 20 g 6.25wt% PAA.

down to submicrometer level.

In this study, a 50 kDa PAA was used to form sacrificial layers. PAA was neutralized by mixing it with sodium hydroxide (NaOH). A titration experiment was carried out to determine amount of NaOH required to neutralize the PAA, shown in Figure 3.27. The pH value of the PAA mixture was brought up to 7.5. The neutralized PAA (25wt%) was spin coated onto PDMS layer on silicon wafers and cured in a convection oven. Figure 3.28 shows the PAA coated PDMS layers after the PAA layers were cured. Due to the high shrinkage of PAA, PDMS structures peeled off from the silicon wafers in all cases.

PAA was also studied on patterned SU-8 photoresist structures on silicon wafers. Due to the hydrophobic nature of the SU-8, corona treatment was required for the PAA mixture to wet the SU-8 surface. After the corona treatment of SU-8, PAA

a) 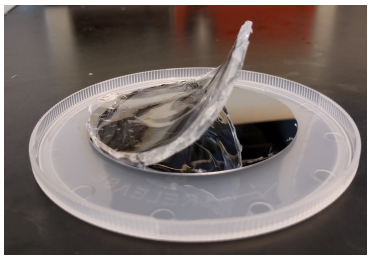 b) 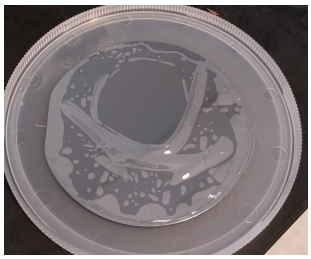 c)

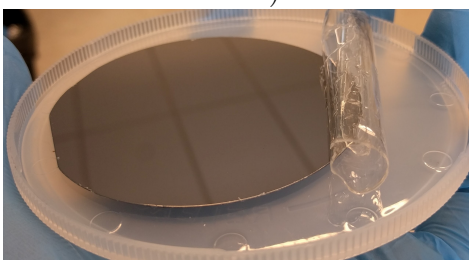

Figure 3.28: (a) PAA on PDMS, spin coated at 500 rpm for 30 seconds, cured at 80°C, (b) PAA on PDMS, spin-coated at 1000 rpm for 30 seconds, cured at 80 °C, (c) PAA on PDMS, spin coated at 500 rpm for 30 seconds, cured at 50 °C. The thicknesses of the PDMS layers in (b) and (c) are equal and are smaller than the thickness of the PDMS in (a).

was spin coated onto the SU-8 surface and cured in the oven. Figure 3.29 shows the resulting PAA coating on SU-8 structures. In Figure 3.29 (a), PAA, which was cured at 150°C, seems to peel off from the SU-8 substrate. Figures 3.29 (b) and (c), show a better PAA integrity on the SU-8 structures. However, the color distribution across the surface of the SU-8 indicates that the thickness of the coating is non-uniform.

The PAA coated SU-8 structures were coated with PDMS to evaluate the possibility of using PAA as a releasing agent for PDMS. After curing the PDMS layer, the silicon wafer was submerged in water. PAA layer dissolved from between the PDMS and the SU-8 layers. However, it took a longer amount of time for water to reach the patterned areas of the SU-8 and since the coating had non-uniformities, PDMS was not entirely detached from the SU-8 layer.

It was concluded that the water soluble PAA layer is not ideal for using as a releasing agent between the patterned SU-8 and the PDMS layers. However, it could

a)  b) 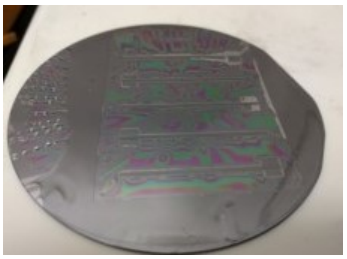 c)

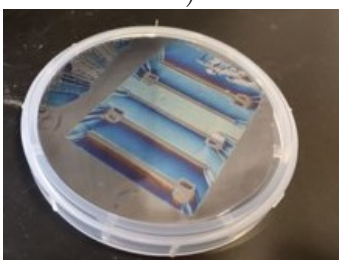

Figure 3.29: PAA layers coated on patterned SU-8 photoresist and cured (a) at 150°C, (b) at 100°C, (c) at 100°C.

be coated onto the silicon wafers before forming the SU-8 structures as an aid to remove the SU-8 layers from the silicon wafers.

3.2.4 Summary

There were several problems regarding the fabrication processes. With the first two methods, removal of the excess conductive slurry was the critical step that limited the repeatability of the experiments. In order to overcome this problem, various methods were tried. Method III, provided a solution for this manual removal problem, however, it did introduce a leakage issue. It was observed that the injection distance was kept shorter, the fabrication yield was better. This could also be related to the total time before curing, when the PDMS is exposed to the solvent in the conductive mixture. Table 3.30 summarizes the improvement attempts for each fabrication method and the resulting observation for each one.

Improvement Attempt	Result/Observation(s)
Method I	
Increasing Coating Speed	Non-uniform coating (high viscosity vs small patterns)
Increasing Force for Removal	Deformed dielectric pillars
Method II	
PAA Sacrificial Layer	Not useful for layer isolation Can be used under SU8 to recover Si wafers
Laser Etching	Not accurate enough for small size Stiffening effect
Method III	
Shorter Injection Distance	Increased the fabrication yield Shorter actuators

Figure 3.30: Summary of the improvement attempts for each fabrication method and the observed outcomes from each attempt.

3.3 Modeling of Interdigitated Multilayer DEAs

The multilayer DEA design proposed in this study has some new geometric parameters that need to be taken into account. As the last objective of this study, in order to better understand the effect of these geometric parameters on actuation performance, the interdigitated multilayer structures were modeled in COMSOL. Electromechanics interface, which couples solid mechanics with electrostatics, was used to simulate the actuation of the devices and to obtain the total displacement and actuation ratio. The geometric parameters that could affect the actuation were identified as shown in Fig. 3.31, where L_d, L_c, t_d, t_c, t_e and d_s are dielectric layer length, conductive layer length, dielectric layer thickness, conductive layer thickness, electrode thickness and separation distance between the counter electrodes, respectively.

The theoretical models for studying the elasticity of polymers started to come out in the 1940's after the World War II with the proliferation of natural and synthetic rubber [19, 62]. Since then, there have been many studies and models for describing

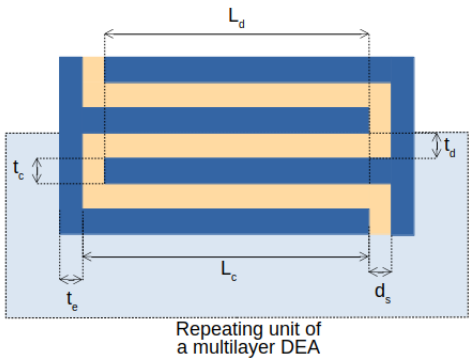

Figure 3.31: Schematic showing the geometric parameters used to model the multi-layer actuators in Comsol.

the mechanical behaviour of polymers and rubber-like materials. Even though there still is not an effective model that describes the behaviour of rubber-like materials in a universal way, there are some models that agree with the experimental data for particular cases [62]. The aim of this section is not to improve upon these models for increasing the accuracy of the simulations but to use the existing models to investigate the effect of different geometric parameters on the actuation of the DEAs. A detailed explanation of the material models used in Comsol can be found in Reference [63].

The simplest model to describe the strain of a rubber-like material is the "Hooke model" or the "spring model", where the strain is proportional to the force applied on the material, as shown in Equation 3.1 where f is the force, Δx is the displacement or change in length, and k is the spring constant [19].

$$f = k\Delta x \tag{3.1}$$

For a linear elastic material, Hooke's law can be used to relate stress tensor and the elastic strain tensor:

$$\sigma = \sigma_{ex} + C : \epsilon_{el} = \sigma_{ex} + C : (\epsilon - \epsilon_{inel}) \tag{3.2}$$

where σ is the stress tensor, C is the 4th order elasticity tensor, ϵ, ϵ_{el} and ϵ_{inel} are the total strain, elastic strain and the inelastic strain respectively. σ_{ex} can be any initial stress before the material goes through deformation and : stands for the double-dot tensor product [63].

Comsol calculates the total stress in 3D as:

$$S - S_0 = C : (\epsilon - \epsilon_0 - \epsilon_{inel}) \tag{3.3}$$

The strain ϵ is calculated as

$$\epsilon = \frac{1}{2}[(\nabla u)^T + \nabla u + (\nabla u)^T \nabla u] \tag{3.4}$$

In 1948, Ronald Rivlin along with other scientists proposed new models, one of which is the neo-Hookean model, to replace the Hooke model for explaining the elastic behaviour of polymers [64]. Neo-Hookean model is used to predict the stress-strain behaviour of a hyperelastic material undergoing large deformations in three dimensions [64]. A hyperelastic material can store deformation as elastic energy (or strain energy) and the stresses can be computed from this strain energy potential or the strain energy density function [65]. The strain energy potential can be defined in different forms using different material parameters depending on the material model, such as the neo-Hookean, Mooney-Rivlin, Ogden potential, Yeoh potential etc. [66]. The Neo-Hookean model is a special case of Mooney-Rivlin model that can be used for relatively small strains and with limited data related to the material parameters [67]. The strain energy density in the Neo-Hookean model is given as:

$$W_s = \frac{1}{2}\mu(I_1 - 3) + \mu ln(J_{el}) + \frac{1}{2}\lambda[ln(J_{el})]^2 \tag{3.5}$$

where μ and λ are Lamé parameters,

$$\mu = \frac{E}{2(1+\nu)} \qquad \lambda = \frac{E\nu}{(1+\nu)(1-2\nu)} \tag{3.6}$$

I_1 is the first invariant of the right Cauchy-Green deformation tensor and J_{el} is the elastic volume ratio. However, this model is applicable to compressible and nonlinear elastic materials as well as incompressible materials. In this study, the deformation of the polymer materials is considered:

- incompressible (or nearly incompressible),
- isochoric (constant volume),
- isotropic (deformation does not depend on the direction),
- linear elastic (strain lower than 20%, see Figure 3.1).

For an incompressible material, the neo-Hookean strain energy density can be defined as:

$$W_s = \frac{1}{2}\mu(I_1 - 3) + \frac{1}{2}K(J_{el} - 1)^2 \tag{3.7}$$

where K is the bulk modulus of the material, μ is the Lamé parameter, which is equal to the shear modulus of the material ($G = \mu$).

Assuming a single DEA unit with initial dimensions of x_0, y_0 and z_0 in x, y and z axes respectively, when a potential difference between the bottom and top plates is introduced, the actuator will contract in z-direction. Due to conservation of volume, it will also expand in x and y directions. The stretch ratio in each direction could be calculated by dividing the final length in a given direction by the original length in that direction:

$$\lambda_x = x/x_0, \qquad \lambda_y = y/y_0, \qquad \lambda_z = z/z_0. \tag{3.8}$$

Since the material is incompressible and the deformation process is isochoric, $\lambda_x\lambda_y\lambda_z = 1$. The main displacement due to the electrostatic pressure is in the z-direction, due to isotropy, the other two stretch ratios can be written in terms of λ_z:

$$\lambda_x = \lambda_y = \frac{1}{\sqrt{\lambda_z}} \tag{3.9}$$

The strain invariant 'J' in Equation 3.7 is defined as the determinant of the deformation gradient tensor ($\mathbf{F}$), which is defined by the stretch ratios:

$$\mathbf{F} = \frac{\partial z}{\partial Z} = \begin{pmatrix} \lambda_x & 0 & 0 \\ 0 & \lambda_y & 0 \\ 0 & 0 & \lambda_z \end{pmatrix} = \begin{pmatrix} \frac{1}{\sqrt{\lambda_z}} & 0 & 0 \\ 0 & \frac{1}{\sqrt{\lambda_z}} & 0 \\ 0 & 0 & \lambda_z \end{pmatrix} \tag{3.10}$$

$$J = det(F) = \tfrac{1}{\sqrt{\lambda_z}}\tfrac{1}{\sqrt{\lambda_z}}\lambda_z = 1 \tag{3.11}$$

I_1 in Equation 3.7 is defined as the trace function (first invariant) of the right Cauchy-Green deformation tensor (C), which is

$$C = F^T F \tag{3.12}$$

$$I_1 = tr(C) = \lambda_x^2 + \lambda_y^2 + \lambda_z^2 \tag{3.13}$$

For PDMS, Poisson's ratio can be considered 0.5 [28], however, it is taken as 0.499 for numerical calculations since 0.5 would make the value of the bulk modulus undefined. As explained by Sönnerlind, setting the Poisson's ratio equal to 0.499 can cause undesirable simulation results (locking problem) such as overly stiff models, checkerboard stress patterns or other errors or warnings [68]. When dealing with such a problem, "mixed formulation" should be enabled in Comsol by selecting the "Nearly incompressible material" option, under the linear elastic material settings.

In Comsol, three different stress measures, Cauchy stress (σ), First Piola-Kirchoff stress ($\mathbf{P}$) and Second Piola-Kirchoff stress ($\mathbf{S}$) are used. The Cauchy stress is defined as force/deformed area in fixed spatial directions. For the First Piola-Kirchoff stress, the forces in the spatial directions are related to the area in the original material frame. In the Second Piola-Kirchoff stress, the force and the area are represented in the material configuration, the values are the same as the Cauchy stress but the directions are rotating with the body. These three stresses are related to each other as follows:

$$S = F^{-1}P \tag{3.14}$$

$$\sigma = J^{-1}PF^{T} = J^{-1}FSF^{T} \tag{3.15}$$

In case of nearly incompressible hyperelastic materials, the total elastic energy function is split into two parts $W_s = W_{iso} + W_{vol}$, where W_{iso} and W_{vol} are the isochoric strain energy density and the volumetric strain energy density, respectively.

$$W_{vol}(J_{el}) = \frac{1}{2}K(J_{el} - 1)^2 \tag{3.16}$$

The volumetric pressure can be calculated as:

$$p_m = -\frac{\partial W_{vol}}{\partial J} = -K(J-1) \tag{3.17}$$

From here, the second Piola-Kirchoff stress can be written as:

$$S = -p_m J C^{-1} + 2\frac{\partial W_{iso}}{\partial C} \tag{3.18}$$

Then the Cauchy stress tensor is:

$$\sigma = J^{-1} F S F^T = -p_m I + 2J^{-1} F \frac{\partial W_{iso}}{\partial C} F^T \tag{3.19}$$

As mentioned earlier, in order to avoid the locking problem, the mixed formulation in Comsol replaces p_m with an "interpolated pressure help variable" p_w that adds extra degrees of freedom to the ones defined by the displacement vector $\mathbf{u}$. This modification changes the Equation 3.3 as:

$$S - S_0 = C : (\epsilon - \epsilon_0 - \epsilon_{inel}) - (trace(C : (\epsilon - \epsilon_0 - \epsilon_{inel}))/3 + p_w)I \tag{3.20}$$

For the DEA simulations, a single DEA structure was modeled as shown in Figure 3.32 as the "repeating unit" of the multilayer DEA configuration. At low strain rates, PDMS shows a linear elastic behaviour, as shown in Figure 3.1 and 3.2. Therefore, "linear elastic dielectric" and "linear elastic material", in Comsol electromechanics module, can be used to define the dielectric PDMS layers 3.32 (a) and the conductive PDMS layers (3.32 (b) respectively.

From the COMSOL material library, PDMS was chosen for the dielectric part of

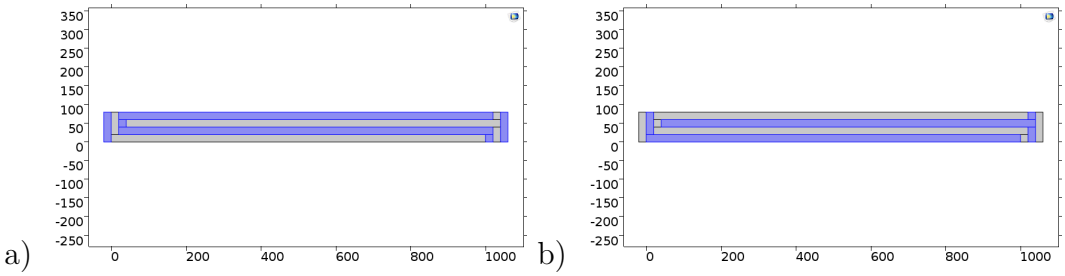

Figure 3.32: Single DEA structure with (a) the dielectric PDMS layers as linear elastic dielectric and (b) the conductive PDMS layers as linear elastic material.

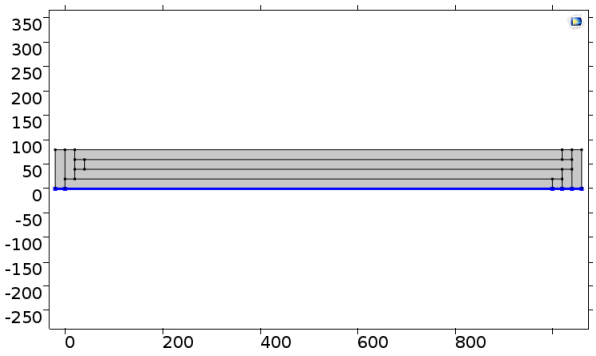

Figure 3.33: Fixed constraint boundary at the bottom of the first layer of the DEA model, where $\sigma = 0$ and $\epsilon = 0$

the actuator structure. The predefined Young's modulus value was replaced by the modulus calculated from the mechanical tests in Section 3.1.1. For Sylgard 184 with 15:1 base to curing agent ratio, Young's modulus was determined to be 400 kPa. For the conductive PDMS, a conductor material was defined with an elastic modulus of 1.1 MPa and a conductivity of 3.35 S/m.

The bottom boundary of the first layer was set as a 'Fixed Constraint' since it would be connected to the electrodes going to the power source and would be stationary, as shown in Figure 3.33. The fixed constraint boundary could be perceived as the reference point for the displacement of the rest of the actuator body.

The conductive layers connected to the left-hand-side electrode were designated as ground and the ones connected to the right-hand-side electrode were designated as

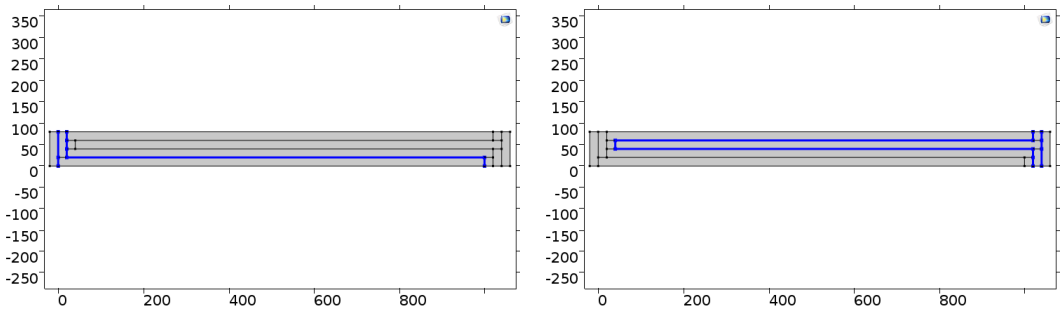

Figure 3.34: The boundaries selected as a) ground ($V = 0$) and b) terminal ($V = V_0$) to create the potential difference for inducing electrostatic pressure on the dielectric layers.

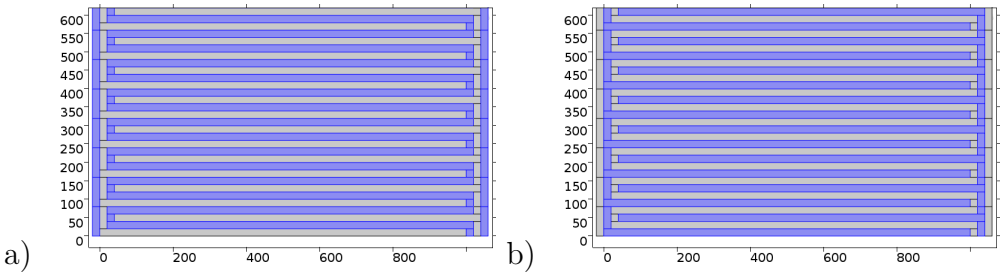

Figure 3.35: Partial view of the multilayer DEA array with a) dielectric domain and b) conductive domain selected.

the terminal. The boundaries selected for the ground and terminal, where the voltage would be V_0 and 0 respectively, are shown in Figure 3.34.

An array of DEA units was created by entering the number of layers (number of DEA units) as the size of the array (set as a 'parameter'). Figure 3.35 shows the array with the dielectric and conductive layers highlighted.

Chapter 4

Results

4.1 Experimental Results

Wires were attached to the fabricated devices by using c-PDMS to encapsulate and secure the connection points. The actuators were tested using a high voltage power source and voltages ranging from 500 V to 2 kV were applied. Figure 4.1 shows the fabricated stacked dielectric elastomer actuator (a) and the same actuator in its actuated state (b). The actuation distance was calculated as the difference between the final and the initial position of the free-end of the actuator in perpendicular direction, as depicted in Figure 4.2. The number of fabricated devices and the number of working devices are shown in Figure 4.11.

The actuation results of the DEAs fabricated through Method I are shown in Figure 4.3. The actuation ratio values seems promising and follows the theoretical trend. However, it should be noted that the results are representative of 20 different DEAs fabricated through the same process and the best actuation results achieved with this method are shown in the figure.

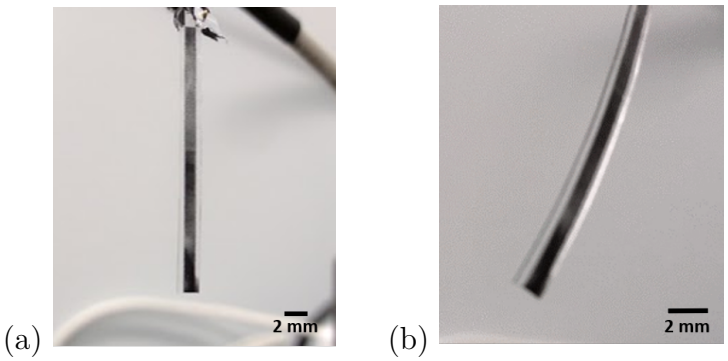

Figure 4.1: a) Representative single stacked actuator fabricated using Method I. b) Microfabricated actuator in its actuated state.

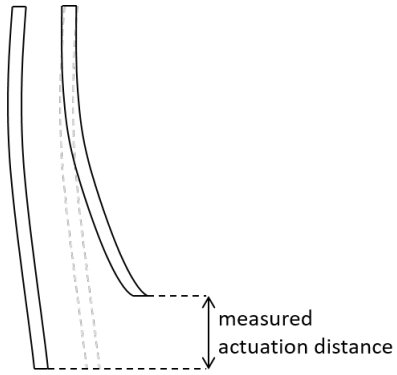

Figure 4.2: Schematic explaining the actuation test measurement. Actuator is at rest on the left, activated on the right.

Figure 4.4 shows the actuation results for the devices obtained using Method II. Compared to Figure 4.3, the most significant difference is that no measurable actuation was observed at 0.6 kV. At 1.2 kV, 6% actuation ratio was obtained with this method.

With Method III, initially, no actuation was observed since the devices had a leaking problem during the injection process. It was seen that the leak generally started near or close to the electrode connections while injecting the cPDMS slurry into the channels, as shown in Figure 4.5 and 4.6.

In order to overcome the leakage problem, a new actuator structure was designed

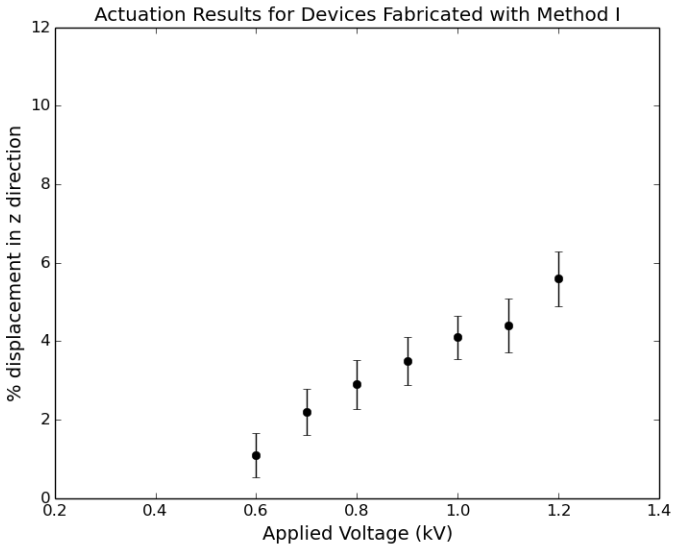

Figure 4.3: Actuation results for the devices fabricated through method I.

that would allow a smoother transition from the electrodes into the interdigitated channels in the PDMS. The duration of the corona treatment step was also increased to improve the adhesion of the two PDMS layers. In addition, the surface roughness (uniformity of the photoresist thickness) of the PDMS was investigated and the spin coating parameters were adjusted to allow a more uniform feature height across the whole device. Figure 4.7 shows the electrode connections that have a smoother transition from the large electrode area through the smaller channels in the device.

After the improvements, actuation measurements were taken with the devices fabricated through the injection method. It should be noted, however, that the total length of the devices used for this actuation test were about half of the length of the actuators used for the measurements from Method I and II. This decreases the total actuation length but does not affect the total actuation ratio. The results are shown in Figure 4.8.

Throughout the actuation tests, no signifant difference was observed in the actu-

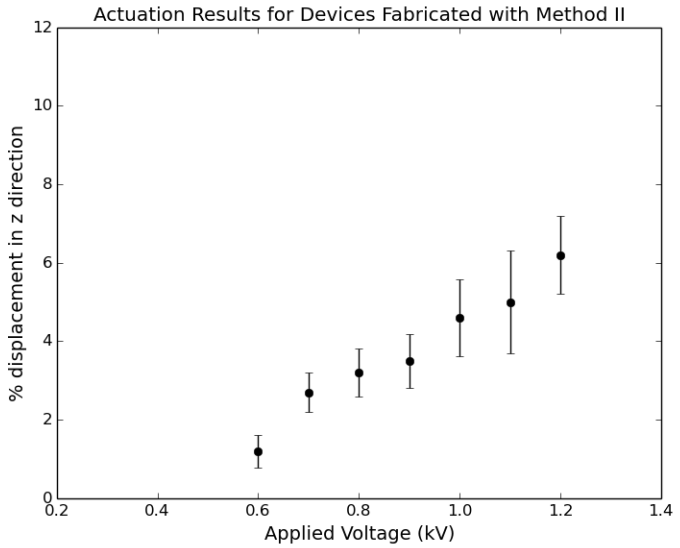

Figure 4.4: Actuation results for the devices fabricated through method II.

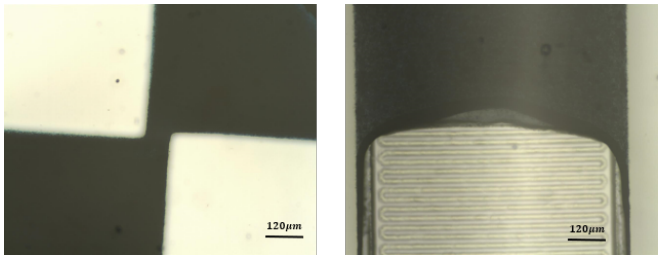

Figure 4.5: Sealed DEAs during the injection process. a) The corner between the electrode connections and the beginning of the interdigitated pattern. b) cPDMS slurry leaking through the channels, covering the entire area.

ation ratio of the devices depending on their fabrication method. Figure 4.9 shows a comparison of the actuation ratios of the microfabricated stacked DEAs (with dielectric layer thicknesses of 20 μm) and compares the actuation ratio of microfabricated DEAs with the macro-scale DEAs (with dielectric layer thicknesses of 50μm) fabricated layer by layer. The values for the actuation of the 20 μm actuator represent the average actuation values of all the devices fabricated through the different microfabrication approaches. Microfabricated DEAs were actuated at voltages between 0.5 kV

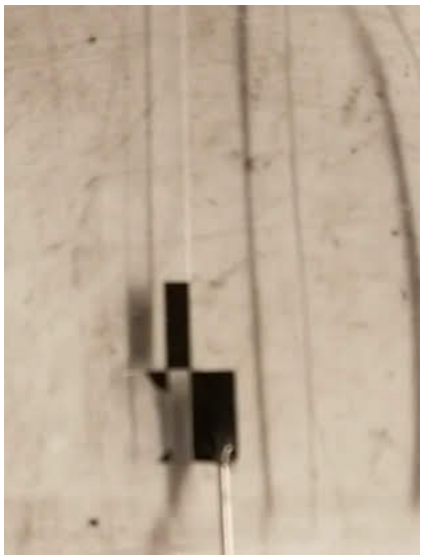

Figure 4.6: cPDMS slurry starting to leak from one electrode to the other.

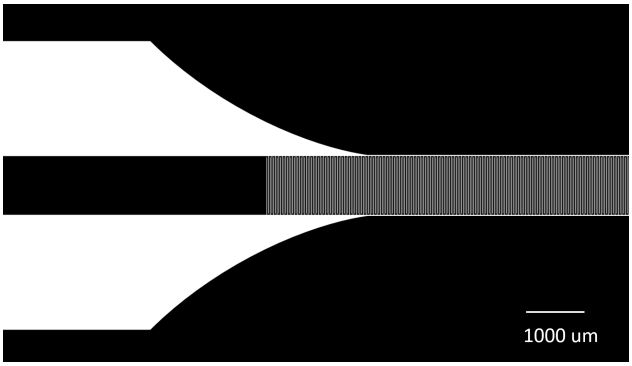

Figure 4.7: The improved actuator design with a smoother arc shaped connection.

and 1.2 kV. A maximum actuation, which was observed with the samples fabricated through Method II, was measured at around 6% at 1.2 kV, after which point the devices failed due to dielectric breakdown.

One important point to note is that the actuation ratio was measured as the difference between the height of the end point of the actuator at an activated state and passive state. However, the actuators have a slight curvature from the side and when they are actuated, the resulting actuation is not purely compression, but a combina-

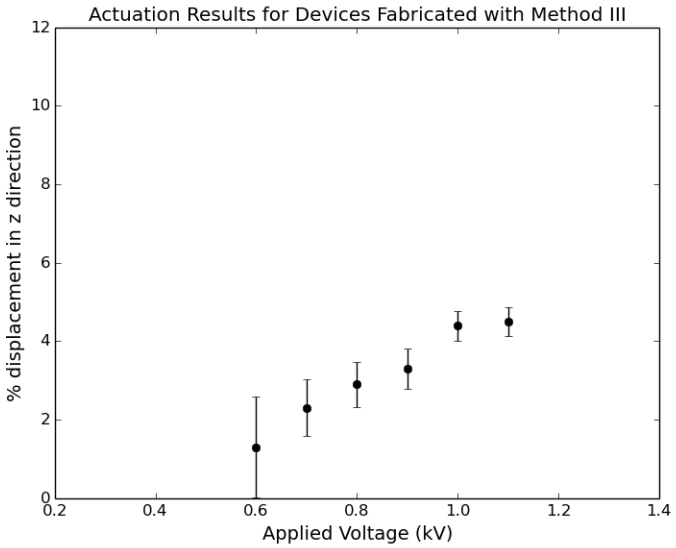

Figure 4.8: Actuation results for the devices fabricated through method III.

tion of compression and bending movement, as shown in Figure 4.2. Depending on the end-application, for which the actuators will be used, bending movement might be desirable. However, if only compressive motion is required from the actuator, bending should be eliminated. Bending of the actuators can be caused by the difference in thickness of PDMS layers at the bottom and the top while fabricating the devices. A thicker layer can resist larger forces while a thin layer bends more easily. Therefore, the actuator starts bending in one direction as the attraction force between the conducting layers increases. For eliminating bending, the thickness of non-working parts on opposite sides must be equal to each other, which is possible by applying identical fabrication steps on each side. Ideally, all layers for encapsulation should also be as thin as possible to minimize the resistance (counter forces) to actuation by the materials.

When compared with the theoretical actuation curve, obtained from Eq. 2.9, the results differ from the theoretical data, but they follow the trend of the theoretical

curve. The difference between the two could be due to numerous reasons including the effect of the passive area around the interdigitated structure, possible voltage drop through the length of the device, or other differences in the mechanical properties of the devices and the assumed values for calculation.

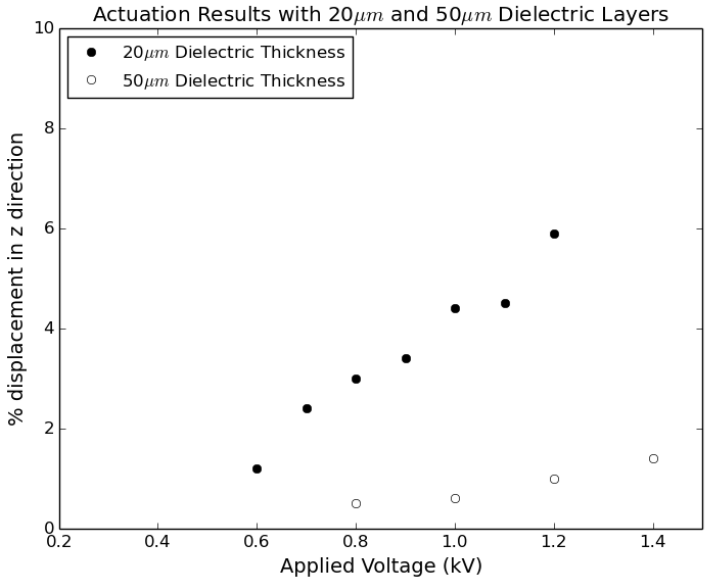

Figure 4.9: Actuation test results represented as % displacement (in length of the stacked structure) vs applied voltage.

Repeatability

In this study, it was shown that utilizing different microfabrication tools and techniques, it is possible to fabricate free-standing stacked dielectric elastomer actuator structures. With the first two fabrication approaches, the main challenge was the removal of the excess c-PDMS from the surface after coating, as illustrated in Figure 4.10. This problem diminished the repeatability of the fabrication process. Applying a larger force helped remove the excess solution, but also damaged the mold and deformed the dielectric elastomer. Applying an additional high speed spinning step

(1000 rpm for 20 s) removed some of the excess material, but also resulted in an uneven filling of the features in some cases.

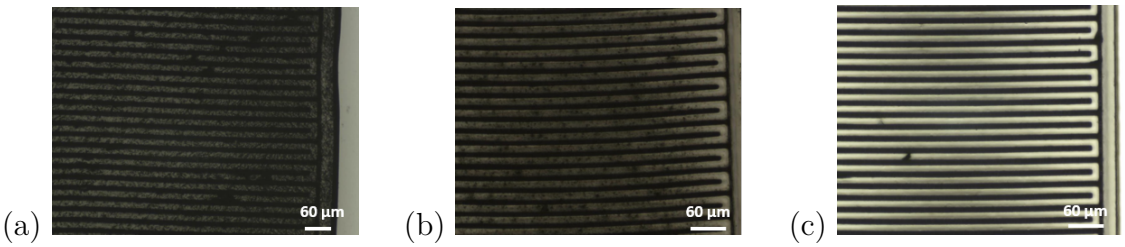

Figure 4.10: Microscope images (top view) showing into one side of the fabricated stacked DEA structures, a) dielectric layers covered with conductive material, b) less conductive material on the dielectric parts, c) almost no conductive material on dielectric layers but with small defects. Image from Ref. [69].

Figure 4.10 represents three different stacked DEAs fabricated through the same fabrication process (Method II) with slightly different parameters. The force applied for removal of the excess solution is larger and the spin coating speed is increased from (a) through (c). Although 4.10 (c) appears to depict what an ideal device should look like, there are local defects and non-uniformities throughout the device.

Using Method II, it was observed in Figure 4.1 (b) that the actuation occurs as a combination of compression and bending. This was due to the difference in thickness of the PDMS layers on each side of the actuator. The compression force was more effective on one side of the actuator while it was inhibited by the counteracting stress caused by the thicker PDMS layer on the other side. This can be adjusted by fine tuning the coating parameters on either side of the structure. When the thickness is uniform and equal on each side, the device should only contract, while it is also possible, as shown in the figure, to introduce a bending mechanism by changing the thickness on either side.

The injection method (Method III) was observed to work better than the two other methods, however only for a short injection distance. There may be two pos-

sible ways to improve the injection method: bonding between the two PDMS layers could be improved through a different surface treatment or functionalization or a less viscous PDMS could be used for preparing the conductive composite material. However, thinning the PDMS mixture requires an additional solvent, which causes swelling of PDMS and causes physical breakdown of the sealed device. An additional enhancement for the injection fabrication process could be done by using a micromanipulator to inject the conductive mixture into the channels in a more precise and accurate manner.

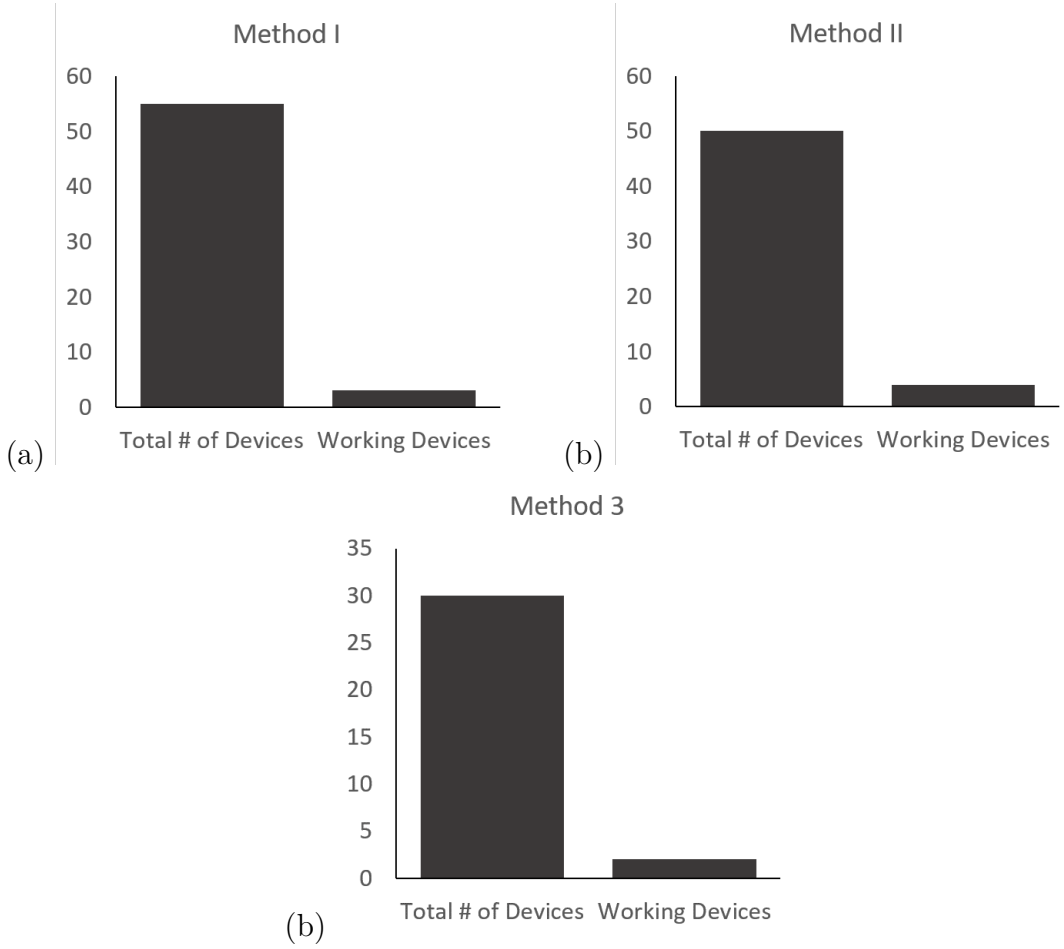

Figure 4.11: Comparison of the total number of devices and number of devices that were observed to work, fabricated via (a) Method I, (b) Method II and (c) Method III.

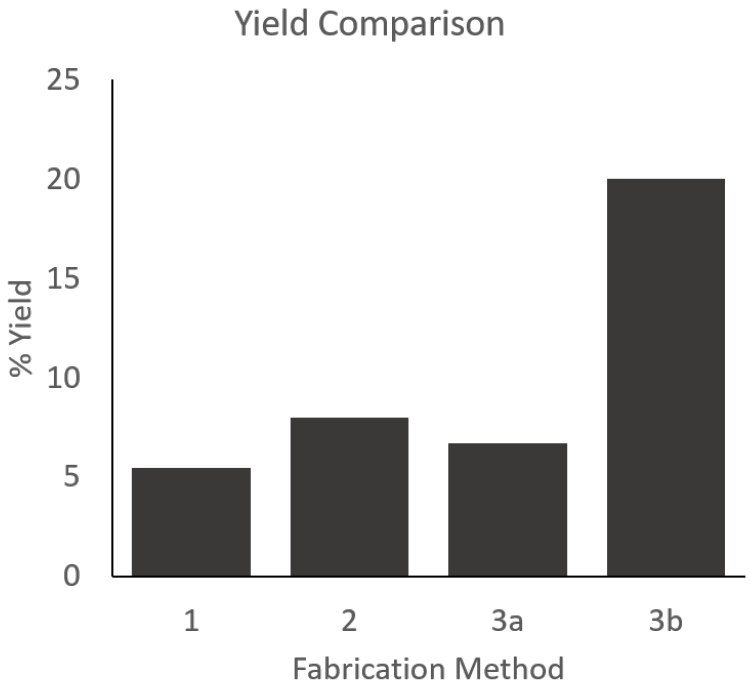

Figure 4.12: Percentage of the working devices. 1, 2, 3 represent fabrication methods I, II, and III respectively. 3b represents the devices fabricated through Method III, where the injection distance was kept at 40% of the original actuator length.

Figure 4.11 compares the total number of devices with the number of working devices for each method. In Figure 4.12, all three fabrication methods are compared in terms of percent yield. The plot includes the yield for Method III overall (3a), as well as the yield for the devices where the injection distance was kept shorter than the original actuator length (3b).

4.2 Simulation Results

The devices were modeled in Comsol as described in Section 3.3. The first model was designed to match the specifications of the fabricated devices and the simulation results were compared with the experimental data. All the thickness values (t_d, t_c, t_e, d_s)

were set to 20 μm and the conductive layer length was set to 1000 μm, bringing the total device width to 1060 μm. The total actuation distance was defined as the difference between the initial length of the actuator and the final length of the actuator. The actuation ratio was defined as the ratio of the total actuation distance and the initial actuator length.

Figure 4.13 shows the results of the simulation at different operating voltages. Actuation ratio is represented on the y-axis and the total actuator length is on the x-axis.

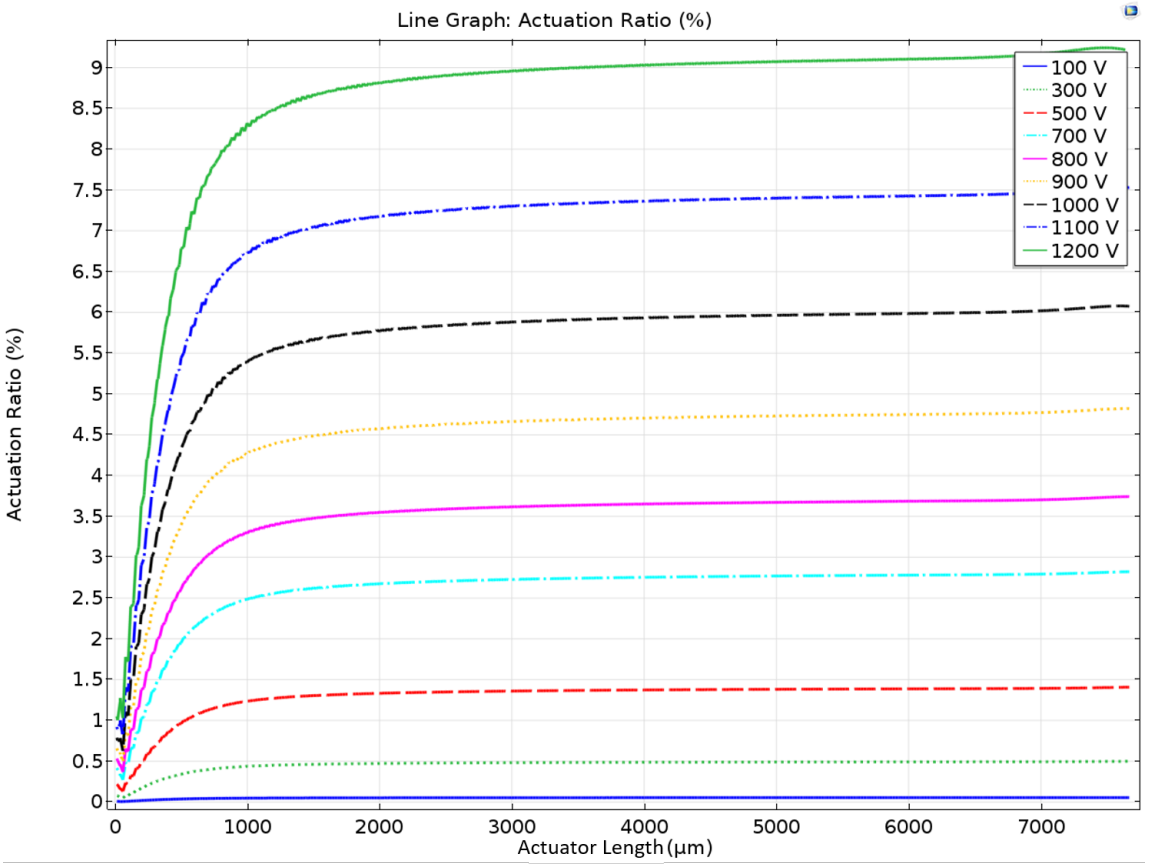

Figure 4.13: Actuation ratio of the modeled device (with the default parameters) working at different input voltages ranging from 100 V to 1.2 kV.

Figure 4.13 shows that the actuation ratio is increasing as the voltage is increasing

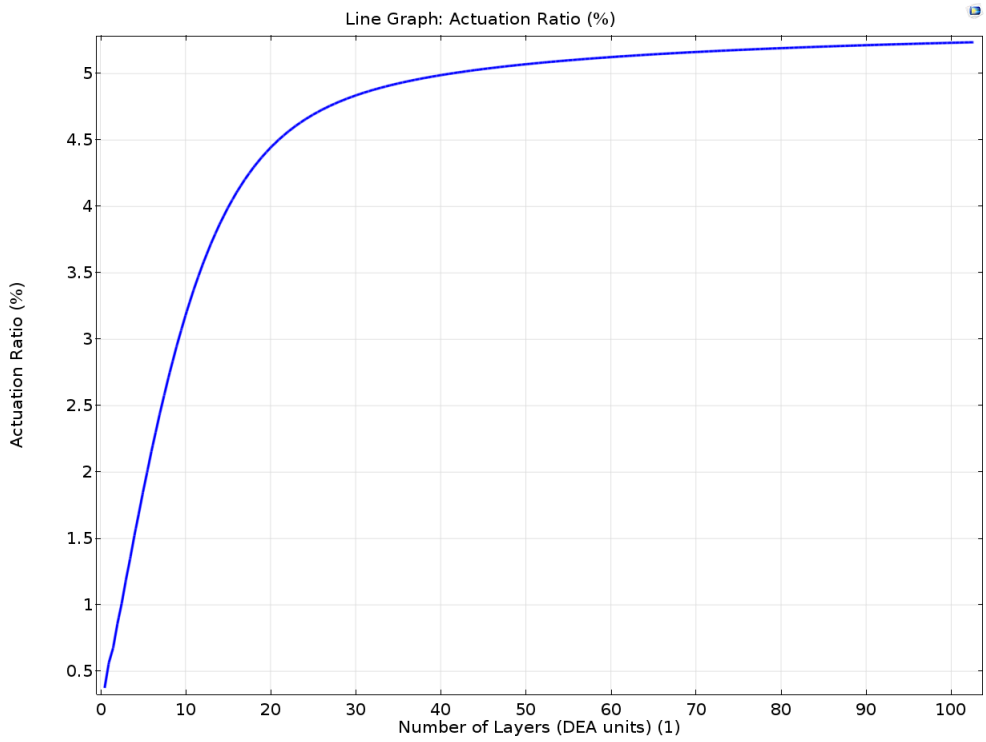

Figure 4.14: Actuation ratio as a function of the number of layers at 1 kV applied voltage.

as expected. It is also observed that the actuation ratio is increasing up to a certain distance of the actuator and then it is stabilizing after reaching to a maximum point. There is only a slight increase but it is relatively constant, with a slope close to zero. This indicates that given that all the geometric parameters are constant, increasing the number of layers (after the actuation ratio reaches to the plateau region) does not significantly affect the actuati on ratio. It does, however, increase the total actuation distance as shown in Figure 4.13.

In Figure 4.14, the actuation ratio with the default configurations is plotted as the number of layers change. It is observed that after about 40 layers, the increase in the actuation ratio diminishes and after 100 layers, it plateaues. Since the increase in the number of layers does not significantly affect the actuation ratio, for the rest of the

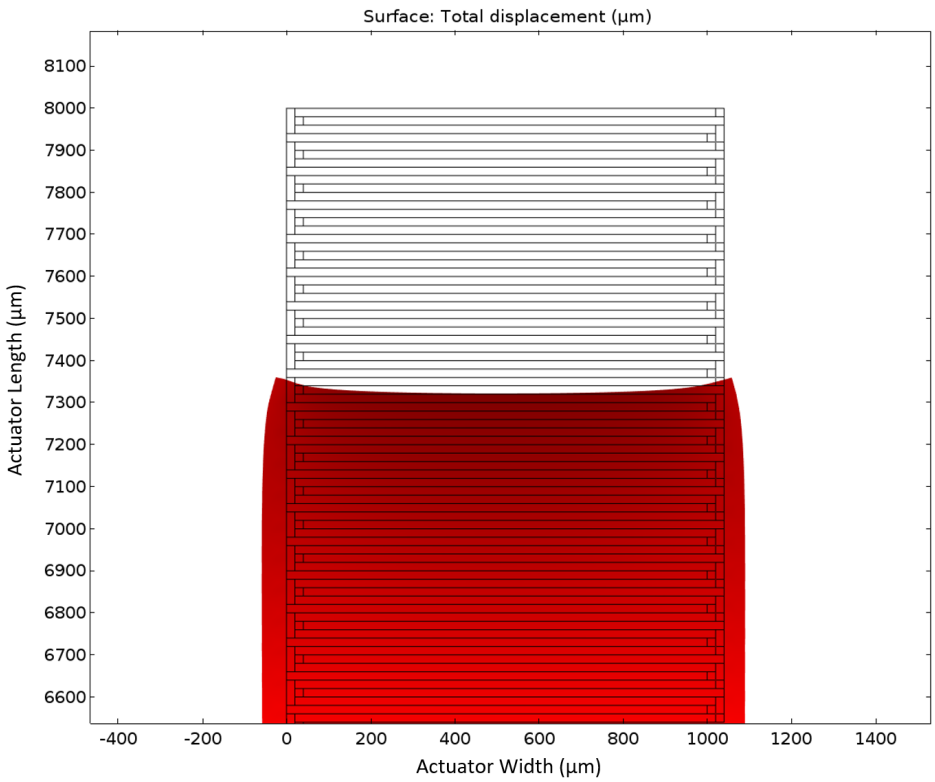

Figure 4.15: The free end (6.5 to 8.2 mm from the fixed end) of the simulated actuator with 20 μm layer thickness at 1 kV input voltage. This modeled actuator was not used for analysis, only simulated for demonstration purposes.

study, 100 layers will be simulated to decrease the computing power consumption.

The free end of a simulated actuator is shown in Figure 4.15. It can be seen in the figure that the displacement reaches its maximum at the center of the actuator in x-axis. The electrode connections on both sides and the dielectric materials cause internal stress and inhibit the actuation motion at the edges.

In a DEA device, the conductive layers do not contribute to the actuation, they act as passive layers within the actuator. Therefore, decreasing the thickness of the conductive layers should increase the actuation ratio. In Figure 4.16 and Figure 4.17, the effect of conductive layer thickness on the actuation ratio is shown. In Figure 4.17, total actuation percent is calculated as displacement in y direction divided by

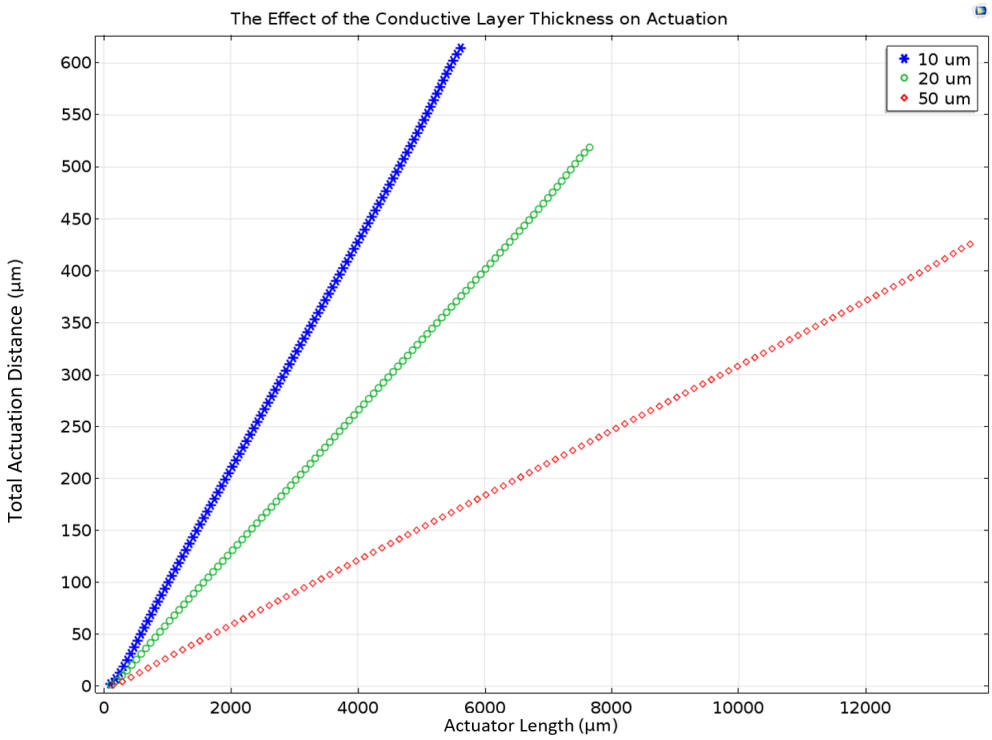

Figure 4.16: The effect of changing conductive layer thickness on the total deformation of the actuator. All other geometric parameters are kept constant.

the distance in the y direction. The applied voltage is set to 1 kV for this comparison. The simulation results follow the expected behaviour where the actuation ratio is increasing as the conductive layer thickness is decreasing.

One of the other passive regions that restrain the actuation motion is the electrodes on both sides of the actuator. Decreasing the thickness of the electrodes would increase the active area and would increase the actuation ratio, as reported in earlier studies by Kovacs et al. [13].

The actuation ratio plotted in Figure 4.18 follows this trend. Although the difference gets smaller as the electrode thickness is decreasing, the differences with larger electrode thickness values are significant. It should also be noted that since the other

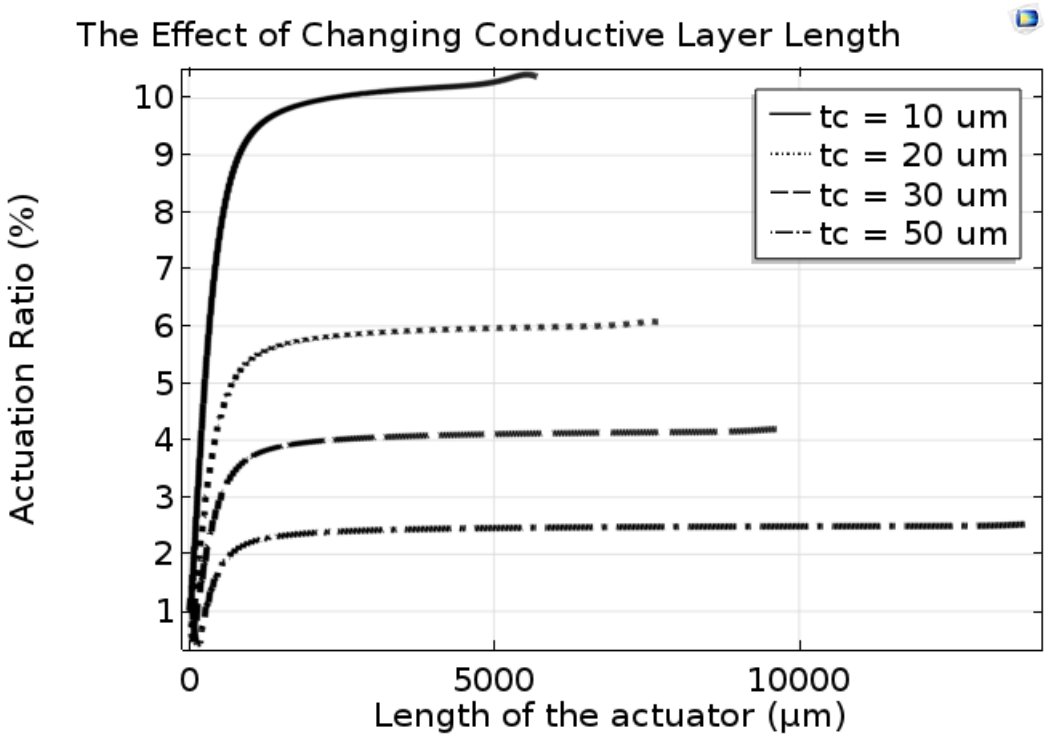

Figure 4.17: Actuation ratio as a function of distance in the vertical axis as the conductive layer thickness (tc) changes.

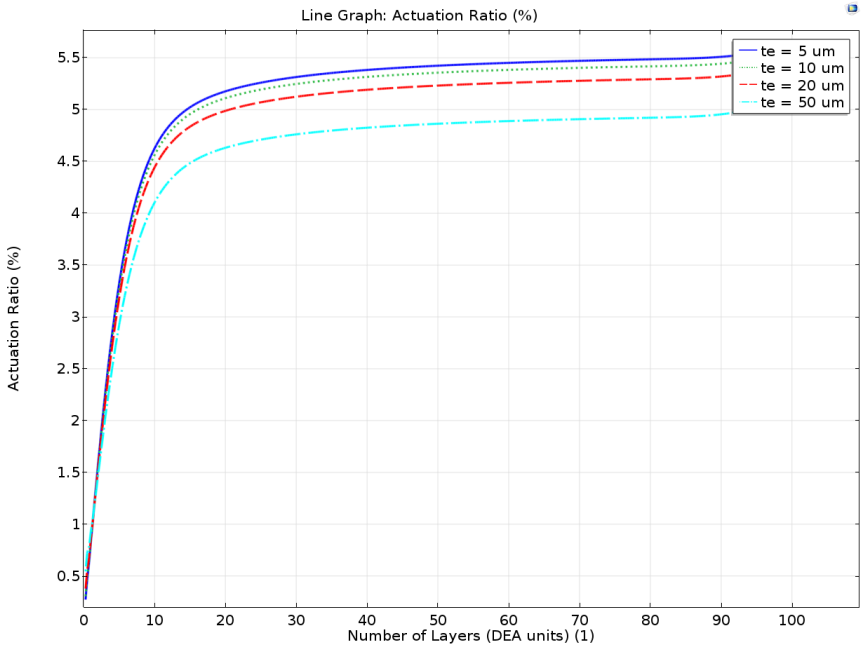

Figure 4.18: The change in the actuation ratio as the electrode thickness (t_e) changes (at 1 kV input voltage).

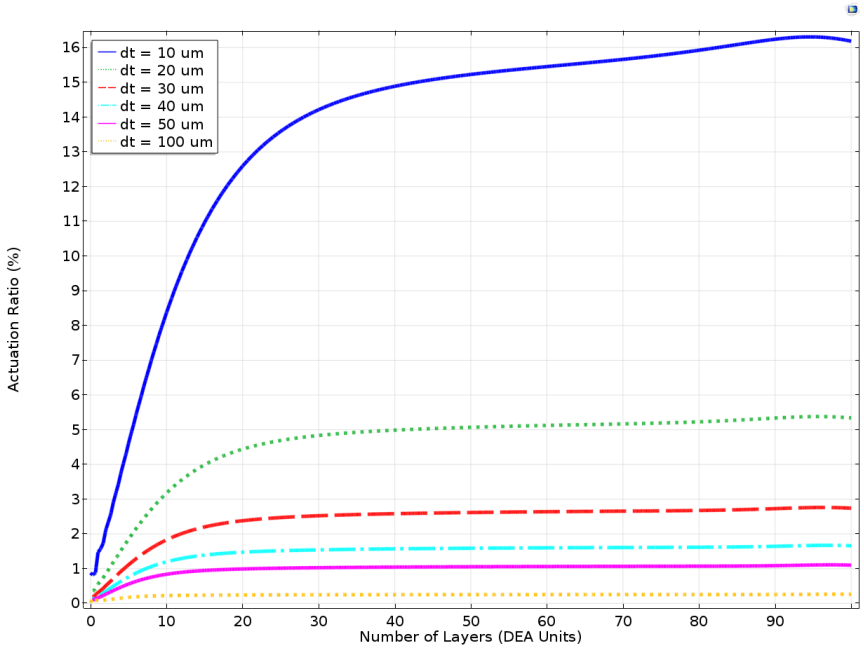

Figure 4.19: Actuation ratio vs the number of DEA layers with changing dielectric layer thickness.

parameters are kept constant, the change in the electrode thickness with respect to the size of the actuator is decreasing as the electrode thickness value is getting smaller. This could explain why the effect of change in t_e is diminshing as the value is getting smaller.

Theoretically, the cross-sectional area of the multilayer DEAs should not affect the actuation ratio since the actuation is a function of the generated force per unit area. Figure 4.21 displays the total displacement (actuation distance) along the y-axis as the conductive layer width is changing. It is observed that the displacement is increasing as the layer width is increasing up to 1000 μm. After 1000 μm, the change in the displacement is diminished. For a better comparison, the ratio of active surface distance to total distance should be calculated. With 20 μm electrode thickness and separation distance, passive surface distance would be 80 μm (40 μm on each side). Therefore the ratio of the active surface to total surface ratio for a 100 μm conductive

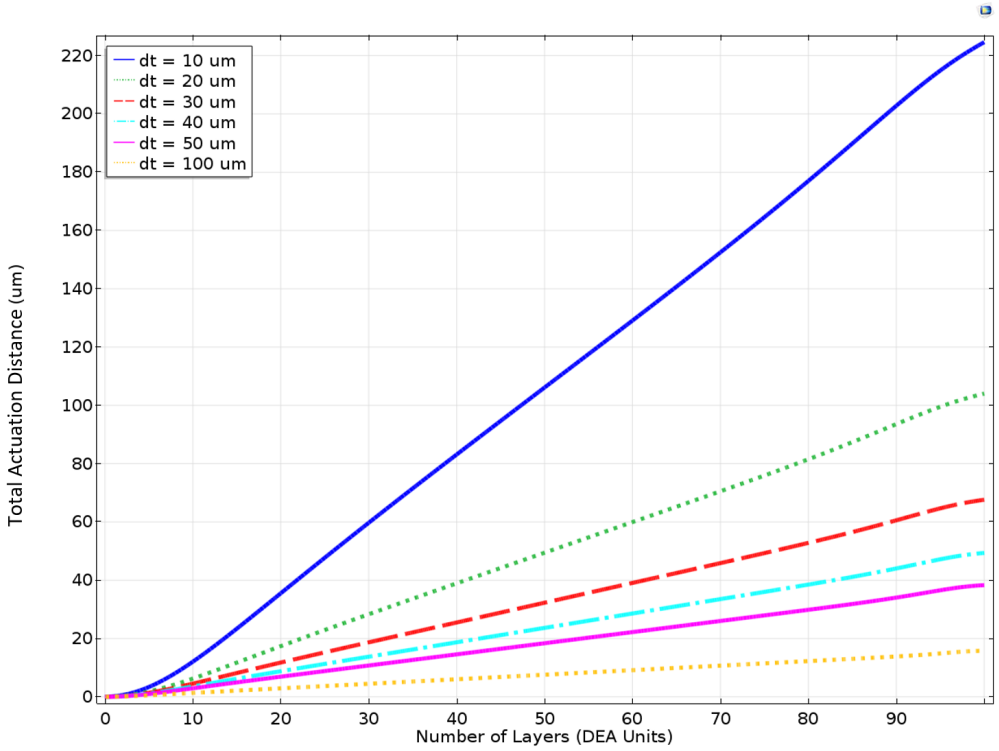

Figure 4.20: Total actuation distance vs the number of DEA layers with changing dielectric layer thickness.

layer width would only be 55.5% (100/180). At 1000 μm width, this ratio goes up to 92.6%. It can be concluded that, for the given geometric configuration, this is the critical ratio of active surface area to total surface area for designing an efficient actuator. The increase in the actuation ratio is smaller as the ratio of active surface to total surface area increases above 92%.

Validation of the Simulation Results

After the fabricated devices were modeled in Comsol and simulated for actuation measurement, the results were compared with the experimental results and the analytical results calculated using Equation 2.9. As shown in Figure 4.22, the experimental results follow the general trend of the simulation results closely but deviates from it

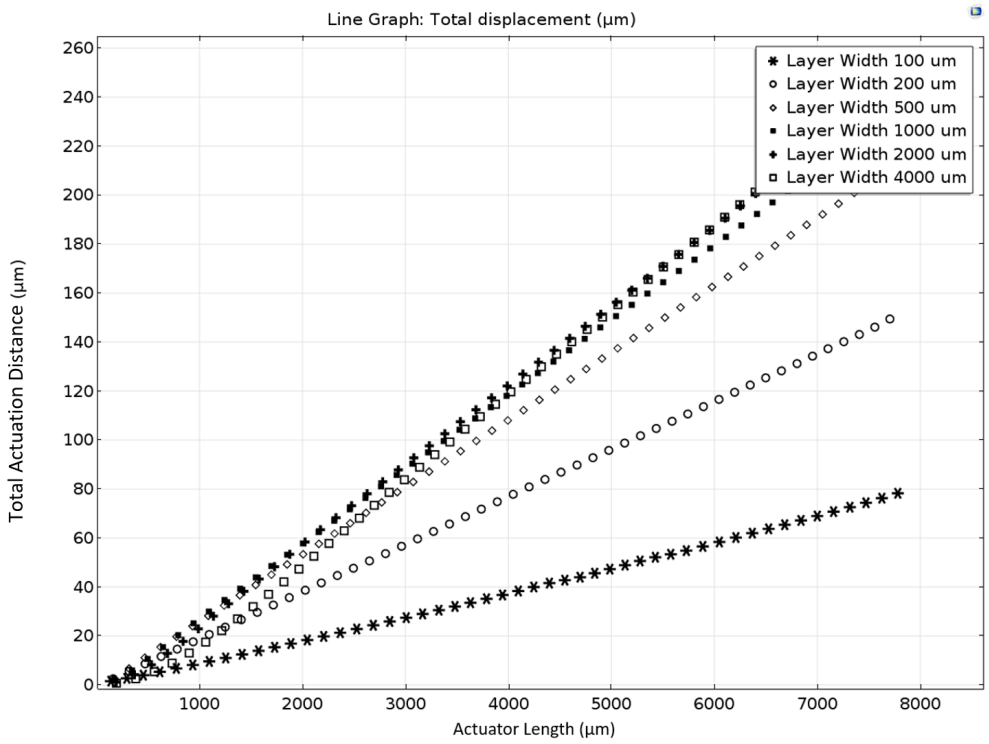

Figure 4.21: Total displacement of 20 μm layer actuators with varying layer width. The actuation distance is increasing up to 1000 μm.

slightly as the voltage goes up. This could be due to the extra PDMS layer at the bottom of the actuator introduced in the fabrication process and was not included in the numerical model. This is similar to the effect of increasing the electrode thickness on both sides and creating extra passive cross-sectional area that counteracts the actuation force generated by the actuator. Figure 4.18 supports this theory, as the actuation ratio decreases with the increase in electrode thickness.

There is also a difference between the analytical calculations and the simulation results. The analytical results, shown in Figure 4.22, were obtained by using Equation 2.1. This is an oversimplification of the multilayer model. It assumes the actuation ratio for the multilayer structure is the same as it is for a single DEA unit. For the analytical calculations, only the Young's modulus was utilized whereas in the

simulations, bulk modulus and the shear modulus are used. The Young's modulus for the analytical calculations was taken as the average of the two materials (conductive and dielectric). In the simulations, the electrode connections (side-walls) and the remaining passive surface area are also considered when calculating the actuation ratio, whereas in the analytical calculations, they are neglected.

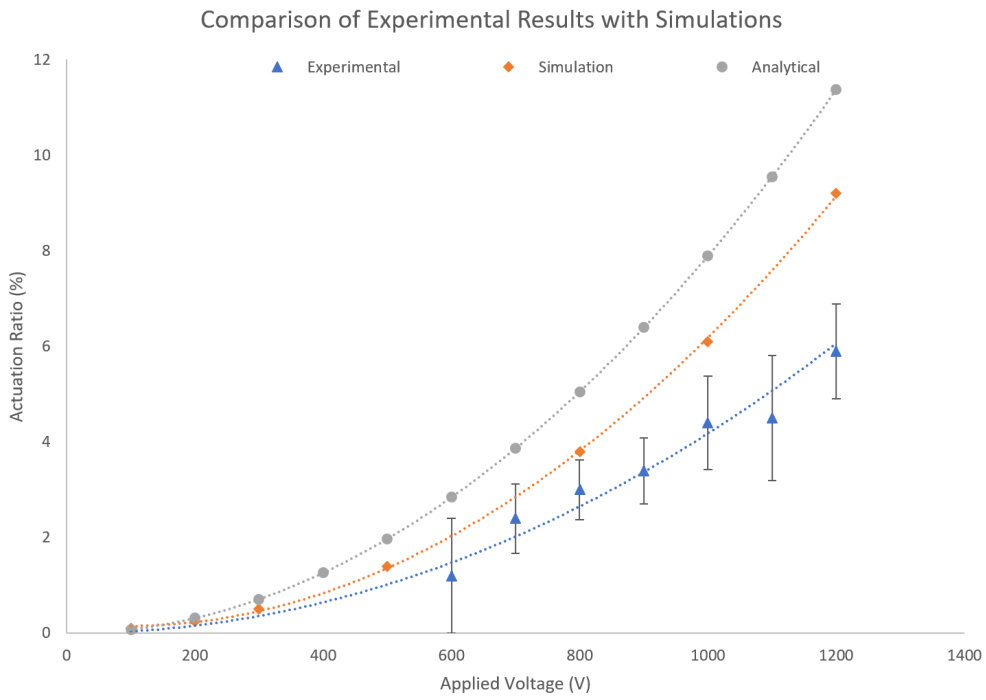

Figure 4.22: Comparison of the actuation ratio obtained from the simulations with the experimental results for actuators with $20\mu m$ dielectric and conductive layer thickness.

Chapter 5

Discussion of the Results

The study introduced three fabrication approaches to implement existing microfabrication techniques for the fabrication of multilayer DEAs consisting of micro-sized DEA units. The results proved that using existing microfabrication techniques, it is possible to fabricate multilayer DEAs comprised of micro-scale layers that can operate in the sub-kV range.

To address the first research objective, a mechanically compliant MWCNT/PDMS composite was fabricated using a combination of sonication and magnetic stirring. Toluene had to be used for creating a MWCNT suspension before mixing the MWCNTs with PDMS. The toluene in the mixture was evaporated before curing the composite material, however small amounts of toluene were still present in the mixture. Increasing the temperature of the toluene/MWCNT mixture to increase the evaporation speed of toluene resulted in non-conductive polymer after the mixture was cured. The evaporation step elongated the fabrication time by up to two days.

As the second step to address the objectives of this study, proof of concept DEAs were fabricated with the selected materials. It was shown that the fabrication of multilayer DEAs was possible with the selected materials. PDMS provided a good

pot life that allowed working with the materials for an extended period of time before they started crosslinking. MWCNTs were a good conductive dopant for reaching the electrical percolation threshold with low filler content so the elastic properties of the polymer matrix were not impacted significantly. PDMS also provided tunable elastic properties so when the conductive polymer could be modified to match the elastic properties of the dielectric material.

After the actuation proved viable with the macro-scale multilayer DEA, the third and fourth objectives were to design a multilayer DEA in micro-scale to operate in the sub-kV range and to develop a fabrication method for the micro-scale design. Instead of following the conventional layer-by-layer fabrication method, an all-in-one step fabrication approach was proposed. To achieve the fabrication of all elastic layers in one step and all conductive layers in another step, an interdigitated DEA structure was designed. The geometric parameters and the number of layer of the stacked actuators could be modified without affecting the total fabrication time.

Two slightly different approaches were proposed to fabricate the multilayer DEAs. In Method I, the dielectric layers were formed on the photoresist and the conductive mixture was coated on top of the dielectric layers, as shown in Figure 3.18. With Method II, the order was changed and the conductive parts were formed on the photoresist before the conductive layers, as shown in Figure 3.20. With both methods, discarding the excess MWCNT/PDMS and isolating each alternating layer from each other was the most challenging step and decreased the repeatability of the fabrication processes. As depicted in Figure 4.11 (a), With the first fabrication method (Method I), the output efficiency was 5%.

In order to help with isolating the alternating conductive layers, spin coating speed was increased and more pressure was applied during the removal of the con-

ductive slurry. With relatively soft and high aspect ratio PDMS structures, the fabricated pillars tended to deform easily. In order the to overcome this problem, the fabrication order was reversed in Method II, as depicted in Figure 3.20. Using Method II, removing the conductive slurry was easier since the soft PDMS pillars were replaced more rigid photoresist pillars. However, with Method II, another problem in addition to the excess MWCNT/PDMS slurry was the strong adhesion between the cured MWCNT/PDMS composite and the photoresist. Most of the patterned MWCNT/PDMS structures were destroyed while removing the cured MWCNT/PDMS composite from the substrate.

In order to eliminate the excess MWCNT/PDMS slurry problem, Method III was designed introducing the injection of the conductive slurry into the fabricated dielectric channels. With this method, the biggest problem was the high viscosity of PDMS and the toluene in the MWCNT/PDMS mixture. The high viscosity of the conductive slurry required high pressure to inject the slurry into the microchannels. As shown in Figure 3.22, one side of the fabricated PDMS structure was cut open to let the air out. The syringe containing the conductive slurry was attached to the other side of the structure. The device was vacuumed in a vacuum chamber to release the conductive slurry into the microchannels in the PDMS structure. The conductive slurry leaked into the neighboring channels and caused the same short-circuiting problem that were present with methods I and II. To overcome this problem, the amount of toluene in the conductive mixture was reduced and the corona treatment time was elongated to provide a stronger bonding between the patterned PDMS and the thin PDMS sheet. Even though some devices were fabricated using this method, the output efficiency of the fabrication method remained near 6.6%.

As the results indicate, changing the fabrication method did not have a significant

impact on the actuation ratio of the fabricated multilayer actuators. This is due to the fact that the magnitude of the actuation is related to the material properties and the thickness of the DEA layers and the same materials and dimensions were used for all the fabrication methods.

The fabricated multilayer DEAs proved that microfabrication can be used for the fabrication of DEAs for larger than micro-scale actuation systems that do not depend on rigid substrates to operate. The operating voltage can be reduced to sub-kV range without applying prestrain on the materials, solely by reducing the dielectric layer thickness. The fabrication yield for method is shown in Figure 4.11. Even though the yields of the fabrication approaches are low, they can be further improved by automating the fabrication steps and eliminating any manual fabrication. When comparing the overall yield for all three methods, the yield seems to decrease from Method I through Method III. However, Method III seems to be the most promising approach. Even though the total yield was low, when the injection distance was decreased, the yield increased significantly. One way to improve Method III while keeping the original actuator length could be applying vacuum only inside the micro-channels, creating a pressure difference between the outside and inside the channels, thus aiding the sealed dielectric materials keep intact. The conductive material could also be further optimized by controlling the alignment of the carbon nanotubes inside the PDMS slurry.

The last objective of the study was to use a computer aided model of the fabricated multilayer DEAs to try to optimize the actuator configuration. The actuators were modeled in Comsol and different geometrical parameters, that are identified in Figure 3.31 were modified to study the effect of each parameter on the actuation ratio. The environmental variables and any potential change in the internal temperature of

the devices were neglected. The deformation was assumed to be isochoric, isotropic and linear elastic. The elastic modulus was assumed to be constant. The results aligned well with the expectations. The actuation ratio increased significantly with the decrease in dielectric and conductive layer thickness, increased slightly with the decrease in the passive surface area (electrode thickness). It was observed that the actuation ratio was impacted by the number of layers (or the total actuation length) only up to a point depending on the layer thickness, length and electrode thickness. After a certain length, the actuation did not change with the change in the number of layers. However, the elastic modulus of the materials in the simulations were given as constants, whereas in reality the elastic modulus can change as the materials are compressed under stress. As the elastic modulus increases, the actuation ratio would decrease.

Chapter 6

Conclusions

The aim of this study was to investigate whether it was possible to utilize existing microfabrication techniques to fabricate fiber-like multilayer dielectric elastomer actuators that could operate in the sub-kV regime. A conductive MWCNT/PDMS composite was fabricated using commercially available MWCTNs and PDMS through a combination of shear mixing and sonication. The fabricated conductive PDMS was mechanically compliant with the dielectric layers, in which that it did not inhibit the actuation mechanism.

This study utilized existing fabrication methods in a unique way for the fabrication of free-standing multilayer DEAs, comprised of micro-scale DEA units, that can be used for both micro-scale and larger scale applications. The size of the DEAs can be adjusted according to the applications needs by changing the number of layers and/or the actuator width, without compromising on the low operating voltage. Actuation ratios up to 6% were achieved at voltages below or at 1.2 kV. As examplified earlier, there are studies in the literature that investigated the possiblity of fabrication of DEAs operating at low voltages. Although they are successful at achieving actuations near or above 10% at voltages lower than 1 kV, the fabrication methods and the

actuator designs in small scale are not compatible with large scale applications and most of them rely on a rigid substrate to operate, as depicted in Figure 2.3 and 2.4. The geometry of the actuators in this study allows for linear actuation, as compression, as opposed to circular area expansions that is found in conventional DEAs. With the linear actuation mechanism, the fabricated DEAs can be used as artificial muscles in soft robots, as well as in many other areas.

The interdigitated design of the actuators allows the fabrication of DEAs in micro-scale, lowering the voltage but maintaining the total actuation distance. The size of a 'unit DEA' can be further scaled down to reduce the operating voltage, without comprimising from the total actuation distance.

The most significant drawback of the fabrication methods investigated in this study was the repetability of the fabrication processes. It should be noted that the number of working devices for each fabrication method is less than 5. Statistically, this data is not enough to make an accurate assesment of the fabrication methods. The reason behind the rest of the fabricated samples not working could be due to human error during the fabrication process. As explained in the previous chapters, the fabrication methods included some manual steps, that relied on human precision. Although the repetability of the injection method was low, it was observed to be the most promising method since it does not involve as many manual steps as the other two methods. With Method III, the possibility of human error was reduced by eliminating the manual removal of the conductive slurry. The reason for low yield with Method III can be explained by; possible swelling of the PDMS by the toluene in the c-PDMS mixture and the weak bonds between the two PDMS layers formed during steps 5 and 6 in Figure 3.2.2.

Modeling of the actuators provided an analysis of the effect of device geometry

on the actuation ratio. It was shown that as the passive surface area increased, the actuation ratio decreased. Decreasing the thickness of the dielectric layers increased the actuation ratio at a given voltage, significantly. The thickness of the conductive layers also affected the actuation ratio, the actuation ratio decreased with increasing layer thickness, albeit not as sharply. When the actuator width decreased, the actuation ratio also decreased but seemed to converge to a limit with increasing actuator width. This proves that as the ratio of the active surface area and the passive surface area increases, actuation ratio (and actuation distance) goes up. When designing multilayer DEAs, the actuator width should be calculated considering the electrode thickness and the separation distance between the counter electrodes.

By microfabricating multilayer DEAs, operating voltage can be reduced, linear compressive actuation can be obtained, actuation ratio can be increased. If the unit DEAs can be fabricated in nano-scale, the operating voltage could be further reduced down below 10 V. There are some limiting factors, such as the size of carbon nanotubes used for the conductive polymer. However, the potential problems related to scaling down can be overcome by using alternative materials (such as liquid metals) or modifying fabrication the processes.

Soft robotics is an emerging field and the need for soft robots is increasing everyday, as robots become more and more integrated into our daily lives. The fabrication methods introduced in this study provide an alternative approach to traditional DEAs. Even though the yields for the fabrication processes are low, this study proves that there is still so much room for the advancement of dielectric elastomer actuators. The microfabrication approach can be a transition stage for the next generation of DEAs.

6.1 Suggested Future Work

6.1.1 Development of a Stretchable Photocurable Conductive Polymer

As previously described, one problem with the fabrication procedure followed in the study was the inconsistency associated with the isolation of conducting paths. An alternate approach to overcome most of the problems in this microfabrication strategy would be using a stretchable, conductive and photocurable polymer. Such a polymer would provide the mechanical properties needed for actuation, and it would eliminate all the additional chemicals used in the process. If both dielectric and conducting layers could be cured using a light source, photoresists would not be required, the thickness of the polymer at each step could be controlled more accurately, and polymers in undesired locations could be washed away easily.

Figure 6.1 depicts the possible fabrication approach assuming a stretchable and photocurable conductive polymer is used for fabrication. As shown in the figure, the fabrication process would not require any manual step and would include fewer steps, which would decrease the total fabrication time. However, developing a photocurable polymer must have high transmittance so that the light can reach to the bottom of the polymer layer. Otherwise, the polymer would start polymerizing at the top and never polymerize at the bottom. It might be possible to design such a polymer by using different functional groups that would provide conductivity and photo-sensitivity.

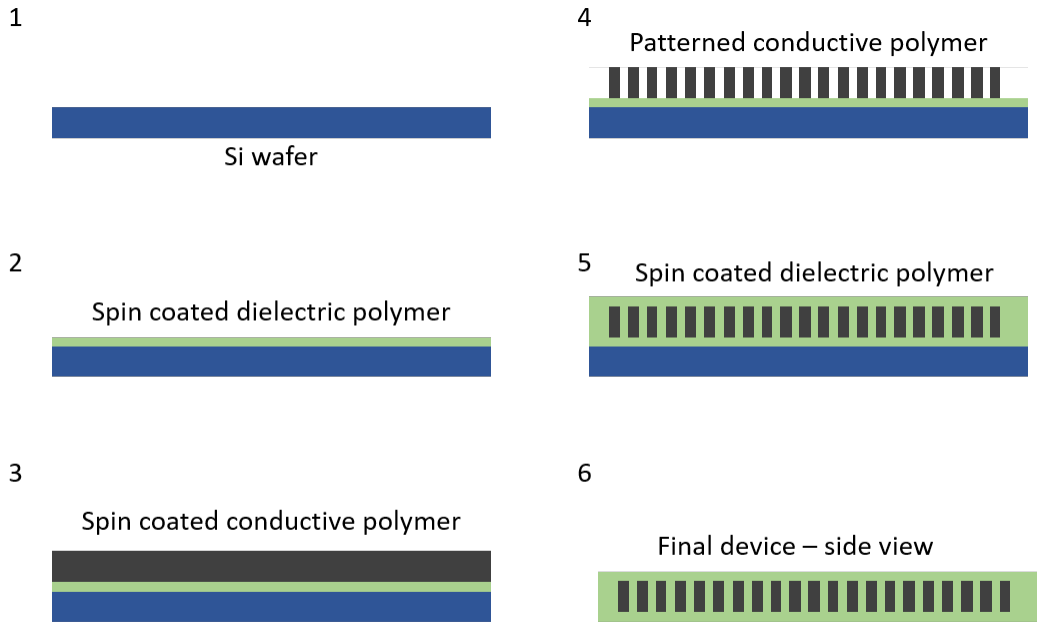

Figure 6.1: Possible fabrication steps for microfabrication of DEAs using photocurable strechable conductive polymer.

6.1.2 Bundling of DEA Fibers to Form Artificial Muscles

The micro-sized multilayer stacked actuators fabricated using the investigated methods resemble the natural muscle fibers in humans due to their geometry and actuation directionality. Once the fabrication of micro-sized DEAs has been optimized, a control system can be integrated to achieve an artificial muscle structure for user-end applications. Theoretically, these 'muscle fibers' can be used like natural muscles by combining a sufficient number of them to form a stronger muscle structure, like the skeletal muscle structure represented in Figure 6.2. They can be connected in parallel to increase the generated output force and to control the direction of actuation.

Figure 6.3 shows crude schematics for a simple possible configuration of micro-DEA structures. In the figure, there are 5 identical actuators placed next to each other

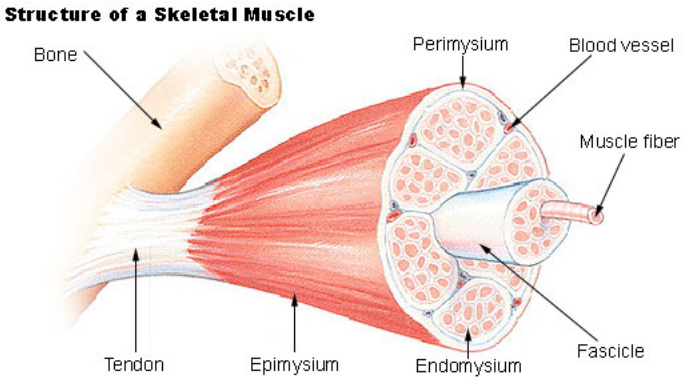

Figure 6.2: Human skeletal muscle structure. *Source:* ***http://people.eku.edu/ritchisong/301images/muscle_structure.jpg***

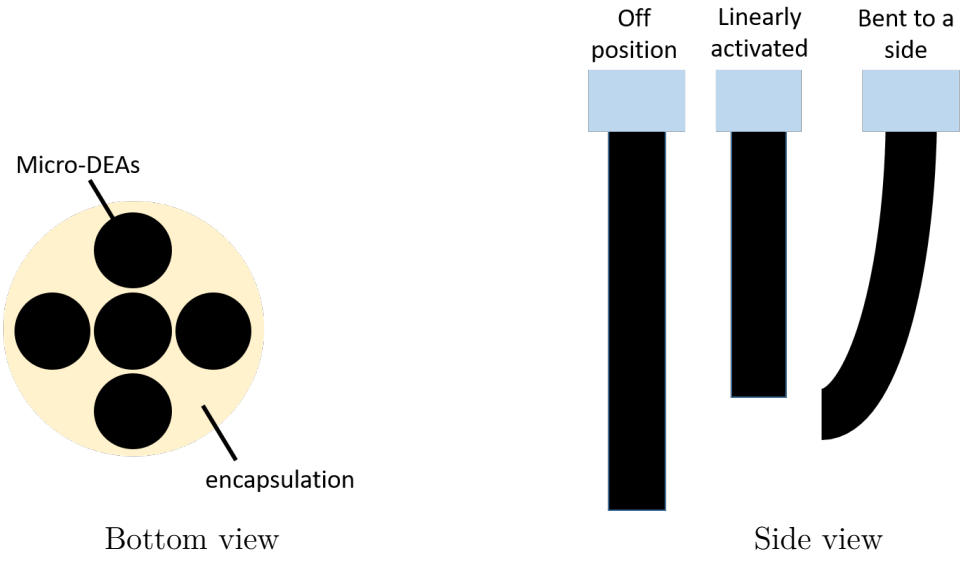

Figure 6.3: Possible configuration for the directional control of micro-DEAP actuator fiber structures.

and encapsulated with a soft polymer to protect the integrity of the structure and to isolate the electrical connections from outside. If all the actuators in the structure are activated at once, the device will actuate linearly due to the compressive motion. If only two or three of the actuators are activated, the device will bend in the direction of the activated actuators. For example, in the bottom view, activation of the top and left actuators would result in a bending motion -45^o in the x-y plane (northeast

direction). The amount of bending motion is a function of the applied voltage.

Another possibility would be connecting the micro-sized DEAs to rigid frames, resembling a skeletal muscle-bone structure in animals and humans. Figure 6.4 shows how basic skeletal muscles work. The bicep muscle, which consists of smaller muscle fibers as shown in Figure 6.2, are connected to skeletal bones via tendons. Micro-DEA structures could be assembled in a similar structure to provide the same movement mechanism for rigid bodies, which also extends the use of DEAP actuators beyond soft structures.

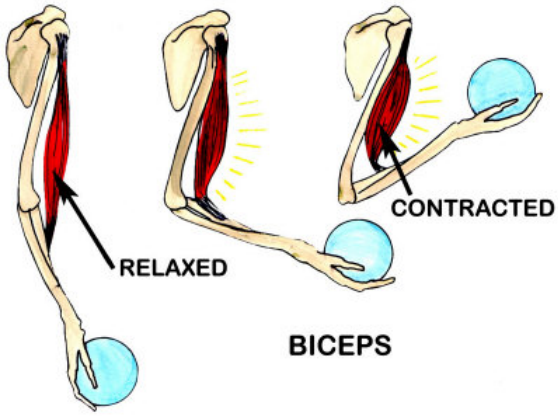

Figure 6.4: Movement of the bones by activation of skeletal muscles *Source:* ***http://wizznotes.com/wp-content/uploads/2012/02/image0071.jpg***

6.1.3 Packaging: Attaching Microchips to Actuators

One of the next steps after developing a repeatable fabrication method for micro-DEAs would be packaging them in a suitable and compact way to integrate in to user end applications. Micro-DEAs can be directly wired to a power source or an external circuit for control. However, as the size of the DEAs gets smaller and the number of

DEAs used in a single device gets larger, it will get more difficult to make compact and clean connections with the electrical circuit.

In 2016, Chang et al. [70] introduced a method for attaching microchips on soft substrates. The study used surface tension to selectively attach microchips onto desired locations on a soft substrate. The authors fabricated a superhydrophobic PDMS surface by transferring the nanostructures of black silicon onto the PDMS. Then they formed hydrophilic pads on a superhydrophobic PDMS background and used these regions for attaching the microchips onto the polymer. A similar approach could be used for attaching a microchip, with a desired control circuit, onto the PDMS based micro-DEA structures. This would provide an easy and compact control mechanism for the actuators.

Bibliography

[1] *The Cambridge Companion to Greek Mythology:*. Cambridge Companions to Literature. Cambridge University Press, Nov 2007.

[2] Stephanie Dalley and John Peter Oleson. Sennacherib, Archimedes, and the Water Screw: The Context of Invention in the Ancient World. *Technology and Culture*, 44(1):1–26, 2003.

[3] Michael E Moran. The da Vinci robot. *Journal of endourology / Endourological Society*, 20(12):986–90, dec 2006.

[4] Shimon Y. Nof. *Handbook of Industrial Robotics*. John Wiley & Sons, Inc., New York, NY, USA, 2nd edition, 1999.

[5] Robot Hall of Fame. Unimate. Accessed: 2016-07-24.

[6] International Federation of Robotics. International robot statistics, 2015. Accessed: 2016-07-24.

[7] Filip Ilievski, Aaron D. Mazzeo, Robert F. Shepherd, Xin Chen, and George M. Whitesides. Soft Robotics for Chemists. *Angewandte Chemie International Edition*, 50(8):1890–1895, feb 2011.

[8] Y Bar-Cohen. Electroactive Polymers as Artificial Muscles: A Review. *Journal of Spacecraft and Rockets*, 39(6):822–827, 2002.

[9] W. C. Röntgen. Ueber die durch Electricität bewirkten Form- und Volumenänderungen von dielectrischen Körpern. *Annalen der Physik und Chemie*, 247(13):771–786, 1880.

[10] Ron Pelrine. High-Speed Electrically Actuated Elastomers with Strain Greater Than 100%. *Science*, 287(5454):836–839, feb 2000.

[11] Kwang J. Kim and Satoshi Tadokoro, editors. *Electroactive Polymers for Robotic Applications*. Springer London, London, 2007.

[12] Y Bar-Cohen. Electroactive Polymers as Artificial Muscles - Reality and Challenges. *Adv. Piezoelectr. Mater.*, pages 1–13, 2001.

[13] G. Kovacs, L. Düring, S. Michel, and G. Terrasi. Stacked dielectric elastomer actuator for tensile force transmission. *Sensors and Actuators, A: Physical*, 155:299–307, 2009.

[14] Hidenori Okuzaki, Satoshi Takagi, Fumiya Hishiki, and Ryo Tanigawa. Ionic liquid/polyurethane/PEDOT:PSS composites for electro-active polymer actuators. *Sensors and Actuators, B: Chemical*, 194:59–63, 2014.

[15] Craig D Near. Piezoelectric actuator technology. In Inderjit Chopra, editor, *Smart Materials Bulletin*, number 1, pages 246–258, may 1996.

[16] Yoseph Bar-cohen. *Electroactive polymer (EAP) actuators as artificial muscles reality, potential, and challenges*. SPIE Press, Bellingham, WA, 2004.

[17] Woosung Yang, Hyonkwang Choi, Suho Choi, Minhyon Jeon, and Seung-Yop Lee. Carbon nanotube-graphene composite for ionic polymer actuators. *Smart Materials and Structures*, 21(5):055012, may 2012.

[18] C O Blattmann, G A Sotiriou, and S E Pratsinis. Rapid synthesis of flexible conductive polymer nanocomposite films. *Nanotechnology*, 26(12):125601, mar 2015.

[19] Guggi Kofod. *Dielectric elastomer actuators*. PhD thesis, The Technical University of Denmark, 2001.

[20] James Biggs, Karsten Danielmeier, Julia Hitzbleck, Jens Krause, Tom Kridl, Stephan Nowak, Enrico Orselli, Xina Quan, Dirk Schapeler, Will Sutherland, and Joachim Wagner. Electroactive polymers: developments of and perspectives for dielectric elastomers. *Angewandte Chemie (International ed. in English)*, 52(36):9409–21, sep 2013.

[21] L.J. Romasanta, M.A. Lopez-Manchado, and R. Verdejo. Increasing the performance of dielectric elastomer actuators: A review from the materials perspective. *Progress in Polymer Science*, 51:188–211, dec 2015.

[22] Samuel Rosset and Herbert R. Shea. Flexible and stretchable electrodes for dielectric elastomer actuators. *Applied Physics A*, 110(2):281–307, 2013.

[23] Samin Akbari, Samuel Rosset, and Herbert R. Shea. Improved electromechanical behavior in castable dielectric elastomer actuators. *Applied Physics Letters*, 102(7):071906, feb 2013.

[24] James E. Mark. *Polymer Data Handbook (2nd Edition)*. Oxford University Press, 2009.

[25] Chao-Xuan Liu and Jin-Woo Choi. Strain-Dependent Resistance of PDMS and Carbon Nanotubes Composite Microstructures. *IEEE Transactions on Nanotechnology*, 9(5):590–595, sep 2010.

[26] Guocheng Shao, Jiahao Wu, Ziliang Cai, and Wanjun Wang. Fabrication of elastomeric high-aspect-ratio microstructures using polydimethylsiloxane (PDMS) double casting technique. *Sensors and Actuators, A: Physical*, 178:230–236, 2012.

[27] A-L Deman, M Brun, M Quatresous, J-F Chateaux, M Frenea-Robin, N Haddour, V Semet, and R Ferrigno. Characterization of C-PDMS electrodes for electrokinetic applications in microfluidic systems. *Journal of Micromechanics and Microengineering*, 21(9):1–8, 2011.

[28] I D Johnston, D K McCluskey, C K L Tan, and M C Tracey. Mechanical characterization of bulk Sylgard 184 for microfluidics and microengineering. *Journal of Micromechanics and Microengineering*, 24(3):035017, mar 2014.

[29] D. P J Cotton, a. Popel, I. M. Graz, and S. P. Lacour. Photopatterning the mechanical properties of polydimethylsiloxane films. *Journal of Applied Physics*, 109(5):054905, 2011.

[30] Zhuo Li, Rongwei Zhang, Yan Liu, Taoran Le, and C. P. Wong. Highly conductive, flexible, bio-compatible poly-urethane based isotropic conductive adhesives for flexible electronics. *Proceedings - Electronic Components and Technology Conference*, pages 406–411, 2012.

[31] Songmin Shang, Wei Zeng, and Xiao-ming Tao. High stretchable MWNTs/polyurethane conductive nanocomposites. *Journal of Materials Chemistry*, 21(20):7274, 2011.

[32] Cheng Huang, Q. M. Zhang, Gal DeBotton, and Kaushik Bhattacharya. All-organic dielectric-percolative three-component composite materials with high electromechanical response. *Applied Physics Letters*, 84(22):4391–4393, 2004.

[33] M. Norkhairunnisa, a. Azizan, M. Mariatti, H. Ismail, and L. Sim. Thermal stability and electrical behavior of polydimethylsiloxane nanocomposites with carbon nanotubes and carbon black fillers. *Journal of Composite Materials*, 46(8):903–910, 2011.

[34] Klaus Flittner, Michael Schlosser, Peter Lotz, Marc Matysek, and Helmut F. Schlaak. Integration of dielectric elastomer stack actuators in micro systems. *Proceedings of SPIE*, 7642:76422W–1–76422W–8, 2010.

[35] Luc Maffli, Samuel Rosset, Michele Ghilardi, Federico Carpi, and Herbert Shea. Ultrafast all-polymer electrically tunable silicone lenses. *Advanced Functional Materials*, 25(11):1656–1665, 2015.

[36] Bavani Balakrisnan and Elisabeth Smela. Challenges in the Microfabrication of Dielectric Elastomer Actuators. *Electroactive Polymer Actuators and Devices*, 7642:76420K–76420K–10, 2010.

[37] Peter Lotz, Marc Matysek, and Helmut F. Schlaak. Fabrication and application of miniaturized dielectric elastomer stack actuators. *IEEE/ASME Transactions on Mechatronics*, 16(1):58–66, 2011.

[38] Philippe Dubois, Samuel Rosset, Sander Koster, Johann Stauffer, Serguei Mikhaïlov, Massoud Dadras, Nico-F. de Rooij, and Herbert Shea. Microactuators based on ion implanted dielectric electroactive polymer (EAP) membranes. *Sensors and Actuators A: Physical*, 130-131(3):147–154, aug 2006.

[39] Aaron P. Gerratt, Bavani Balakrisnan, Ivan Penskiy, and Sarah Bergbreiter. Batch fabricated bidirectional dielectric elastomer actuators. *2011 16th International Solid-State Sensors, Actuators and Microsystems Conference, TRANSDUCERS'11*, pages 2422–2425, 2011.

[40] Alexandre Poulin, Samuel Rosset, and Herbert R. Shea. Printing low-voltage dielectric elastomer actuators. *Applied Physics Letters*, 107(24), 2015.

[41] Mihai Duduta, Robert J. Wood, and David R. Clarke. Multilayer Dielectric Elastomers for Fast, Programmable Actuation without Prestretch. *Advanced Materials*, 28(36):8058–8063, 2016.

[42] David McCoul, Samuel Rosset, Samuel Schlatter, and Herbert Shea. Inkjet 3D printing of UV and thermal cure silicone elastomers for dielectric elastomer actuators. *Smart Materials and Structures*, 26(12), 2017.

[43] Xiaobin Ji, Alae El Haitami, Francesca Sorba, Samuel Rosset, Giao T.M. Nguyen, Cédric Plesse, Frédéric Vidal, Herbert R. Shea, and Sophie Cantin. Stretchable composite monolayer electrodes for low voltage dielectric elastomer actuators. *Sensors and Actuators, B: Chemical*, 261:135–143, 2018.

[44] Michael Wissler and Edoardo Mazza. Modeling and simulation of dielectric elastomer actuators. *Smart Materials and Structures*, 14:1396–1402, 2005.

[45] Michael Wissler and Edoardo Mazza. Electromechanical coupling in dielectric elastomer actuators. *Sensors and Actuators, A: Physical*, 138(2):384–393, 2007.

[46] Dominik Tepel, Christian Graf, and Jürgen Maas. Modeling of mechanical properties of stack actuators based on electroactive polymers. volume 8687, page 86871C, apr 2013.

[47] Henry Haus, Marc Matysek, Holger Mößinger, and Helmut F Schlaak. Modelling and characterization of dielectric elastomer stack actuators. *Smart Materials and Structures*, 22(10):104009, oct 2013.

[48] R Zhang, P Iravani, and P S Keogh. Modelling dielectric elastomer actuators using higher order material characteristics. *Journal of Physics Communications*, 2(4):045025, apr 2018.

[49] ASTM International. Standard test method for tensile properties of plastics. *ASTM International*, 08:46–58, 2003.

[50] V Popov. Carbon nanotubes: properties and application. *Materials Science and Engineering: R: Reports*, 43(3):61–102, jan 2004.

[51] Hailin Cong and Tingrui Pan. Photopatternable Conductive PDMS Materials for Microfabrication. *Advanced Functional Materials*, 18(13):1912–1921, jul 2008.

[52] Alexandre Larmagnac, Samuel Eggenberger, Hanna Janossy, and Janos Vörös. Stretchable electronics based on Ag-PDMS composites. *Scientific reports*, 4:7254, 2014.

[53] Ajit Khosla. Nanoparticle-doped Electrically-conducting Polymers for Flexible Nano-Micro Systems. *ECS Interface*, 21(3-4):67–70, 2012.

[54] Chao-Xuan Liu and Jin-Woo Choi. Patterning conductive PDMS nanocomposite in an elastomer using microcontact printing. *Journal of Micromechanics and Microengineering*, 19(8):085019, 2009.

[55] R Andrews and M.C Weisenberger. Carbon nanotube polymer composites. *Current Opinion in Solid State and Materials Science*, 8(1):31–37, jan 2004.

[56] Fangjun Liu, Weijie Sun, Zhendong Sun, and John T. W. Yeow. Effect of CNTs alignment on electrical conductivity of PDMS/MWCNTs composites. In *14th IEEE International Conference on Nanotechnology, IEEE-NANO 2014*, pages 711–714. IEEE, aug 2014.

[57] Peng Cheng Ma, Naveed a. Siddiqui, Gad Marom, and Jang Kyo Kim. Dispersion and functionalization of carbon nanotubes for polymer-based nanocomposites: A review. *Composites Part A: Applied Science and Manufacturing*, 41(10):1345–1367, 2010.

[58] A. Chiolerio, M. Castellino, P. Jagdale, Mauro Giorcelli, Stefano Bianco, and Alberto Tagliaferro. Electrical Properties of CNT-Based Polymeric Matrix NanoComposites. *Intechopen.Com*, 2004.

[59] Yan Yan Huang and Eugene M. Terentjev. Dispersion of carbon nanotubes: Mixing, sonication, stabilization, and composite properties. *Polymers*, 4(1):275–295, 2012.

[60] Samuel Rosset and Herbert R. Shea. Small, fast, and tough: Shrinking down integrated elastomer transducers. *Applied Physics Reviews*, 3(3):031105, sep 2016.

[61] Vincent Linder, Byron D. Gates, Declan Ryan, Babak A. Parviz, and George M. Whitesides. Water-Soluble Sacrificial Layers for Surface Micromachining. *Small*, 1(7):730–736, jul 2005.

[62] Luis Dorfmann and Raymond W Ogden Editors. *Nonlinear Mechanics of Soft Fibrous Materials*, volume 559 of *CISM International Centre for Mechanical Sciences*. Springer Vienna, Vienna, 2015.

[63] Comsol. Comsol structural mechanics user's guide, version 5.2a, 2016.

[64] R.W. Ogden. *Non-linear Elastic Deformations*. Dover Civil and Mechanical Engineering. Dover Publications, 1997.

[65] Fridtjov Irgens. *Continuum Mechanics*. Springer Berlin Heidelberg, Berlin, Heidelberg, 2008.

[66] L Lampani. Finite element modeling of dielectric elastomer actuators for space applications. 2005.

[67] Majid Shahzad, Ali Kamran, Muhammad Zeeshan Siddiqui, and Muhammad Farhan. Mechanical Characterization and FE Modelling of a Hyperelastic Material. *Materials Research*, 18(5):918–924, 2015.

[68] Henrik SÃűnnerlind. Modeling linear elastic materials - how difficult can it be?, Jun 2015.

[69] Mert Corbaci, Kathleen Lamkin-Kennard, and Wayne Walter. Optimization study for fabrication of micro-scale stacked dielectric elastomer actuators. In Yoseph Bar-Cohen, editor, *Proc. SPIE 10163, Electroactive Polymer Actuators and Devices (EAPAD)*, volume 101631I, page 101631I, apr 2017.

[70] Bo Chang, Quan Zhou, Zhigang Wu, Zhenhua Liu, Robin Ras, and Klas Hjort. Capillary Self-Alignment of Microchips on Soft Substrates. *Micromachines*, 7(3):41, mar 2016.